Search for electroweak production of charginos and neutralinos in proton-proton collisions at $\sqrt{s} = 13\,\text{TeV}$

The CMS Collaboration[*]

Abstract

A direct search for electroweak production of charginos and neutralinos is presented. Events with three or four leptons, with up to two hadronically decaying τ leptons, or two same-sign light leptons are analyzed. The data sample consists of $137\,\text{fb}^{-1}$ of proton-proton collisions with a center of mass energy of $13\,\text{TeV}$, recorded with the CMS detector at the LHC. The results are interpreted in terms of several simplified models. These represent a broad range of production and decay scenarios for charginos and neutralinos. A parametric neural network is used to target several of the models with large backgrounds. In addition, results using orthogonal search regions are provided for all the models, simplifying alternative theoretical interpretations of the results. Depending on the model hypotheses, charginos and neutralinos with masses up to values between 300 and 1450 GeV are excluded at 95% confidence level.

Submitted to the Journal of High Energy Physics

[*]See Appendix A for the list of collaboration members

1   Introduction

Supersymmetry (SUSY) is a promising extension of the standard model (SM) with the potential to solve several of the outstanding problems in particle physics by introducing a new symmetry between bosons and fermions [1–5]. This symmetry leads to the prediction of many new particles, called superpartners of the SM particles [6]. The addition of superpartners can mend the hierarchy problem by introducing cancellations between the large loop corrections to the mass of the Higgs boson (H). Additionally, SUSY models in which R-parity [3] is conserved, implying pair production of superpartners, provide a suitable dark matter candidate in the form of the lightest SUSY particle (LSP).

Searches for the production of SUSY particles have already been carried out in a multitude of final states by the ATLAS and CMS Collaborations at the CERN LHC, however none resulted in evidence of the existence of new particles. Particularly stringent exclusion limits have been placed on the production of strongly interacting superpartners (squarks and gluinos) due to the relatively large production cross section of such processes [7–16]. The absence of any evidence for the production of such particles could mean that colored superpartners are too heavy to be produced at the LHC. The lower production cross sections associated with electroweak production directly lead to the currently softer exclusion limits on the superpartner masses. This makes searches for electroweak SUSY production especially interesting. Such superpartners might still be observed, even if their strongly interacting counterparts are out of reach at the LHC.

In this paper, we present a search for the direct production of charginos ($\tilde{\chi}_1^\pm$) and neutralinos ($\tilde{\chi}_2^0$), mixed states of the SUSY partners of the electroweak gauge and Higgs bosons, in final states with multiple leptons (ℓ). Events with three or four leptons, with up to two hadronically decaying τ leptons (τ_h), as well as events with two light leptons (electrons or muons) of the same sign are analyzed. A data set of proton-proton (pp) collision events collected with the CMS detector from 2016 to 2018 is used, corresponding to an integrated luminosity of 137 fb^{-1}. Previous searches in these final states were performed on data samples of approximately 36 fb^{-1} by ATLAS [17–19] and CMS [20, 21], resulting in exclusion limits on chargino masses up to 1150 GeV for particular model assumptions. The use of parametric neural networks [22], the re-optimization of the search strategy, and the increased data volume, significantly extend the reach of this search compared to previous results.

This paper is structured as follows. Section 2 contains a brief description of the CMS detector. Descriptions and diagrams of all targeted models can be found in Section 3. Section 4 outlines the baseline requirements imposed to select events corresponding to final states of interest in the search. Details on the simulation of the different background and signal processes that populate such selections are included in Section 5. Section 6 includes a description of the search strategies developed to isolate the different signals from the background processes. The different techniques used for the estimation of the contributions of the SM backgrounds are detailed in Section 7. A summary of all sources of uncertainty affecting the interpretation of the results is included in Section 8. A comparison between the observed data and the expectations for the different signal extraction strategies are presented in Section 9. Section 10 is composed of an interpretation of such information in terms of several SUSY models. Finally, Section 11 contains a brief summary of the obtained results.

2   The CMS detector

The central feature of the CMS detector is a superconducting solenoid of 6 m internal diameter, providing a magnetic field of 3.8 T. Silicon pixel and strip trackers, a lead tungstate crystal electromagnetic calorimeter, and a brass and scintillator hadron calorimeter, each composed of a barrel and two endcap sections, reside within the solenoid. Forward calorimeters extend the pseudorapidity (η) coverage provided by the barrel and endcap detectors. Muons are detected in gas-ionization detectors embedded in the steel flux-return yoke outside the solenoid. A more detailed description of the CMS detector, together with a definition of the coordinate system used and the relevant variables, can be found in Ref. [23].

A two-tiered trigger system [24] is used to reduce the rate of recorded events and select those of interest. The first level, composed of custom hardware processors, uses information from the calorimeters and muon detectors to select events at a rate of 100 kHz within a time latency of less than 4 μs. The second level consists of a processor farm which runs a version of the full event reconstruction, optimized for fast processing, and decreases the event rate to around 1 kHz before data storage.

3   Signal models

This search is aimed at the production of charginos and neutralinos, specifically in decay modes that lead to final states with three or more leptons. The results will be interpreted in the context of several simplified models in which the only free parameters are the superpartner masses [25, 26]. Interpretations are performed for both $\tilde{\chi}_1^\pm \tilde{\chi}_2^0$ production and effective $\tilde{\chi}_1^0 \tilde{\chi}_1^0$ production in gauge mediated models with mass degenerate $\tilde{\chi}_1^0$, $\tilde{\chi}_2^0$ and $\tilde{\chi}_1^\pm$. In the former models $\tilde{\chi}_1^\pm$ and $\tilde{\chi}_2^0$ are assumed to be wino-like, i.e. mass-degenerate mixtures of superpartners of the $SU(2)_L$ gauge field, while $\tilde{\chi}_1^0$ is the LSP and bino-like, i.e. the superpartner of the $U(1)_Y$ field. The latter models consider Higgsino-like $\tilde{\chi}_1^\pm$, $\tilde{\chi}_2^0$, and $\tilde{\chi}_1^0$ that are nearly mass-degenerate with $\tilde{\chi}_1^0$ being the next-to-LSP (NLSP), and a gravitino being the LSP. In all models, the other superpartners are assumed to be heavy and decoupled. The lightest of the CP even bosons inside the Higgs sector of the minimal supersymmetric SM is assumed to have SM-like properties, including the mass and branching fractions [27], and is referred to as the Higgs boson. The rest of the bosons inside the Higgs sector are assumed to be heavy and decoupled. An overview of all specific models used for the interpretation of the search is given below. Scenarios in which the mass splitting between any of the superpartners in the decay chain is small are referred to as "compressed" in this paper, and generally have one or more decay products with low p_T. Cases where the mass splittings between all superpartners are relatively large, resulting in high p_T decay products, are called "uncompressed".

3.1   Production of $\tilde{\chi}_1^\pm \tilde{\chi}_2^0$ with decays via intermediate sleptons

Charginos and neutralinos can decay to leptons and the LSP via intermediate sleptons ($\tilde{\ell}$) and sneutrinos ($\tilde{\nu}$), the respective superpartners of charged leptons and neutrinos (ν). These decays are shown in Fig. 1. We only target diagrams in which at least three leptons are produced. Whether the decays are more likely to result in τ leptons than the other lepton flavors depends on the combination of gauge eigenstates making up $\tilde{\chi}_1^\pm$ and $\tilde{\chi}_2^0$, and their masses [6]. Three scenarios are considered:

The "flavor-democratic" scenario, in which the $\tilde{\chi}_1^\pm$ and $\tilde{\chi}_2^0$ decays are mediated by left-handed sleptons, resulting in decays to all lepton flavors with equal probability.
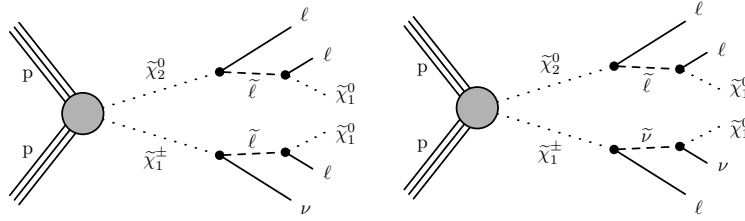
Figure 1: Production of $\tilde{\chi}_1^{\pm}\tilde{\chi}_2^0$ with subsequent decays via sleptons (left) and a slepton and a sneutrino (right).

The "τ-enriched" scenario, where $\tilde{\chi}_1^{\pm}$ couples only to right-handed sleptons, while the decay of $\tilde{\chi}_2^0$ still goes via left-handed sleptons. Right-handed sleptons only couple to the Higgsino component of $\tilde{\chi}_1^{\pm}$, resulting in $\tilde{\chi}_1^{\pm}$ decays that strongly favor the heavier τ leptons. The decay of $\tilde{\chi}_2^0$ will still result in all lepton flavors with equal probability.

The "τ-dominated" scenario with both $\tilde{\chi}_1^{\pm}$ and $\tilde{\chi}_2^0$ decays mediated by τ sleptons because the other slepton flavors are heavy and decoupled [6]. In this case both $\tilde{\chi}_1^{\pm}$ and $\tilde{\chi}_2^0$ decay exclusively to τ leptons.

In each of these scenarios the branching fraction to leptons is assumed to be 100%, and both charged $\tilde{\chi}_1^{\pm}$ and $\tilde{\nu}$ masses are assumed to lie between $m_{\tilde{\chi}_2^0}$ and $m_{\tilde{\chi}_1^0}$, where we take $m_{\tilde{\chi}_1^{\pm}}$ to be equal to $m_{\tilde{\chi}_2^0}$. The kinematics of the leptons and LSPs vary depending on the mass difference between $\tilde{\chi}_2^0$ and $\tilde{\ell}$. A parameter x is introduced that governs the $\tilde{\ell}$ mass as follows: $m_{\tilde{\ell}} = x m_{\tilde{\chi}_2^0} + (1-x) m_{\tilde{\chi}_1^0}$. The interpretation of the search is done using three different values of x as benchmarks for possible manifestations of SUSY in nature:

$x = 0.5$: The slepton mass lies in the middle between $m_{\tilde{\chi}_2^0}$ and $m_{\tilde{\chi}_1^0}$. Each of the leptons and neutrinos emitted in the decay will carry half of the mass difference so they all have identical momentum spectra.

$x = 0.95$: The slepton mass is close to $m_{\tilde{\chi}_2^0}$, resulting in softer leptons from the initial $\tilde{\chi}_2^0$ and $\tilde{\chi}_1^{\pm}$ decays to sleptons.

$x = 0.05$: The slepton mass is similar to $m_{\tilde{\chi}_1^0}$. The second lepton produced in the $\tilde{\chi}_2^0$ decay will be soft.

3.2 Production of $\tilde{\chi}_1^{\pm}\tilde{\chi}_2^0$ with decays via H, W or Z bosons

If the sleptons are too heavy, $\tilde{\chi}_2^0$ is forced to decay to the LSP by emitting either an H or Z boson, while $\tilde{\chi}_1^{\pm}$ decays to a W boson and the LSP. These decays are illustrated in Fig. 2. Final states with multiple leptons can occur by means of subsequent decays of the electroweak bosons to leptons. In the case of WZ (WH) mediated $\tilde{\chi}_1^{\pm}\tilde{\chi}_2^0$ decays, a branching fraction of 3.3 (2.9)% to multiple leptons is expected, much lower than what is assumed for the slepton-mediated decays.

3.3 Production of $\tilde{\chi}_1^0\tilde{\chi}_1^0$ with decays via H or Z bosons

Lastly, we consider $\tilde{\chi}_1^0$ pair production in a gauge-mediated SUSY breaking model with Higgsino-like neutralinos and charginos, and a near massless gravitino (G) as the LSP [28–30]. The cross section for direct pair production of neutralinos is expected to be vanishingly small [31–33], so
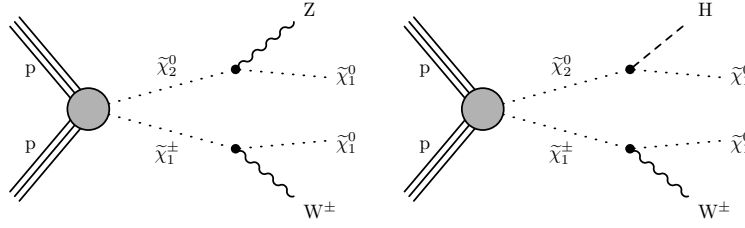
Figure 2: Production of $\tilde{\chi}_1^\pm \tilde{\chi}_2^0$ with subsequent decay of $\tilde{\chi}_1^\pm$ via a W boson and $\tilde{\chi}_2^0$ via a Z boson (left) or H boson (right).

we consider a model in which $\tilde{\chi}_2^0$, $\tilde{\chi}_1^0$, and $\tilde{\chi}_1^\pm$ are almost mass-degenerate. In such a model, $\tilde{\chi}_1^\pm$ and $\tilde{\chi}_2^0$ decay to $\tilde{\chi}_1^0$ via soft particles that escape detection, resulting in effective $\tilde{\chi}_1^0$ pair production. The $\tilde{\chi}_1^0 \tilde{\chi}_1^0$ pair subsequently decays to LSPs by emitting H or Z bosons, as depicted in Fig. 3.
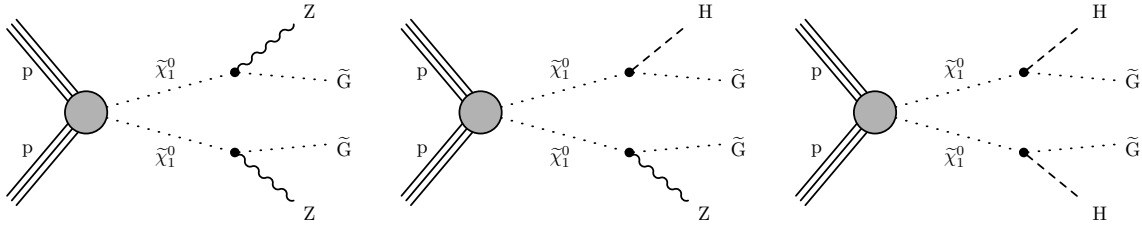

Figure 3: Effective $\tilde{\chi}_1^0$ pair production with decays mediated by Z or H bosons.

4 Event selection

This analysis employs the particle-flow (PF) algorithm [34] for event reconstruction. The algorithm aims to identify and reconstruct the individual particles in an event from an optimized combination of various elements in the CMS detector. Particles reconstructed by the PF algorithm (PF candidates) are classified into charged and neutral hadrons, photons, electrons, and muons.

After reconstruction, PF candidates are clustered into jets using the anti-k_T algorithm [35], with a distance parameter of 0.4, implemented in the FASTJET package [36, 37]. Several selection criteria are applied, designed to remove jets that are likely to originate from extraneous energy deposits in the calorimeters [38]. The missing transverse momentum vector $p_\mathrm{T}^\mathrm{miss}$ is defined as the negative vector sum of transverse momenta (p_T) of all PF candidates in the event, taking into account jet energy corrections [39, 40]. Its magnitude is referred to as $p_\mathrm{T}^\mathrm{miss}$. The vertex with the largest squared p_T sum of all objects returned by the jet finding algorithm, with the tracks associated with this candidate vertex as inputs, as well as the $p_\mathrm{T}^\mathrm{miss}$ computed from the vector sum of the p_T of those jets, is taken to be the primary pp interaction vertex.

Electrons are reconstructed from a combination of the tracker and the electromagnetic calorimeter measurements. They are required to satisfy $|\eta| < 2.5$, ensuring they are within the volume of the tracker, and $p_\mathrm{T} > 10\,\mathrm{GeV}$. Additionally, requirements are placed on the shower shape, and on a multivariate discriminant based on the shower shape and track quality of the electrons [41]. Electrons that are matched to a secondary vertex consistent with a photon conversion or have a missing hit in the tracker are vetoed.

Muon reconstruction uses a global fit combining information from the tracker, muon spec-

trometers, and calorimeters. Muons must be within the acceptance of the muon spectrometers, $|\eta| <$ 2.4, and have $p_\mathrm{T} >$ 10 GeV. Selected muons further pass criteria on the geometrical matching between the track in the inner tracker and the muon spectrometers, and on the quality of the global fit [42].

Both electron and muon candidates must be consistent with originating from the primary pp interaction vertex. This is ensured by requiring the transverse impact parameter (d_0) to be smaller than 0.5 mm, and the longitudinal one (d_z) not to exceed 1.0 mm. The significance of the impact parameter must satisfy $d_\mathrm{3D} / \sigma_{d_\mathrm{3D}} <$ 8, where d_3D and σ_{d_3D} are, respectively, the three-dimensional impact parameter and its uncertainty. Electrons and muons must also fulfill several prerequisites on their relative mini-isolation ($I_\mathrm{rel}^\mathrm{mini}$), defined as the scalar p_T sum of all other PF candidates in a cone of p_T dependent radius around the lepton's direction, divided by the lepton p_T. The radius of this cone is given by $\Delta R = p_\mathrm{T}$ $\overline{\sqrt{\Delta\eta^2 + \Delta\phi^2}}$ 10 GeV/min max p_T , 50 GeV , 200 GeV in (η, ϕ) space, where ϕ is the azimuthal angle in radians, taking into account increased particle collimation at high lepton p_T values [43]. All electrons and muons must satisfy $I_\mathrm{rel}^\mathrm{mini} <$ 0.4. The lepton selection discussed up to here is referred to as the baseline selection.

In order to select leptons resulting from superpartner production, it is important to identify "prompt" leptons that originate from the decay of electroweak bosons or superpartners. Prompt leptons have to be separated from other genuine leptons produced in hadron decays, as well as particles in jets that are incorrectly reconstructed as leptons. Such lepton candidates are collectively called "nonprompt".

A gradient boosted decision tree (BDT) trained to distinguish prompt from nonprompt light leptons is used [44, 45]. This BDT uses the properties of the jet, as returned by the jet clustering algorithm, containing the lepton: its DEEPFLAVOR [46] b tagging score, the ratio of the lepton p_T to that of the jet, and the component of the jet momentum that is transverse to the lepton's direction. Other input variables are p_T, η, $I_\mathrm{rel}^\mathrm{mini}$, d_0, d_z, and $d_\mathrm{3D} / \sigma_{d_\mathrm{3D}}$ of the lepton. The BDT additionally has access to the muon segment compatibility for muons and to the earlier mentioned multivariate discriminant for electrons. Two selection criteria on the BDT output are used in the analysis, one for events with three or more leptons, and a tighter one for events with two leptons of the same sign. The latter results in a smaller nonprompt background at the cost of slightly lower selection efficiencies for superpartner production. For prompt muons, the BDT-based selection results in typical efficiencies ranging 90–99%. Misidentification rates for nonprompt muons passing the baseline selection range 5–10%. Prompt electrons are identified with an efficiency of around 75% in events with three or more leptons, with a corresponding misidentification rate of about 5% for nonprompt electrons passing the baseline selection. The efficiency is typically in the range 50–60% for the tighter same-sign dilepton selection, with a misidentification rate around 2%.

Reconstruction of τ_h candidates is performed using the "hadron-plus-strips" algorithm [47]. The τ_h candidates are required to be consistent with one- or three-pronged hadronic τ lepton decays, and must have $|\eta| <$ 2.3 and $p_\mathrm{T} >$ 20 GeV. In order to reject a large background from hadrons misidentified as τ leptons, the τ_h candidates must pass a stringent selection on a BDT discriminant aimed at identifying prompt τ_h candidates [47]. This selection has typical efficiencies around 50% for prompt τ_h candidates in the analysis, while having a misidentification rate of 0.2% for quantum chromodynamics (QCD) jets. Additional selection criteria based on the consistency between the measurements from the tracker, calorimeters and muon detectors are required to reduce the proportion of electrons and muons misidentified as τ_h candidates.

Leptons passing the BDT-based selection criteria mentioned above are labeled "tight" leptons.

Electrons or muons are "loose" if they either pass the same BDT discriminant or pass additional requirements on the properties of the jet containing the lepton in case they fail the BDT selection. Similarly, loose τ_h candidates are those passing a looser requirement on the BDT discriminant. Tight leptons always satisfy the conditions of the loose selection, but not the other way around. The final analysis selection consists of tight leptons, while loose leptons are used to categorize events based on their lepton content and to predict the background from nonprompt leptons. The loose definition of electrons and muons is tuned to facilitate this background prediction, as explained in Section 7.

In events with two same-sign light leptons, with or without an additional τ_h candidate, further requirements are placed on tight leptons to ensure that their sign is well-measured. For electrons, the sign is determined by the position of a linear extrapolation of the deposits in the pixel detector to the inner calorimeter surface relative to the calorimeter deposit, and compared to the sign determined from the full fit used for electron reconstruction. Electrons in which the two sign measurements are inconsistent are not considered tight. Tight muons are required to have $\sigma_{p_T}/p_T < 0.2$ where, p_T and σ_{p_T} are respectively the p_T as measured from a tracker-only fit and the associated uncertainty. These requirements are found to reduce the sign mismeasurement probability to under 0.0001 (0.3)% with efficiencies for prompt well measured leptons greater than 99.9 (99)% for muons (electrons).

Jets retained for analysis must satisfy $p_T > 25\,\text{GeV}$, $|\eta| < 2.4$, and have a separation of $\Delta R > 0.4$ from any loose lepton. Jets originating from the hadronization of b quarks are identified with the DEEPCSV algorithm [48]. Jets satisfying the tight working point of this algorithm are referred to as b-tagged jets. The chosen working point corresponds to a typical efficiency of 50% for correctly identifying b quark jets, with a misidentification probability of 2.4 (0.1)% for c quark (light-flavor) jets.

Events that have at least three loose leptons, or two loose light leptons of the same sign, are selected for further analysis. To enter the nominal analysis selection either all loose leptons, or at least four leptons, must be tight. Events in which one or more of the loose leptons fail the tight selection are used to predict the background from nonprompt leptons, following the procedure explained in Section 7. Events with one or more b-tagged jets are vetoed to reduce the backgrounds from processes involving top quarks. To match the analysis selection to the online selection, events must satisfy the requirements of trigger algorithms selecting one, two, or three electrons or muons. The lepton p_T cuts mentioned in Section 6 are designed to ensure selected events efficiently pass the trigger selection. Events with any opposite-sign and same flavor (OSSF) pair of light leptons passing the baseline selection, with a dilepton invariant mass below 12 GeV, are vetoed to reduce the background from photon conversions and low-mass resonances.

5 Simulation

Monte Carlo (MC) simulated event samples are used for the estimation of most of the backgrounds, the determination of signal efficiencies, and the training of the parametric neural networks used in the analysis. Separate samples, simulating the data–taking conditions in 2016, 2017, and 2018, are used for each process.

Signal samples are generated with the MADGRAPH5_aMC@NLO program [49, 50] at leading order (LO) in perturbative QCD, with up to two additional partons in the matrix element computations. Background samples of diboson WZ, $qq \to ZZ$ and $H \to ZZ$ production are generated at next-to-LO (NLO) precision using the POWHEG v2 [51–54] generator. MCFM v7.0 [55]

has been used to generate the gluon induced diboson processes $gg \to ZZ$. Other major background samples (Zg, Wg, $t\bar{t}g$, VH, WWW, WWZ, WZZ, ZZZ, $t\bar{t}Z$, $t\bar{t}W$, $t\bar{t}H$, $t\bar{t}t\bar{t}$, tZq) are simulated using MADGRAPH5_aMC@NLO, at NLO in QCD. The small contributions from processes involving two top quarks and two massive bosons ($t\bar{t}ZZ$, $t\bar{t}ZH$, $t\bar{t}WZ$, $t\bar{t}WH$, $t\bar{t}HH$, $t\bar{t}WW$) are simulated using MADGRAPH5_aMC@NLO at LO in QCD. Version 2.2.2 (2.4.2) of MADGRAPH5_aMC@NLO is used for simulating 2016 (2017 and 2018) collisions in each case.

The NNPDF3.0 [56] (NNPDF3.1 [57]) parton distribution function (PDF) sets are used in the simulation of 2016 (2017 and 2018) collisions. The perturbative order in QCD used for the PDFs is LO for the signal samples and NLO (NNLO) for the 2016 (2017 and 2018) background samples. The simulation of hadronization, parton showering and the underlying event is performed by PYTHIA 8.212 (8.230) [58] with the CUETP8M1 [59, 60] (CP5 [61]) tune in samples matching 2016 (2017 and 2018) conditions. Double counting of partons generated by PYTHIA and MADGRAPH5_aMC@NLO is eliminated with the FxFx [62] (MLM [63]) matching scheme in NLO (LO) simulations. For signal samples, the same setup is used but using the CP2 tune [61] instead for 2017 and 2018 samples.

Signal samples of $\tilde{\chi}_1^\pm \tilde{\chi}_2^0$ production are normalized to cross sections computed at NLO plus next-to-leading logarithmic (NLL) precision using the Resummino framework [31–33, 64] in the limit of mass-degenerate wino-like $\tilde{\chi}_1^\pm$ and $\tilde{\chi}_2^0$, and bino-like $\tilde{\chi}_1^0$. Cross sections at the same precision are computed for effective $\tilde{\chi}_1^0 \tilde{\chi}_1^0$ production, assuming mass-degenerate Higgsino-like $\tilde{\chi}_1^\pm$, $\tilde{\chi}_2^0$ and $\tilde{\chi}_1^0$. All other superpartners are always assumed heavy and decoupled.

Each event is overlaid with additional inelastic pp collisions generated in PYTHIA to mimic the presence of additional collisions in the same or adjacent bunch crossings (pileup). The simulated number of interactions per bunch crossing is reweighted to match the one observed in data. Simulated background events include a full GEANT4-based [65] detector simulation, while signal events use the CMS fast simulation package [66] to simulate the detector response. All simulated events are subsequently reconstructed using the same software employed for collision data.

6 Search strategy

As explained in Section 3, the search targets several models for the production of charginos and neutralinos in final states with multiple leptons. In each model we work under the assumption of R-parity conservation, meaning that the LSP is stable, giving a significant p_T^{miss} in most cases. Many final states, including events with two leptons of the same sign, three leptons, and four or more leptons are selected to target several possible SUSY signals that might be present in the collision data. In the case of same-sign dilepton events, only electrons or muons are considered, whereas up to two τ_h candidates are selected in the other final states. Events are further categorized according to the lepton flavors and signs to focus on various signal hypotheses. A summary of this categorization is presented in Table 1. In each of these categories, a set of search regions is defined based on the kinematics of the events to further separate potential signal events in data from the SM backgrounds. Because of the large background in events with three light leptons including an OSSF pair of leptons, and the difficulty of optimizing kinematic bins for sensitivity to a host of models, parametric neural networks are trained for separating signal and background in this region.

Table 1: Brief description of the categories used to classify events in the search.

Category	Requirements
2 SS	Two light leptons with the same sign
3 A	Three light leptons including one or more OSSF pairs
3 B	Three light leptons including no OSSF pairs
3 C	A pair of light leptons forming an OSSF pair and a τ_h candidate
3 D	A pair of light leptons of different flavor and opposite sign and a τ_h candidate
3 E	A pair of light leptons of same sign and a τ_h candidate
3 F	A light lepton and two τ_h candidates
4 G	Four light leptons including two independent OSSF pairs
4 H	Four light leptons including one or less OSSF pairs
4 I	Three light leptons and a τ_h candidate
4 J	Two light leptons and two τ_h candidates, including two OSSF pairs
4 K	Two light leptons and two τ_h candidates, including one or no OSSF pair

6.1 Same-sign dilepton events

The signal models described in Section 3 yield final states with three or more leptons. In models where the mass difference between the NLSP and LSP is small, or the slepton mass is close to either the NLSP or LSP mass, one or more of the leptons in the final state could have a high probability to fail the lepton selection. The sensitivity of the analysis to such models is increased by retaining events with two leptons. Dilepton events with an opposite-sign lepton pair suffer from a very large SM background, but events with same-sign lepton pairs are relatively rare in the SM. For this reason, we select only events in which both leptons have the same sign (2 SS).

To ensure efficient triggering on these events, the leading lepton is required to have p_T 20 GeV in $\mu\mu$ events, and p_T 25 GeV in $e\mu$ and ee events. The subleading lepton must satisfy p_T 15 10 GeV in case it is an electron (muon). Events in which a third loose light lepton or tight τ_h candidate is present are vetoed to ensure orthogonality with the other event categories. As this category mainly targets signal events with a lepton that fails the selection or fails to be reconstructed, we do not veto events with a third lepton passing the baseline selection, as long as it fails the loose selection. When a third lepton passing the baseline selection is present, it is not allowed to form a mass within a 15 GeV window around the Z boson mass (m_Z) with another lepton in the event. This requirement is found to reduce the SM WZ background while keeping a signal efficiency over 99% for the most compressed signal scenarios with mass splittings between the NLSP and the LSP under 50 GeV. Events with more than one jet with p_T 40 GeV are rejected to reduce the $t\bar{t}$ background, while still allowing for some hadronic recoil in signal events. Finally, p_T^{miss} 60 GeV is required.

Events are then binned according to their kinematic properties to maximally separate SUSY signal from the background. The stransverse mass M_{T2}, defined to have an endpoint at the parent particle's mass for events with two semi-invisible decays [67], is used, because its tails tend to be populated by signal events with high p_T^{miss}. Additional discriminating variables are the p_T of the dilepton system (p_T), which tends to be high in uncompressed models, and p_T^{miss}. Bins with expected yields sufficient for an accurate background description are further split according to the sign of the leptons, as positively charged background events are more likely due to the pp nature of the collision data. The full set of search regions is shown in Table 2.

Table 2: Definition of the search regions used for events with two same-sign light leptons (SSXX). The symbols ( ) and ( ) represent requirements on the sign of the leptons. The first M_{T2} bin contains only events where M_{T2} is exactly 0 [68], whereas the second bin contains events where M_{T2} is larger than 0 and less than or equal to 80 GeV. The last M_{T2} bin contains events where M_{T2} exceeds 80 GeV.

2ℓSS : two light leptons of the same sign

M_{T2} (GeV)	p_T (GeV)	60 < p_T^{miss} < 100 GeV	100 < p_T^{miss} < 200 GeV	p_T^{miss} > 200 GeV
0	> 70	SS01	SS01	SS01
0	< 70	SS02	SS03 ( )	SS05 ( )
0	< 70	SS02	SS04 ( )	SS06 ( )
0–80	> 30	SS07 ( )	SS07 ( )	SS09
0–80	> 30	SS08 ( )	SS08 ( )	SS09
0–80	< 30	SS10	SS10	SS10
80	> 200	SS11	SS12 ( )	SS14 ( )
80	> 200	SS11	SS13 ( )	SS15 ( )
80	< 200	SS16	SS17 ( )	SS19 ( )
80	< 200	SS16	SS18 ( )	SS20 ( )

6.2 Three-lepton events

All signal models considered in this analysis yield at least three leptons in the final state, so the analysis retains all events with three or more leptons, with up to two τ_h candidates. This section describes the search strategy for events with exactly three leptons, while events with four or more leptons are discussed in Section 6.3.

The leading light lepton is required to satisfy $p_T > 25\ (20)$ GeV if it is an electron (muon). If two or more light leptons are present, the subleading light lepton must have $p_T > 15\ (10)$ GeV. In events with just a single muon, where this is also the leading light lepton, the muon must satisfy $p_T > 25$ GeV. These p_T requirements are added in addition of those specified in Section 4, in order to ensure efficient triggering on the events by at least one of the leptonic triggers used in the analysis. As we target signals with escaping particles, we require $p_T^{\text{miss}} > 50$ GeV, significantly reducing the background from processes without particles evading detection.

6.2.1 Three light leptons with an OSSF pair

If no τ leptons are present in the decay, the signal models in Section 3 mainly give final states with an OSSF pair of leptons. As such, these events will dominate the sensitivity to $\tilde{\chi}_1^{\pm} \tilde{\chi}_2^0$ production with flavor-democratic decays through sleptons, or decays via the emission of a W and a Z boson. Meanwhile, this event category also suffers from the largest amount of background among all analysis categories, dominated by SM WZ production. Because of the category's importance and the relatively large background, several parametric neural networks are trained to distinguish the signal models from the background in this region. Additionally, a set of search regions is also defined, which are less sensitive than the neural networks, but that facilitate alternative interpretations of the results. This event category is referred to as 3ℓA as shown in Table 1.

Our signal model has several varying parameters, namely the masses of the NLSP and LSP. One could search for such a model by training a single machine learning discriminant based on reconstructed quantities, or by training one such discriminant for each value of the signal parameters. If the event kinematics depend on the signal parameters, the former approach will

be suboptimal for most or all signal points, while the latter introduces a great deal of complexity. Additionally, the second approach of training separate discriminants for each signal point does not allow for the interpolation of the results to signal parameters not seen while training the discriminant. A solution to these problems is the training of a "parametric" machine learning discriminant [22]. On top of a set of reconstructed quantities, such a discriminant uses one or more signal parameters as additional input features. In the training each background event is given a value randomly drawn from the parameter distribution in the signal simulation. This results in a discriminant that learns to optimally distinguish each signal hypothesis from the background, and that can be evaluated using signal parameters not seen during training.

The kinematics of the signal events are largely determined by the mass splitting $\Delta m \equiv m_{\tilde{\chi}_1} - m_{\tilde{\chi}_1^0}$, with relatively small kinematic differences between signal points having equal Δm, but differing $m_{\tilde{\chi}_1}$ values. This is exploited by training a neural network parametric in Δm for each of the four different signal models: $\tilde{\chi}_1^\pm \tilde{\chi}_2^0$ production with decays through W and Z bosons, and $\tilde{\chi}_1^\pm \tilde{\chi}_2^0$ with slepton-mediated decays at $x \approx 0.95$, 0.50 and 0.05, with x being the parameter governing the mass splitting between the NLSP and the sleptons. The following reconstructed input variables are used when training the neural networks: the mass of the OSSF lepton pair that is closest to m_Z out of all such pairs in the event ($M_{\ell\ell}$), the transverse mass of the lepton not forming the Z boson candidate and p_T^{miss} (M_T), p_T^{miss}, the transverse mass of the trilepton system and p_T^{miss} (M_T^3), the trilepton invariant mass (M_3), the scalar sum of lepton p_T's and p_T^{miss} ($L_T + p_T^{\text{miss}}$), and the scalar sum of the p_T of all jets in the event (H_T). For each of these variables the distribution is compared between the fast simulation of the CMS detector used in the signal simulation and the nominal GEANT4-based simulation. This comparison is made for several representative signal points: compressed, noncompressed and at Δm close to m_Z. No significant differences are observed between the distributions.

The neural networks are fully connected feed-forward networks with a single output node representing the probability that an event is signal. They are trained in TENSORFLOW [69] using the KERAS [70] interface. To reinforce the learning of the parametrization, the signal parameter is fed as an additional input to each hidden layer of the network, and the Δm values assigned to background events are resampled from the signal distribution for each training epoch. The gradient descent of the network weights for training is done with a variant of the Adam [71] algorithm using Nesterov momentum [72]. Batch normalization [73] is added between all of the hidden layers to reduce the internal covariance shift of the network, speeding up training and increasing the final performance. To regularize the network, dropout [74] is added to each hidden layer. At each node a parametric rectified linear unit activation function is used, except for the output node, which uses a sigmoid activation. The number of nodes in each layer of the network, the number of hidden layers, the learning rate, the learning rate decay, the dropout rate, and the used activation function, are all varied in grid scans, training the neural network each time with a different configuration. The performance of each configuration is then evaluated, in terms of the area under the receiver operating characteristic curve (AUC), on a validation set. The optimal values of these parameters are chosen for the final training of each network. The results of the grid scan optimization are cross-checked with a custom–made evolutionary algorithm designed to optimize the neural network hyperparameters. The evolutionary algorithm results in an equivalent final neural network performance, though with significantly fewer training iterations than needed in the grid scan.

It is explicitly verified that the trained parametric networks are optimally performing at each Δm point, and able to interpolate to unseen points. The ability of the network to interpolate to a particular point is checked by training a parametric neural network excluding all events at a
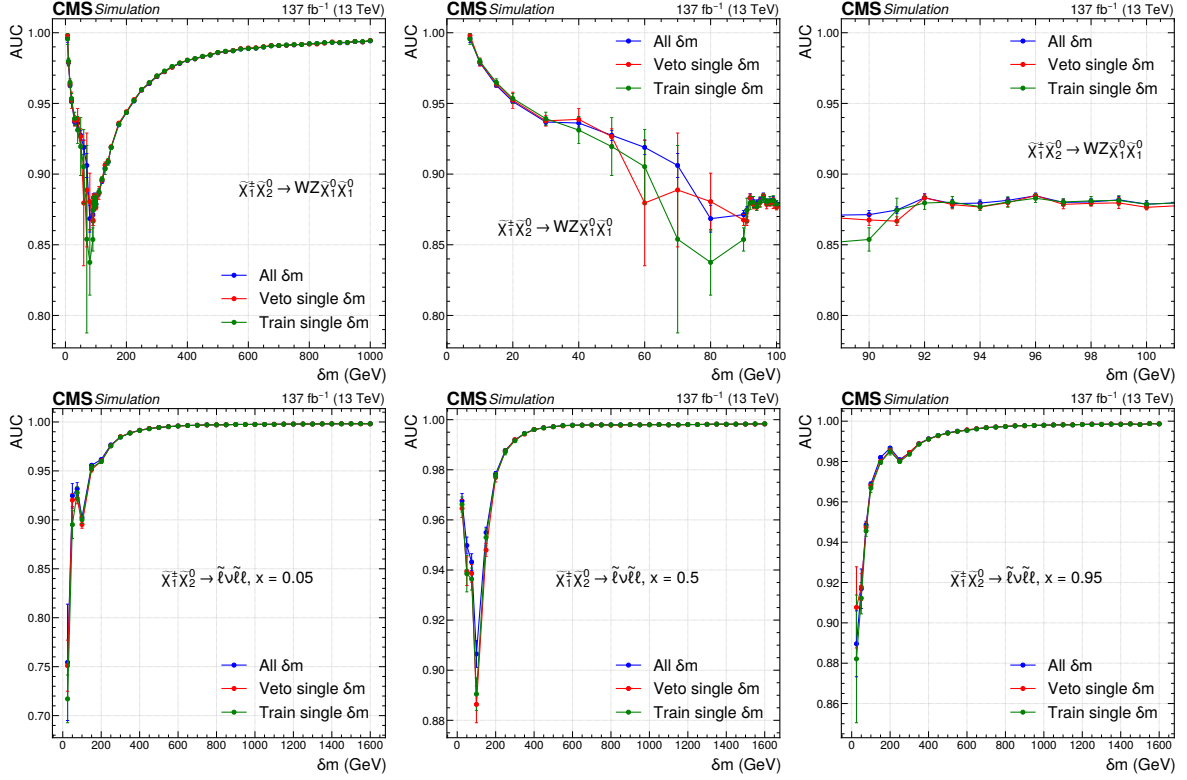
Figure 4: The AUC performance of the parametric neural networks for discriminating the signal from the total background predicted in simulation, as a function of δm for the trainings targeting different signal models. The top row corresponds to the neutral network targeting signals with WZ-mediated decays with different mass ranges to show all points. The bottom row corresponds to the models with slepton-mediated decays at $x = 0.05$ (left), $x = 0.5$ (middle) and $x = 0.95$ (right). Neural network models shown in blue are trained using all available δm points, those in red are trained with all available points except the point for which the performance is shown. The models in green are not parametric and only trained to find a signal at the point where the performance is indicated. Each neural network is retrained ten times, and the mean performances are shown, with error bars indicating the standard deviation computed from ten performance values. This means that each red and green point correspond to ten neural network trainings. The entire blue curve in each figure also corresponds to ten trainings.

particular δm value as well as a nonparametric network trained for just events at this δm value. If both the new parametric model and our nominal one perform equally well it implies that the latter performs equally well on seen and unseen parameter points. The comparison between the nominal model and the nonparametric network tells us if the network's parametrization performs optimally or not. This check is repeated for each δm point present in each of the signal models, training 10 neural networks of each type at each point to estimate the variations due to random weight initializations. It is found that the parametric network is able to achieve optimal performance at each δm point present in the signal simulation even without explicitly seeing it during training, as shown in Fig. 4.

The signal and background predictions, as well as the yield in data, are then evaluated for each of the four neural networks at every δm value present in the signal simulation. For the interpretation of the results in a particular signal model at a given δm only the corresponding neural network output is used. At each δm value, the neural network output is binned in terms

Table 3: Definition of the search regions used for events with three light leptons, at least two of which form an OSSF pair, excluding those with $75 < M_{\ell\ell} < 105\,\mathrm{GeV}$ (AXX).

$3\ell\mathrm{A}$: three light leptons with at least one OSSF pair, $M_{\ell\ell} \leq 75\,\mathrm{GeV}$ or $M_{\ell\ell} \geq 105\,\mathrm{GeV}$

M_{T} (GeV)	M_{T}^3 (GeV)	$M_{\ell\ell} \leq 50\,\mathrm{GeV}$	$50 < M_{\ell\ell} < 75\,\mathrm{GeV}$	$105 < M_{\ell\ell} < 250\,\mathrm{GeV}$	$M_{\ell\ell} \geq 250\,\mathrm{GeV}$
0–100	0–50	A01	A06	A13	A19
	50–100	A02	A06	A13	A19
	100–400	A03	A07	A14	A20
	400	A03	A08	A14	A20
100–200	0–200	A04	A09	A15	A21
	200	A04	A10	A16	A21
200	0–400	A05	A11	A17	A22
	400	A05	A12	A18	A22

of the expected background yields. The last bin is defined to have a single expected background event in the 2016 data set, corresponding to $35.9\,\mathrm{fb}^{-1}$, and each preceding bin has twice the expected yield of the following bin. The shape of the outputs of the neural networks varies substantially with the Δm parameter, and this method allows for a robust binning definition across all values of Δm.

Aside from the neural network, a set of search regions is also defined to extract the signals from the background in a cut-based manner. Most of the SM WZ background, as well as $\tilde{\chi}_1^\pm \tilde{\chi}_2^0$ production with W and Z boson mediated decays result in $M_{\ell\ell}$ values close to the Z boson mass. For this reason, the search regions with $75 < M_{\ell\ell} < 105\,\mathrm{GeV}$ are optimized for finding WZ-mediated signal decays, while the other search regions are optimized for finding slepton-mediated decays. The search region definitions are given in Tables 3 and 4, using some, but not all, of the neural network input variables to define the bins. The WZ background falls off quickly when M_{T} exceeds the W boson mass (m_{W}), making it a powerful tool to reduce the background. For signal events with slepton-mediated decays, $M_{\ell\ell}$ and M_{T}^3 provide sensitivity to Δm, and are used to separate signal and background events. The search regions targeting WZ-mediated superpartner decays are further binned in $p_{\mathrm{T}}^{\mathrm{miss}}$ and H_{T}. Due to escaping LSPs in signal events, their $p_{\mathrm{T}}^{\mathrm{miss}}$ spectrum tends to be harder than that of SM events, a fact which is further enhanced at large H_{T}.

The neural network analysis and search regions use the same data and thus can not be analyzed simultaneously. The results of both approaches are interpreted separately, and shown in Section 10. The neural network approach has higher sensitivity, while the search region results are easier to reinterpret.

6.2.2 Three light leptons without an OSSF pair

Events with three light leptons that do not contain an OSSF pair (3ℓB) do not occur frequently in the SM, because most events with multiple leptons involve a Z boson decay. This category of events is particularly sensitive to signal models with nonresonant lepton production from the decay of an H. Since SM production of an H with an additional lepton is exceedingly rare, the search regions are designed to target possible $H \to WW$ decays in signal events. The events are binned in the minimum ΔR between any two leptons in the event ($\min \Delta R_{\ell,\ell}$), exploiting the increased collimation of leptons in $H \to WW$ events when compared to events with nonprompt leptons or nonresonant WW production. The search region definitions are given in Table 5.

Table 4: Definition of the search regions used for events with three light leptons, at least two of which form an OSSF pair, and which satisfy 75 < M < 105 GeV (AXX).

3ℓA : three light leptons with at least one OSSF pair, $75 < M_{\ell\ell} < 105\,$GeV

M_T (GeV)	p_T^{miss} (GeV)	$H_T < 100\,$GeV	$100 < H_T < 200\,$GeV	$H_T > 200\,$GeV
0–100	50–100	A23	A36	A49
	100–150	A24	A37	
	150–200	A25	A38	A50
	200–250	A26	A39	
	250–350	A27	A40	A51
	350			A52
100–160	50–100	A28	A41	A53
	100–150	A29	A42	A54
	150–200	A30	A43	A55
	200–250	A31	A44	A56
	250–300			A57
	300			A58
160	50–100	A32	A45	A59
	100–150	A33	A46	A60
	150–200	A34	A47	A61
	200–250	A35	A48	A62
	250–300			A63
	300			A64

Table 5: Definition of the search regions used for events with three light leptons, none of which form an OSSF pair (BXX).

3ℓB: three light leptons without an OSSF pair

min $\Delta R < 0.4$	$0.4 < $ min $\Delta R < 1$	min $\Delta R > 1$
B01	B02	B03

Table 6: Definition of the search regions for events with a $\mu^+\mu^-$ or e^+e^- pair and an additional τ_h candidate (CXX).

3ℓC: $\mu^+\mu^-$ or $e^+e^- + \tau_h$

p_T^{miss} (GeV)	M_T^2 (GeV)	$M_{T2} < 80\,\text{GeV}$	$80 < M_{T2} < 120\,\text{GeV}$	$M_{T2} > 120\,\text{GeV}$
50–200	0	C01	C02	C03
200–300	0	C04	C05	C06
	0–250	C07		
>300	250–500	C08		
	>500	C09		

Table 7: Definition of the search regions for events with a $e\mu$ pair and a τ_h candidate (DXX).

3ℓD: $e^\pm\mu^\mp + \tau_h$

M_{T2} (GeV)	p_T^{miss} (GeV)	$M < 60\,\text{GeV}$	$60 < M < 100\,\text{GeV}$	$M > 100\,\text{GeV}$
	50–100	D01	D06	D11
	100–150	D02	D07	D12
0–100	150–200	D03	D08	D13
	200–250	D04	D09	D14
	>250	D05	D10	
100	50–200	D15		
	>200	D16		

6.2.3 Three leptons with one or more τ_h candidates

If chargino or neutralino decays are mediated by right-handed sleptons, or the first- and second-generation sleptons are heavy and decoupled, signal events will favor final states with one or more τ leptons. To retain sensitivity to such models, events with τ_h candidates are selected and split into further categories.

The first category consists of events with an OSSF pair of light leptons and a τ_h candidate (3ℓC). These events are mainly sensitive to τ-enriched $\tilde\chi_1^\pm \tilde\chi_2^0$ production and contain a large background from Drell–Yan and top quark pair production ($t\bar{t}$) events with a nonprompt τ_h candidate. Events are required to have $|M_{\ell\ell} - m_Z| > 15\,\text{GeV}$, with $M_{\ell\ell}$ being the mass of the light lepton pair, to veto the bulk of the Drell–Yan background. At low and moderate p_T^{miss} values, M_{T2} is used to reduce the $t\bar{t}$ background. At higher p_T^{miss} values, the transverse mass of the combined dilepton system and p_T^{miss} (M_T^2), a proxy for the $\tilde\chi_2^0$ mass, is found to be a strong discriminator. The full set of search region definitions in this category is given in Table 6.

Events with a single τ_h in which the light leptons do not form an OSSF pair are split according to whether the light leptons have opposite sign (3ℓD) or not (3ℓE). One of the discriminating variables in such events is the opposite-sign lepton pair mass closest to what is expected for a Z boson decay, called M (M_{τ_h}) in 3ℓD (3ℓE) events. The expected reconstructed mass of a Z $\to \tau\tau$ decay is 50 GeV in $e\mu$ pairs and 60 GeV in $e\tau_h$ and $\mu\tau_h$ pairs. For events in 3ℓE where the τ_h is of the same sign as the light leptons, M is set to zero. Additional discrimination power is provided by the stransverse mass, computed with the two light leptons in category 3ℓD (M_{T2}), and with the leading light lepton and τ_h candidate in category 3ℓE (M_{T2}^{ℓ,τ_h}). This variable has a sharply falling distribution beyond m_W in the SM. Definitions of the search regions in category 3ℓD (3ℓE) can be found in Table 7 (8).

Table 8: Definition of the search regions for events with a pair of light leptons of the same sign and a τ_h candidate (EXX).

3ℓE: same-sign light lepton pair + τ_h

$M_{T2}(\ell\ell,\tau_\mathrm{h})$ GeV	p_T^{miss} (GeV)	$M_{\tau_\mathrm{h}} < 50$ GeV	$50 < M_{\tau_\mathrm{h}} < 100$ GeV	$M_{\tau_\mathrm{h}} > 100$ GeV
0–80	50–100	E01	E04	
	100–250	E02	E05	
	250	E03		
80	50–150	E06		E08
	150–200	E07		
	200			E09

Table 9: Definition of the search regions for events with 2 τ_h candidates and one light lepton (FXX).

3ℓF: 2 τ_h + light lepton

$M_{T2}(\ell\ell,\tau_\mathrm{h})$ (GeV)	p_T^{miss} (GeV)	$M_{\tau_\mathrm{h}} < 100$ GeV	$M_{\tau_\mathrm{h}} > 100$ GeV
0–100	50–100	F01	F07
	100–150	F02	F08
	150–200	F03	F09
	200–250	F04	F10
	250–300	F05	
	300	F06	
100	50–200	F11	
	200	F12	

Events with two τ_h candidates provide additional sensitivity to models with τ dominated slepton decays. Events in this category are binned in the invariant mass of the leading τ_h and light lepton ($M_{\ell\tau_\mathrm{h}}$), which tends to be high for uncompressed signal events. The same lepton pair and the p_T^{miss} enter the computation of the stransverse mass ($M_{T2}(\ell\ell,\tau_\mathrm{h})$), which is used to further suppress the SM background. The complete set of bins is shown in Table 9.

6.3 Four or more lepton events

Events with four leptons provide sensitivity to effective $\tilde{\chi}_1^0 \tilde{\chi}_1^0$ production with subsequent decays via H or Z bosons. Further categorization of the events is done depending on the number of OSSF pairs and light leptons. If more than four loose leptons are present in an event, the event categorization and computation of analysis variables uses the four highest p_T leptons.

Decays of $\tilde{\chi}_1^0 \tilde{\chi}_1^0$ via two Z bosons tend to give two OSSF pairs. For this reason, the first category consists of events with four light leptons forming two separate OSSF pairs (4 G). The OSSF dilepton pair with the closest invariant mass to m_Z forms the first Z boson candidate (Z_1), while the remaining OSSF pair is taken to be the second Z boson candidate (Z_2). The M_{T2} computed with both Z boson candidates (M_{T2}^{ZZ}) is expected to have a sharply falling distribution beyond m_{NLSP}, providing a handle to separate different signal points and to discriminate signal from the background. Events are further binned in the mass of the Z_2 candidate (M_{Z2}) to enhance the sensitivity to signal models without two Z bosons in the $\tilde{\chi}_1^0 \tilde{\chi}_1^0$ decay. The search region definitions are listed in Table 10.

Table 10: Definition of the search regions for events with 4 light leptons, including 2 separate OSSF pairs (GXX).

4ℓG: 4 light leptons with 2 separate OSSF pairs

M_{T2} ZZ (GeV)	M_{Z2} 60 GeV	M_{Z2} 60 GeV
0–150	G01	
150–250	G02	G03
250–400	G04	
400	G05	

Table 11: Definition of the search regions for events with 4 leptons with one or more τ_{h}, or without two light-lepton OSSF pairs (XYY).

4ℓH-K : 4 leptons with one or more τ_{h} or without two light-lepton OSSF pairs

M_{Z1} (GeV)	ΔR^{H} 0.8	ΔR^{H} 0.8
0–60	X03	X02
60		X01

The remaining events are further split up as follows: four light leptons forming one or no OSSF pairs (4 H), one τ_{h} candidate and three light leptons (4 I), two τ_{h} candidates and two light leptons forming two OSSF pairs (4 J), and two τ_{h} and two light leptons forming one or fewer OSSF pairs (4 K). The same binning is used in each of these categories, as they are sensitive to the same signal models, and it is shown in Table 11. If at least one OSSF pair is present, the OSSF pair of mass closest to m_{Z} is taken to reconstruct a Z boson candidate (Z1). If no OSSF pair is present, other opposite sign lepton combinations are considered when finding the Z boson candidate. The Z boson candidate mass M_{Z1} is used to discriminate between processes with and without a true on-shell Z boson involved. The remaining two leptons in the event are assigned to be the decay of an H candidate. Events are further subdivided according to the ΔR between those two remaining leptons (ΔR^{H}), as these are expected to be collimated if they are from genuine H decay products.

7 Background estimation

The background contributions in each of the search categories can be subdivided into four distinct categories. Firstly, there are SM events with three or more prompt leptons, or two prompt leptons of same sign. Secondly, external and internal conversions of photons also result in events entering our search region. Backgrounds from both conversions and prompt leptons are estimated using simulated samples. Thirdly, backgrounds involving one or more nonprompt leptons are directly predicted from data. Lastly, events that enter a particular event category due to the mismeasurement of a lepton sign are estimated from data for events in the 2 SS and 3 E categories, while its importance is minute in other event categories and is estimated from simulation.

The dominant background contribution to events in the 3 A category comes from WZ production. With leptonic decays of the Z and W bosons, respectively, WZ production results in events with three prompt leptons and a neutrino giving sizable $p_{\mathrm{T}}^{\mathrm{miss}}$, thus mimicking the topology of $\tilde{\chi}_1^\pm \tilde{\chi}_2^0$ production. The background is estimated from simulation and is validated in a control region that is contained within the search regions but nearly depleted of signal

events. The control region has the same selection criteria as 3ℓA events, with the following additional requirements: $|M_{\ell\ell} - m_Z| > 15\,\text{GeV}$, $50 < p_T^{\text{miss}} < 100\,\text{GeV}$, $50 < M_T < 100\,\text{GeV}$ and $|M_{3\ell} - m_Z| > 15\,\text{GeV}$. A fit is performed to the data in the WZ CR, in which the WZ normalization is free to float. This fit takes into account all relevant analysis uncertainties and assumes that no signal is present. The result is a normalization factor of $r_{WZ} = 1.17 \pm 0.05$ over the POWHEG prediction, which is applied in the analysis. The 3ℓA events are interpreted twice, once using the neural network and once using the search regions. The WZ control region is included into the fit for the signal region interpretation and, to avoid double counting the data, the partially overlapping search regions A23, A36, and A49 are removed from it. When the neural network results are used for the interpretation, the WZ control region is excluded from the fits used for the interpretation of the results in terms of superpartner production.

One of the most important discriminating variables used in both the parametric neural networks and the 3ℓA search regions is M_T, the transverse mass of the lepton not forming the Z boson candidate. Simulation studies indicate that the tails of the M_T distribution mainly originate from the mispairing of leptons when forming the Z boson candidate, leading to M_T being computed with one of the leptons from the Z boson decay. The prediction of such mispaired events is validated by selecting $ee\mu$ and $e\mu\mu$ events in the aforementioned WZ control region. In these events, where there is no ambiguity when assigning leptons to W and Z boson decays, the leptons are intentionally mispaired, and the simulated predictions are validated by comparison to data. A second, though smaller, source of events in the M_T tails comes from p_T^{miss} mismeasurements. This effect is studied in $\mu\mu\gamma$ events enriched in the Wγ process where no possible lepton ambiguity may arise. The muon is required to have $p_T > 25\,(28)\,\text{GeV}$ in 2016 (2017 and 2018) data. To reduce the contribution from final-state radiation (FSR) photons, which affect the M_T distribution, the photon is required to have $p_T > 40\,\text{GeV}$, and be separated by $\Delta R > 0.3$ from the muon. Additional requirements are $M_T > 40\,\text{GeV}$ and $p_T^{\text{miss}} > 50\,\text{GeV}$. After this selection, the simulated Wγ prediction is compared to the data in bins of M_T and p_T^{miss} to derive uncertainties based on the agreement, which are applied to the WZ prediction. The uncertainties vary from around 5% at low p_T^{miss} and M_T to slightly below 30% at high p_T^{miss} and M_T. The relative uncertainties derived in the $\mu\mu\gamma$ region thus provide an upper bound on the uncertainty in the WZ prediction, as a function of M_T and p_T^{miss}.

Production of ZZ with subsequent leptonic Z boson decays leads to final states with four leptons. This process is the largest background in the four-lepton categories, while also entering the three lepton categories in case one of the leptons fails to be identified. The normalization of ZZ is constrained using a four-lepton control region with identical selection to the 4ℓG region, but an inverted requirement $p_T^{\text{miss}} < 50\,\text{GeV}$. The predictions as a function of the analysis variables are also checked in this control region. We perform a fit to the control region, in which the ZZ normalization is free to float, all analysis uncertainties are included and the signal presence is suppressed. The fit results in a normalization factor of $r_{ZZ} = 1.02 \pm 0.10$ over the POWHEG simulation prediction. Contributions from gluon induced (gg $\to$ ZZ), quark induced (qq $\to$ ZZ), and resonant (H $\to$ ZZ) production are split for plotting purposes in the four lepton categories where they are the most relevant background sources. For categories with three or fewer leptons, all contributions to ZZ production are grouped together under the ZZ/H label in figures.

Processes involving one or more top quarks and electroweak bosons can produce many prompt leptons and contribute to all of the analysis final states. The main contributions come from $t\bar{t}t\bar{t}$, $t\bar{t}H$, $t\bar{t}W$, and $t\bar{t}Z$, which are collectively labeled $t\bar{t}X$. Smaller contributions originate from processes with a single top quark or with top quarks and multiple electroweak bosons and are labeled tX. These are minor backgrounds because of their small cross sections, and they are

further reduced by the b veto applied in the event selection. Even smaller contributions appear due to processes in which two top quarks and two massive bosons are produced, labeled $\mathrm{t\bar{t}XX}$, which have cross sections so small that barely one event in total appears at the analysis level. The predictions for the $\mathrm{t\bar{t}Z}$ background are verified in a $\mathrm{t\bar{t}Z}$-enriched control region with the selection of the 3ℓ A category, but requiring at least one b jet, and $|M_{\ell\ell} - m_Z| < 15\,\mathrm{GeV}$. All other contributions are estimated from simulation. For plotting purposes, the $\mathrm{t\bar{t}X}$ and tX contributions are grouped together.

Rare processes involving the production of three or more electroweak bosons (WWW, WWZ, WZZ, ZZZ) can also lead to events with enough prompt leptons to enter the search regions. These processes have extremely small cross sections, and thus constitute only a tiny fraction of the background. Their contributions are estimated from simulation. For plotting purposes this contributions are labeled as multiboson.

Internal and external photon conversions can lead to additional leptons in an event. Such events typically enter the search regions when the conversion is asymmetric and one of the leptons coming from the conversion has a very low p_T and fails to be reconstructed. This background is dominated by Zg for events with three or more leptons, while Wg provides the dominant source for 2ℓ SS events. The conversion background is estimated from simulation, which is validated and normalized in a Zg-enriched control region in data. This region is obtained by applying the 3ℓ A selection with inverted requirements $p_T^{\mathrm{miss}} < 50\,\mathrm{GeV}$, and $M_{\ell\ell} < 75\,\mathrm{GeV}$. The last requirement is applied because asymmetric conversions from Zg tend to have $M_{3\ell}$ rather than $M_{\ell\ell}$ values close to the Z boson mass. Processes involving a final state photon $(\mathrm{Zg}, \mathrm{Wg}, \mathrm{t\bar{t}g})$ which undergoes an asymmetric conversion are included into the Xg background group for plotting and fitting purposes. A fit is performed in the control region, in which the photon conversion process normalization is free to float, all analysis uncertainties are included, and the signal presence is suppressed. This leads to a normalization factor of $r_{\mathrm{Xg}} = 1.12 \pm 1.10$ over the MADGRAPH5_aMC@NLO simulation prediction.

Events with nonprompt leptons entering the search regions come mostly from $\mathrm{t\bar{t}}$ and Drell–Yan production with an additional nonprompt lepton. It is a dominant background source in categories 3ℓ B, 2ℓ SS, and all of the categories involving one or more τ_h candidates. This background contribution is estimated from data using the "tight-to-loose" ratio method, as described in Ref. [43]. The probability for a loose nonprompt lepton to also pass the tight lepton selection, the "nonprompt rate", is measured as a function of p_T and η. For light leptons, this is done in a QCD-enriched sample of single lepton events. The nonprompt rate of τ_h candidates is measured in both Drell–Yan- and $\mathrm{t\bar{t}}$-enriched events. These nonprompt rates differ due to the flavor content of the jets in the event. In the 3ℓ D and 3ℓ E categories the background from nonprompt τ leptons is expected to be dominated by $\mathrm{t\bar{t}}$, so the $\mathrm{t\bar{t}}$ based nonprompt rate measurement is used. For 3ℓ C and 3ℓ F events, Drell–Yan is the dominant background source, and the nonprompt rates measured in Drell–Yan enriched data are used. The measured nonprompt rates are applied to events passing the search region selection but with one or more leptons failing the tight selection while still passing the loose selection. Both simulated events and a data sample enriched in nonprompt leptons are used to validate the method.

Electron sign mismeasurements are an important source of background in 2ℓ SS and 3ℓ E events. This background is reduced by the application of additional requirements on the leptons designed to ensure a well-determined sign, as discussed in Section 4. The remaining background for electron sign mismeasurement is predicted from data in 2ℓ SS and 3ℓ E events. The probability for an electron sign mismeasurement is computed as a function of p_T and η in a large

sample of simulated events from Drell–Yan, $t\bar{t}$, and diboson production. The resulting background contribution in the search regions is then determined by applying this probability to data events with two light leptons of opposite sign. A sample of same-sign dilepton events dominated by Drell–Yan is selected by requiring $M \quad m_Z \quad 10\,\text{GeV}$, in which the predictions are validated, and an integral normalization factor is measured for each data-taking year by which the predictions are scaled. The scale factors are 0.89, 1.26 and 1.17 in the 2016, 2017 and 2018 data sets, respectively. Studies in simulated events indicate that the probability of sign misidentification for muons is negligible, and the minuscule background contribution that results in the search regions is estimated using simulation.

8 Systematic uncertainties

Several sources of systematic uncertainties affect both the background and signal predictions, changing both the total yields and the contribution of each process to the different analysis bins. The experimental sources of uncertainty that affect the simulated samples are pileup modeling, jet energy scale and resolution, b tagging, lepton identification and trigger efficiencies, p_T^{miss} resolution, and the measurement of the integrated luminosity. Additional sources of systematic uncertainty come from the uncertainties in the theoretical calculations used to generate samples of simulated events. The effects of each of these uncertainties, aside from those associated with the integrated luminosity and the trigger efficiency, vary across the analysis bins.

Light lepton identification efficiencies are measured in a Z boson enriched data sample using the "tag-and-probe" technique [41, 42]. The corresponding corrections are applied to simulated events. Uncertainties on these measured corrections, as well as on the validity of their extrapolation to the search regions, are applied to simulated events. Signal events are expected to contain relatively high p_T leptons because of the potentially large superpartner masses. For this reason the lepton efficiencies are measured separately for events with a reconstructed Z boson p_T above and below 80 GeV. The difference between the corresponding corrections at high and low p_T of the Z boson is taken as the uncertainty in the application of these corrections, and is around 0.5% for most of the leptons, but ranges up to 3% for very high and low p_T leptons.

Similarly, identification efficiencies for $_h$ candidates are measured in $_h$ events enriched in Z bosons for p_T values up to approximately 60 GeV. For $_h$ candidates with intermediate p_T values, up to 100 GeV, $t\bar{t}$ enriched $_h$ events are used. At even higher p_T values the efficiencies are measured using single $_h$ events enriched in highly virtual W bosons. The associated uncertainties in the measured efficiencies applied in the analysis range from 1 to 3%.

The uncertainty in the correction of the number of events per bunch crossing applied to simulated events is estimated by varying the total pp inelastic cross section up and down by 4.6% [75]. The uncertainty in the measurement of the integrated luminosity, used to normalize all simulated yields, is 2.3 (2.5)% for the data set collected in 2017 [76] (2016 [77] and 2018 [78]). The integrated luminosity of the total data set has an uncertainty of 1.8%, where the improved understanding comes from the independence of some parts of the uncertainty between data-taking years. The correlated (uncorrelated) components correspond to 1.2, 1.1 and 2.0 (2.2, 2.0 and 1.5%) for the 2016, 2017 and 2018 data-taking years. The trigger efficiency is measured in an unbiased sample of events, triggered on the p_T^{miss} and total hadronic momentum in the event. The uncertainties in the trigger efficiency range from 1.4% for events with three or more light leptons to 3% for events in the 2 SS and 5% for category 3 F events have less redundancy to pass the leptonic trigger requirements. The trigger uncertainties are split into a component correlated across years accounting for possible biases in the method used to measure trigger

efficiencies and an uncorrelated component per year because of the limited data available in the data sideband used for such measurements. The latter accounts for effects of roughly 1% for each category and year with the former accounting for the rest of the uncertainty size.

The uncertainties due to the jet energy scale are computed by varying the scale for all jets up and down within its uncertainty. Similarly, the uncertainties from the jet energy resolution are estimated by smearing the jets according to the resolution uncertainty [39, 40]. Both effects are subsequently propagated to all steps of the analysis, affecting p_T^{miss}, the b veto and all analysis variables calculated using jets or p_T^{miss} [40]. The p_T^{miss} is affected by additional resolution uncertainties due to objects not clustered into jets, which are also propagated to all affected analysis variables. Corrections are applied to account for differences between data and simulation in the b tagging efficiency and misidentification rate. Uncertainties in this correction affect the b veto used in the analysis, and the effects are propagated to all analysis bins. These effects are partially correlated across data-taking years accounting for the possible year dependency of the origin of each source of uncertainty included into these variations. The overall effect of the correlated and uncorrelated components is approximately equal for all data-taking years.

Uncertainties stemming from a limited knowledge of the proton PDFs are estimated using a set of NNPDF3.0 (NNPDF3.1) replicas in simulations corresponding to 2016 (2017 and 2018) data-taking conditions. Uncertainties stemming from missing higher order corrections are estimated by varying the renormalization and factorization scales up and down simultaneously by a factor two and evaluating the effect on simulated events. Both of these theoretical uncertainty sources lead to changes in the predicted cross sections of simulated processes, as well as additional kinematic variations across analysis bins. The shape variations are taken into account for all simulated events, whereas for several processes the cross section uncertainties are replaced by a prior uncertainty which is constrained by a fit to data. This is the case for WZ, ZZ and Zg processes.

The experimental and theoretical uncertainties listed earlier in this section affect all simulated processes, both signal and background, and the effects are considered correlated across processes. A number of additional process-specific systematic uncertainty sources are taken into account.

The modeling of QCD ISR in signal events is done by MADGRAPH5_aMC@NLO and affects the total ISR transverse momentum of the events (p_T^{ISR}). The p_T^{ISR} distribution in 2016 signal events is reweighted based on the Z boson p_T spectrum observed in data [79]. Differences between corrected and uncorrected signal events are taken into account as systematic uncertainties. For 2017 and 2018 data, the p_T^{ISR} distribution was found to be well modeled, but a small correction based on the distribution of the number of reconstructed jets in a Z boson enriched data sample is applied. The size of the corrections are also considered as uncertainties in this case.

As discussed in Section 7, Wg data are used to validate the modeling of events with p_T^{miss} mismeasurements entering the M_T tail in WZ events. The deviations from unity observed in Wg as a function of M_T and p_T^{miss} serve as an upper bound on the potential uncertainties in WZ as the M_T distribution of Wg is more strongly affected by mismeasurements. The resulting uncertainties typically range from 10% at low-M_T and p_T^{miss} to 20% at high-p_T^{miss} values. These uncertainties are mainly driven by the size of the Wg-enriched data sample.

A prior normalization uncertainty of 10% is assigned to WZ events, which is constrained implicitly by the fit to the data in 3 A events. Similarly prior normalization uncertainties of 10% are assigned to both the ZZ and Zg processes, which are further constrained by including their respective control regions in the analysis fit. A normalization uncertainty of 30% is assigned to

the nonprompt lepton background prediction, covering any biases found in simulated studies of the method. Three separate uncorrelated nuisance parameters with priors of the same size are used for nonprompt light leptons, nonprompt τ_h candidates from $t\bar{t}$ and nonprompt τ_h candidates from Drell–Yan production. A 20% uncertainty is assigned to the normalization of the sign misidentification background to cover deviations observed in the Z boson enriched control region mentioned in Section 7.

A summary of the systematic uncertainties applied in the analysis, and their effects on the predicted event yields across analysis bins is shown in Table 12.

Table 12: Systematic uncertainty sources affecting the analysis, with their typical size across signal regions, and the treatment of the correlations across data-taking years. Uncertainties in the jet energy corrections and b tagging efficiencies are considered separately for signal events which use CMS fast simulation, as explained in Section 5, and for the other simulated processes. Both the overall integrated luminosity and all normalization uncertainties have effects on the predicted yields of the corresponding processes that are of the same size across all signal regions. Their quoted typical size corresponds to the size of such variations. All other uncertainties can have different effects on the predicted yields for each process and signal region. Their typical uncertainty corresponds to the range of sizes that such effects take across the analysis search regions.

| Source	Typical uncertainty (%)	Correlation across data-taking years
e/μ efficiency	1–2 per lepton	Correlated
τ_h efficiency	1–3 per lepton	Correlated
Pileup	1–2	Correlated
Integrated luminosity	1.8	Partially correlated
Trigger efficiency	1.4–5	Partially correlated
Jet energy corrections	1	Partially correlated
Jet energy corrections (fast simulation)	1	Correlated
b tagging efficiency	1–3	Correlated
b tagging efficiency (fast simulation)	1–3	Correlated
PDF	1–10	Correlated
Renormalization and factorization scales	1–10	Correlated
Signal ISR	1–5	Correlated
Signal $p_\mathrm{T}^\mathrm{miss}$	1–2	Correlated
WZ shape	5–30	Uncorrelated
WZ normalization	10	Correlated
ZZ normalization	10	Correlated
Conversion normalization	10	Correlated
Nonprompt normalization (e/μ/τ_h)	30	Correlated
Charge misidentification normalization	20	Correlated
$t\bar{t}$X normalization	15	Correlated
Multiboson normalization	50	Correlated
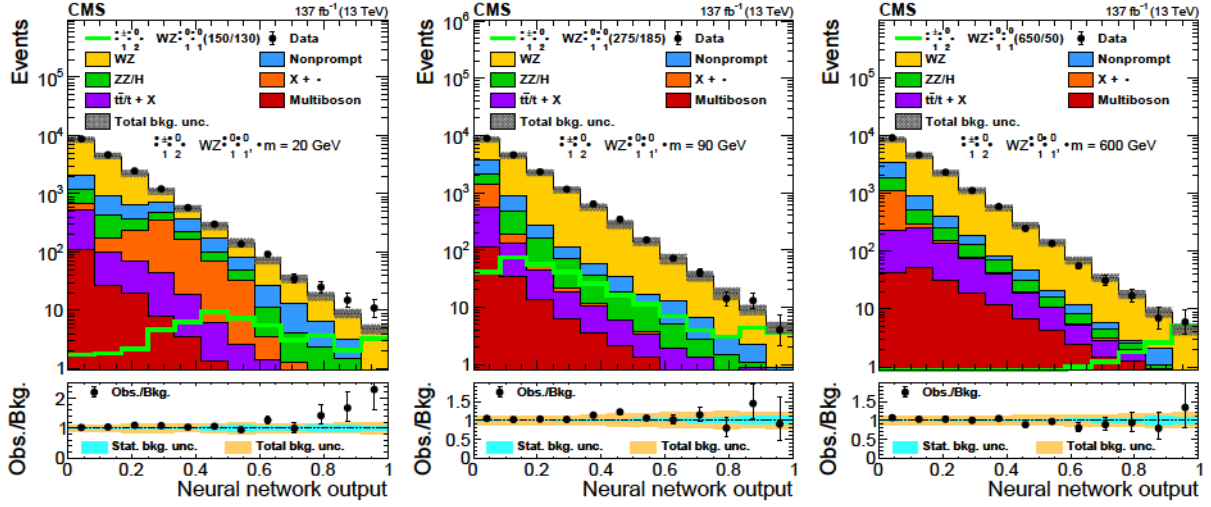
Figure 5: Observed and expected yields as functions of the output of the neural network used to search for $\widetilde{\chi}_1^\pm \widetilde{\chi}_2^0$ production with WZ-mediated decays, evaluated at $\delta m = 20\,\text{GeV}$ (left), 90 GeV (center), and 600 GeV (right). The legends specify the masses of $\widetilde{\chi}_2^0$ and $\widetilde{\chi}_1^0$ for the shown signal distributions as $(m_{\widetilde{\chi}_2^0}/m_{\widetilde{\chi}_1^0})$. The top panels show only the total uncertainty in the background prediction, while the lower panels show the total and statistical uncertainties separately. The following abbreviations are used in the legends of this and the following figures: "bkg." stands for background, "unc." for uncertainty and "obs." for observed.

9 Results

The observed and expected SM yields in each of the search regions introduced in Section 6 are shown in this section. The expected yields are obtained using the background estimation procedures elucidated in Section 7, with systematic uncertainties as explained in Section 8.

The yields as a function of the parametric neural network output in 3ℓA events are respectively shown in Figs. 5–6 for the different $\widetilde{\chi}_1^\pm \widetilde{\chi}_2^0$ production models considered. For each model the neural network discriminant is shown as evaluated at three distinct δm hypotheses, representing low, intermediate, and high δm values. To obtain the final results, the neural network is evaluated at far more δm parameters, separated by 50 GeV for models with slepton-mediated decays and by 25 GeV in case of WZ-mediated decays with δm in excess of 100 GeV. When δm is below 90 GeV in the former models, the neural network is evaluated in δm steps of 10 GeV, and in steps of 1 GeV between 90 and 100 GeV. The expected and observed yields as a function of the search regions in each event category are shown in Figs. 7–14.

In all categories, and in both evaluations of 3ℓA events, based on the neural networks and on the search regions, the data are found to be consistent with the expectation from the SM backgrounds. The agreement in the search regions is summarized in Fig. 15 (upper plot), where the expected test statistic [80] distribution for a background only fit to data is compared to the observed test statistic value. One expects the observed test statistic to lie in a likely region of the expected test statistic distribution in the absence of any unknown physics. A similar plot is shown in Fig. 15 (lower plot) for the neural network targeting WZ-mediated decays of the chargino-neutralino pair. This is the neural network for which the data are evaluated at the most δm values, and the agreement is shown for each one of them.
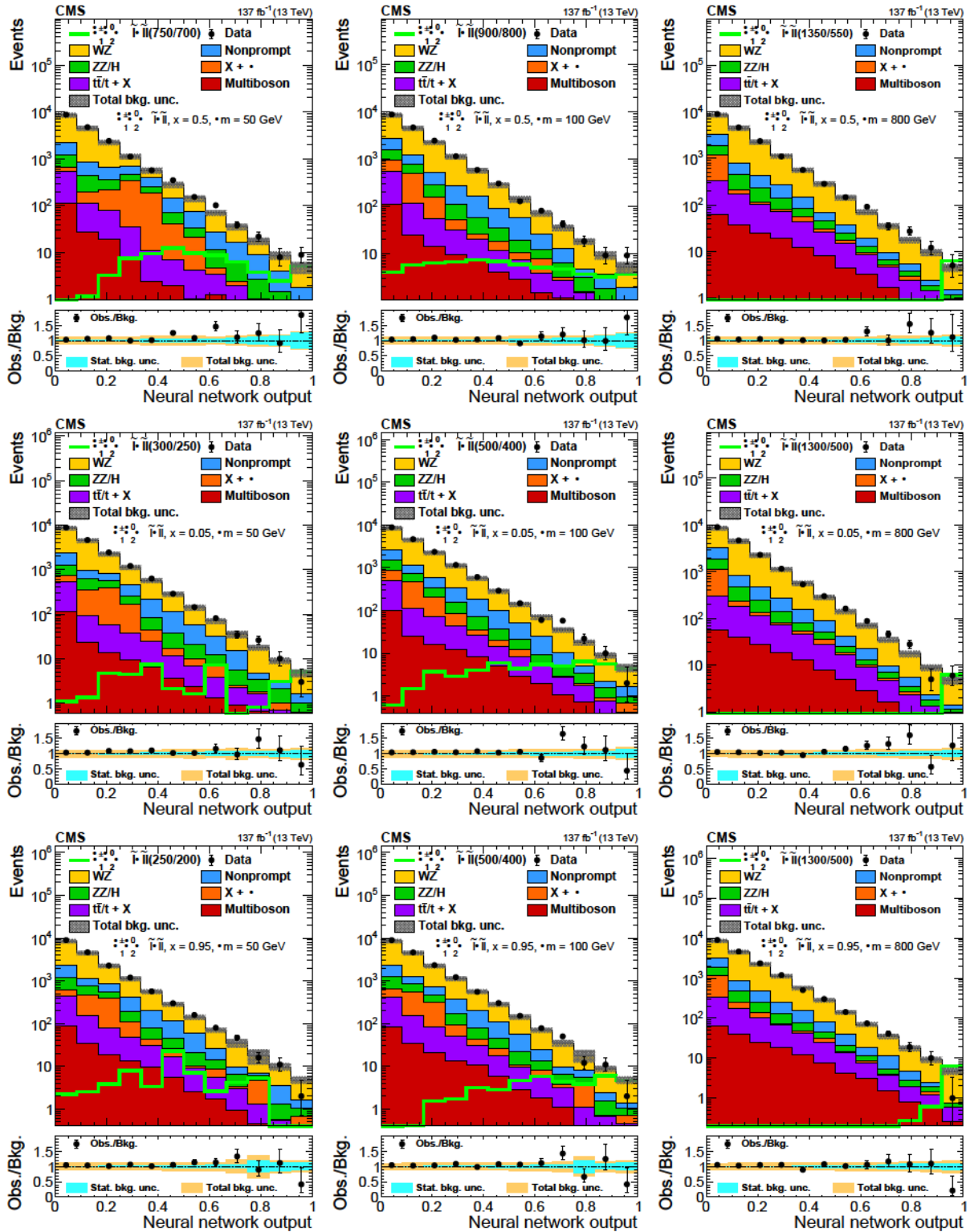
Figure 6: Observed and expected yields as functions of the output of the neural network used to search for $\widetilde{\chi}_1^{\pm}\widetilde{\chi}_2^0$ production with slepton-mediated decays at $x = 0.5$ (upper), 0.05 (middle), and 0.95 (lower), evaluated at $\delta m = 50\,\text{GeV}$ (left), $100\,\text{GeV}$ (center), and $800\,\text{GeV}$ (right). The legends specify the masses of $\widetilde{\chi}_2^0$ and $\widetilde{\chi}_1^0$ for the shown signal distributions as $(m_{\widetilde{\chi}_2^0}/m_{\widetilde{\chi}_1^0})$.
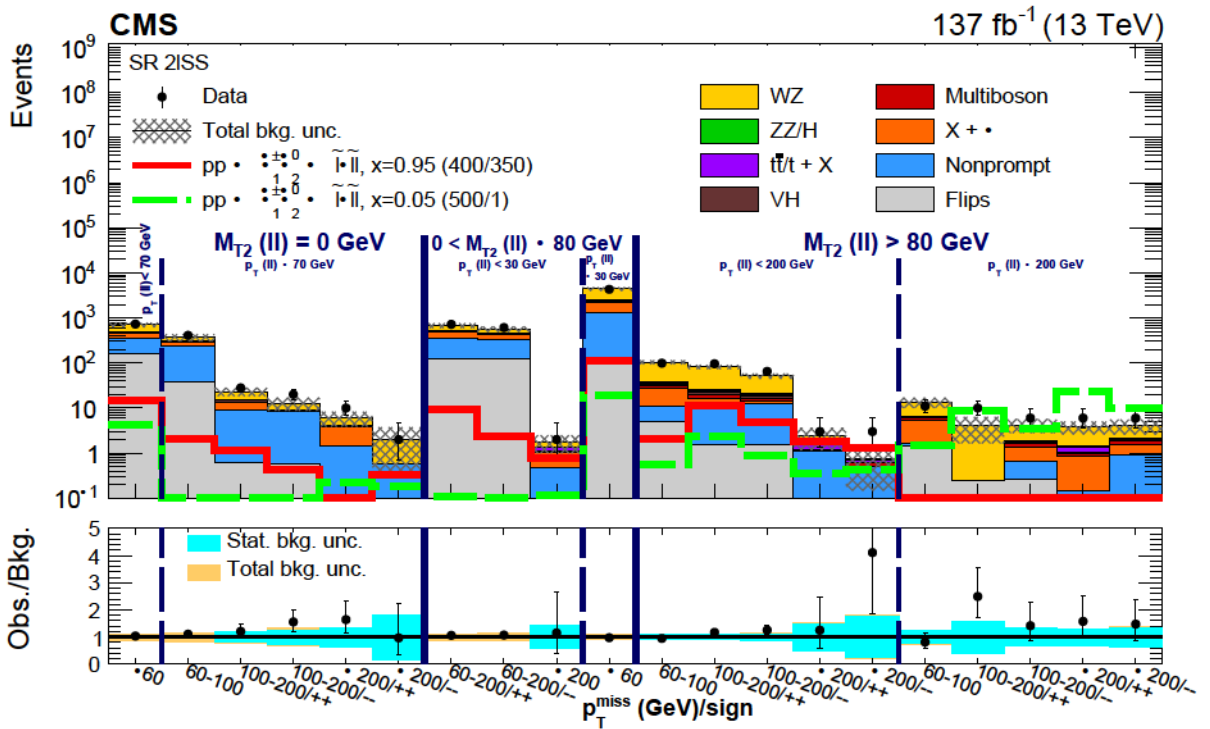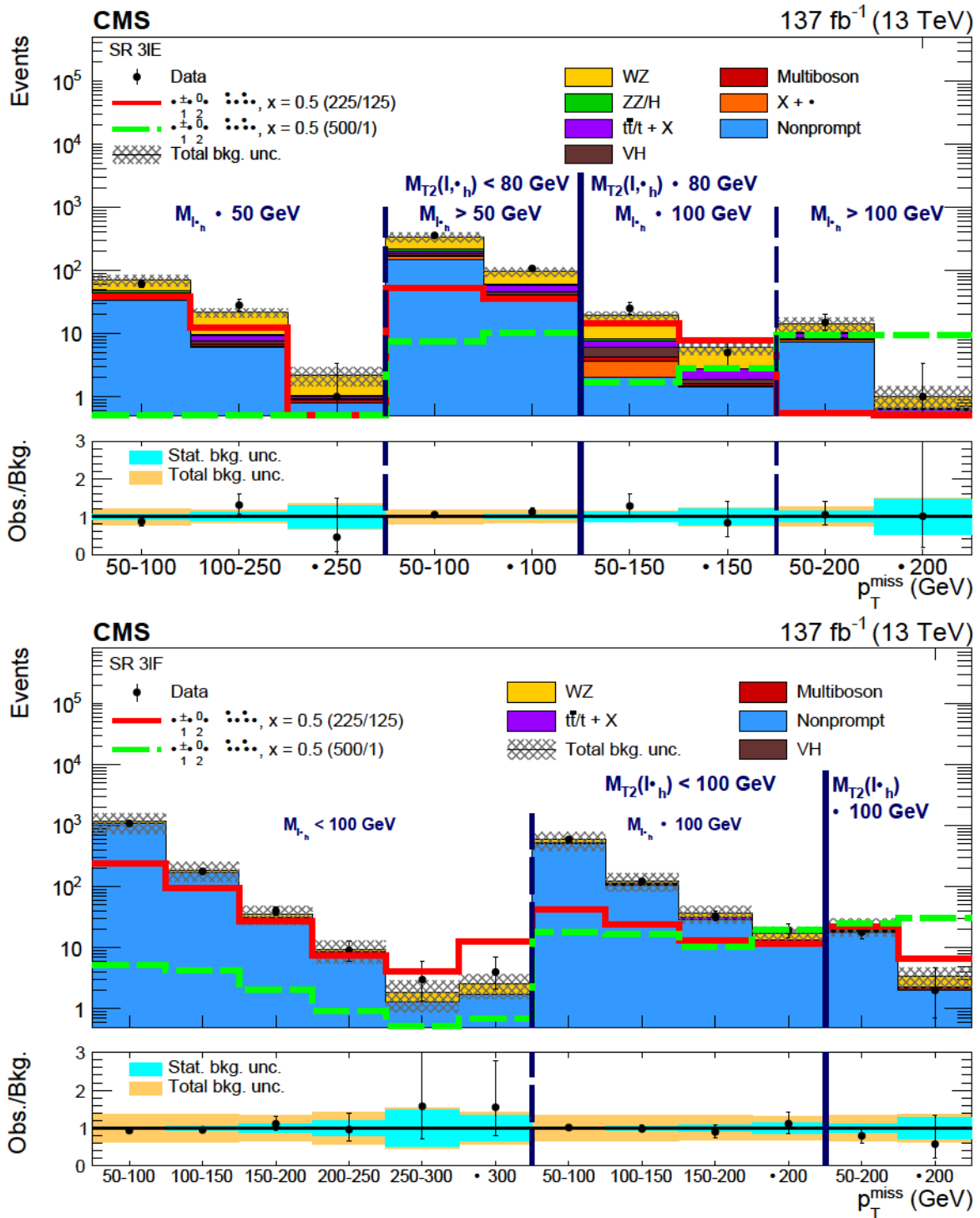
Figure 7: Observed and expected yields across the search regions in events with two same-sign light leptons (2ℓSS). Several signal models are shown superimposed. They correspond to $\widetilde{\chi}_1^{\pm}\widetilde{\chi}_2^0$ production with slepton-mediated decays in the flavor-democratic hypothesis for a compressed $\delta m = 50\,\text{GeV}$ (red line) and uncompressed $\delta m = 500\,\text{GeV}$ (green dashed line) scenario. The legends specify the masses of $\widetilde{\chi}_2^0$ and $\widetilde{\chi}_1^0$ for the shown signal distributions as $(m_{\widetilde{\chi}_2^0}/m_{\widetilde{\chi}_1^0})$.
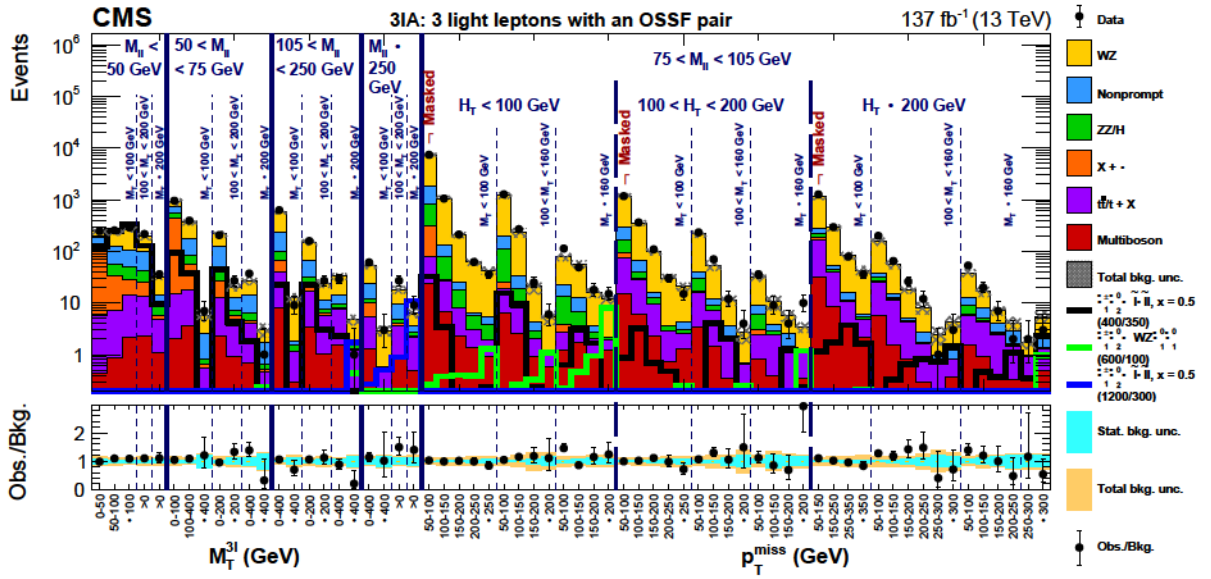
Figure 8: Observed and expected yields across the search regions in events with three light leptons, at least two of which form an OSSF pair (3ℓA). Several signal models are shown superimposed. They correspond to $\tilde{\chi}_1^\pm \tilde{\chi}_2^0$ production with slepton-mediated decays in the flavor-democratic hypothesis for a compressed $\delta m = 50$ GeV (black line) and uncompressed $\delta m = 900$ GeV (blue line) scenario, and for WZ-mediated decays in an uncompressed $\delta m = 500$ GeV scenario (green line). Bins labeled as "Masked" are not considered in the interpretation of the results because of overlap with the WZ control region. The legends specify the masses of $\tilde{\chi}_2^0$ and $\tilde{\chi}_1^0$ for the shown signal distributions as $(m_{\tilde{\chi}_2^0}/m_{\tilde{\chi}_1^0})$.
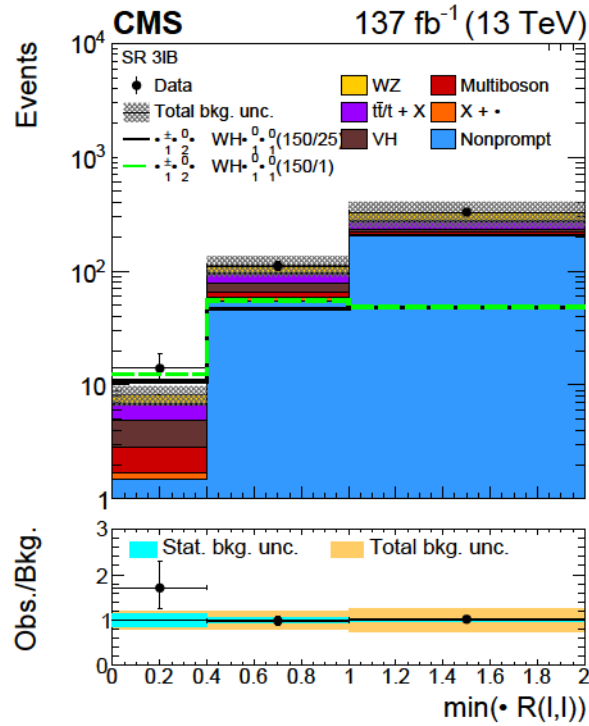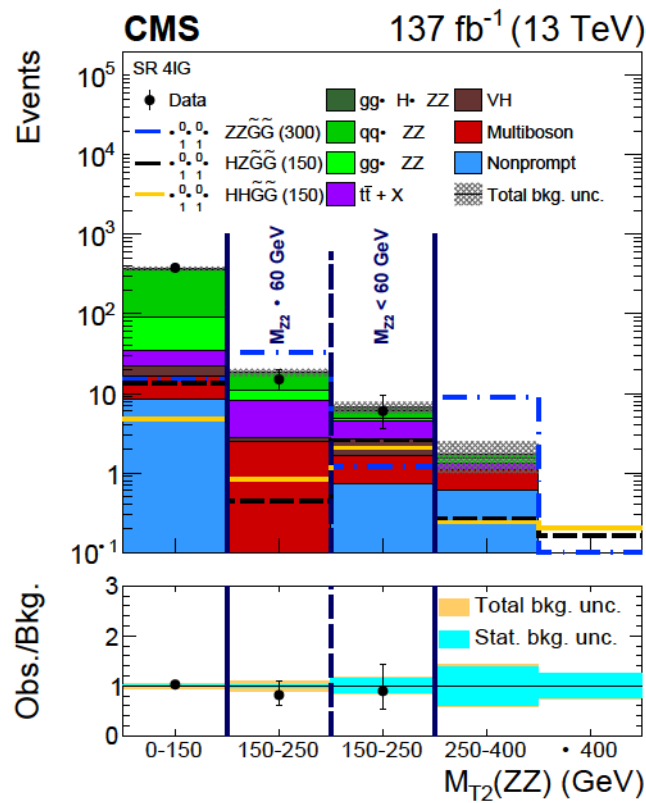
Figure 9: Observed and expected yields across the search regions in events with three light leptons, none of which form an OSSF pair (3ℓB). Several signal models are shown superimposed. They correspond to $\tilde{\chi}_1^\pm \tilde{\chi}_2^0$ production with WH-mediated decays for scenarios corresponding to a H boson like mass splitting $\delta m = 125\,\text{GeV}$ (black line) and a slightly less compressed $\delta m = 150\,\text{GeV}$ (green dashed line) scenario. The legends specify the masses of $\tilde{\chi}_2^0$ and $\tilde{\chi}_1^0$ for the shown signal distributions as $(m_{\tilde{\chi}_2^0}/m_{\tilde{\chi}_1^0})$.
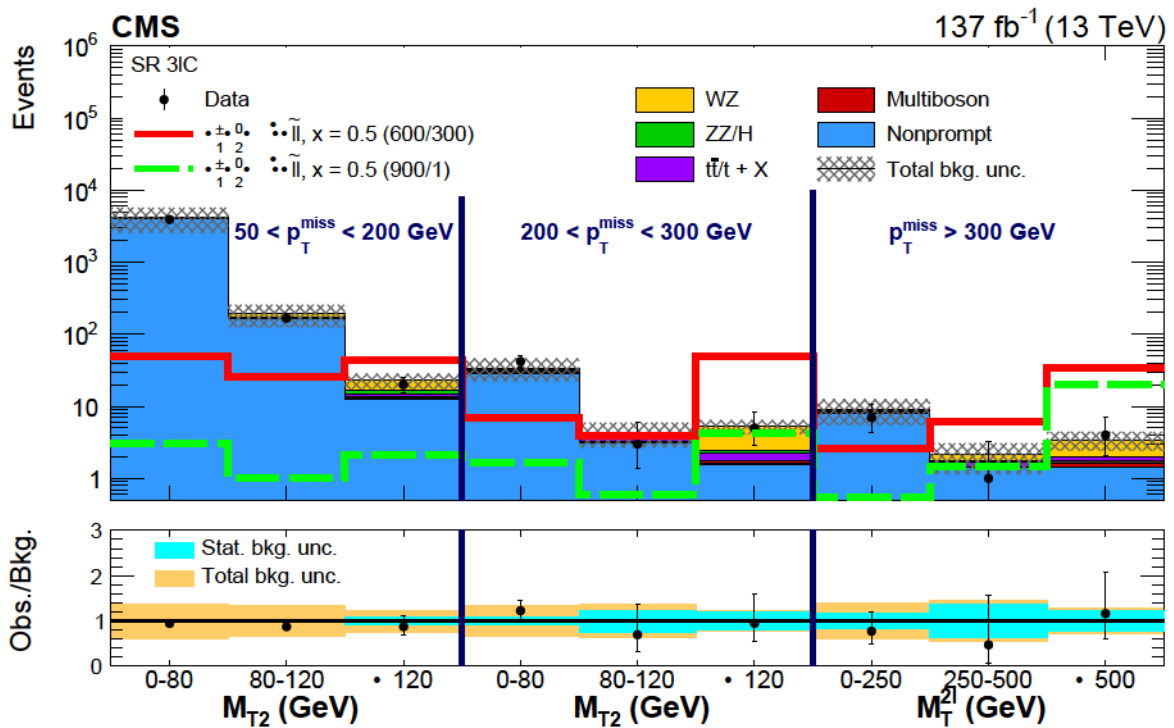
Figure 10: Observed and expected yields across the search regions in events with a $\mu^+\mu^-$ or e^+e^- pair and an additional τ_h candidate (3ℓC). Several signal models are shown superimposed. They correspond to $\widetilde{\chi}_1^{\pm}\widetilde{\chi}_2^0$ production with slepton-mediated decays in the τ lepton enriched hypothesis for a compressed $\delta m = 300\,\text{GeV}$ (red line) and uncompressed $\delta m = 900\,\text{GeV}$ (green dashed line) scenario. The legends specify the masses of $\widetilde{\chi}_2^0$ and $\widetilde{\chi}_1^0$ for the shown signal distributions as $(m_{\widetilde{\chi}_2^0}/m_{\widetilde{\chi}_1^0})$.
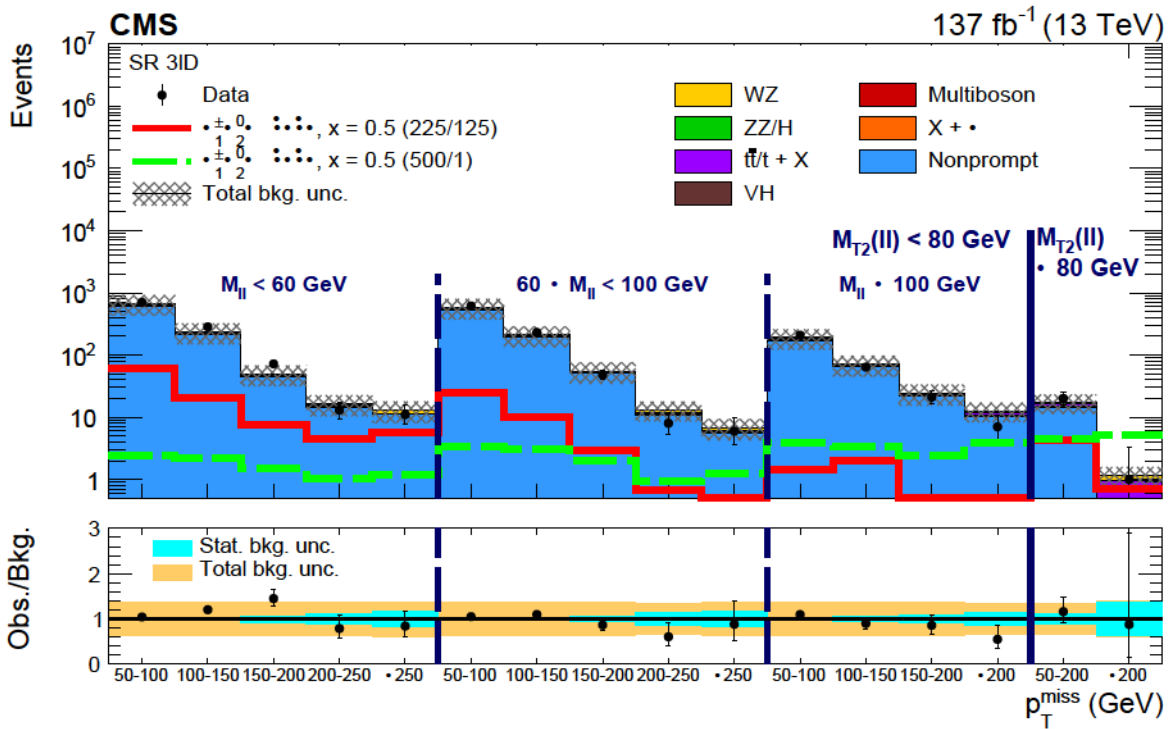
Figure 11: Observed and expected yields across the search regions in events with an $e^{\pm}\mu^{\mp}$ pair and a τ_h candidate (3ℓD). Several signal models are shown superimposed. They correspond to $\widetilde{\chi}_1^{\pm}\widetilde{\chi}_2^0$ production with slepton-mediated decays in the τ lepton dominated hypothesis for a compressed $\delta m = 100\,\text{GeV}$ (red line) and uncompressed $\delta m = 500\,\text{GeV}$ (green dashed line) scenario. The legends specify the masses of $\widetilde{\chi}_2^0$ and $\widetilde{\chi}_1^0$ for the shown signal distributions as $(m_{\widetilde{\chi}_2^0}/m_{\widetilde{\chi}_1^0})$.

Figure 12: Observed and expected yields across the search regions in events (upper plot) with a same-sign light lepton pair and a τ_h candidate (3ℓE), and (lower plot) with two τ_h candidates and one light lepton (3ℓF). Several signal models are shown superimposed. They correspond to $\tilde{\chi}_1^{\pm}\tilde{\chi}_2^0$ production with slepton-mediated decays in the τ lepton dominated hypothesis for a compressed $\delta m = 100\,\text{GeV}$ (red line) and uncompressed $\delta m = 500\,\text{GeV}$ (green dashed line) scenario. The legends specify the masses of $\tilde{\chi}_2^0$ and $\tilde{\chi}_1^0$ for the shown signal distributions as $(m_{\tilde{\chi}_2^0}/m_{\tilde{\chi}_1^0})$.

Figure 13: Observed and expected yields across the search regions in events with four light leptons, including 2 separate OSSF pairs (4ℓG). Several signal models are shown superimposed. They correspond to Higgsino pair production with decays to ZZ (blue dotted line, Higgsino mass of 300 GeV), HZ (black dashed line, Higgsino mass of 150 GeV), and HH (dark yellow line, Higgsino mass of 150 GeV).
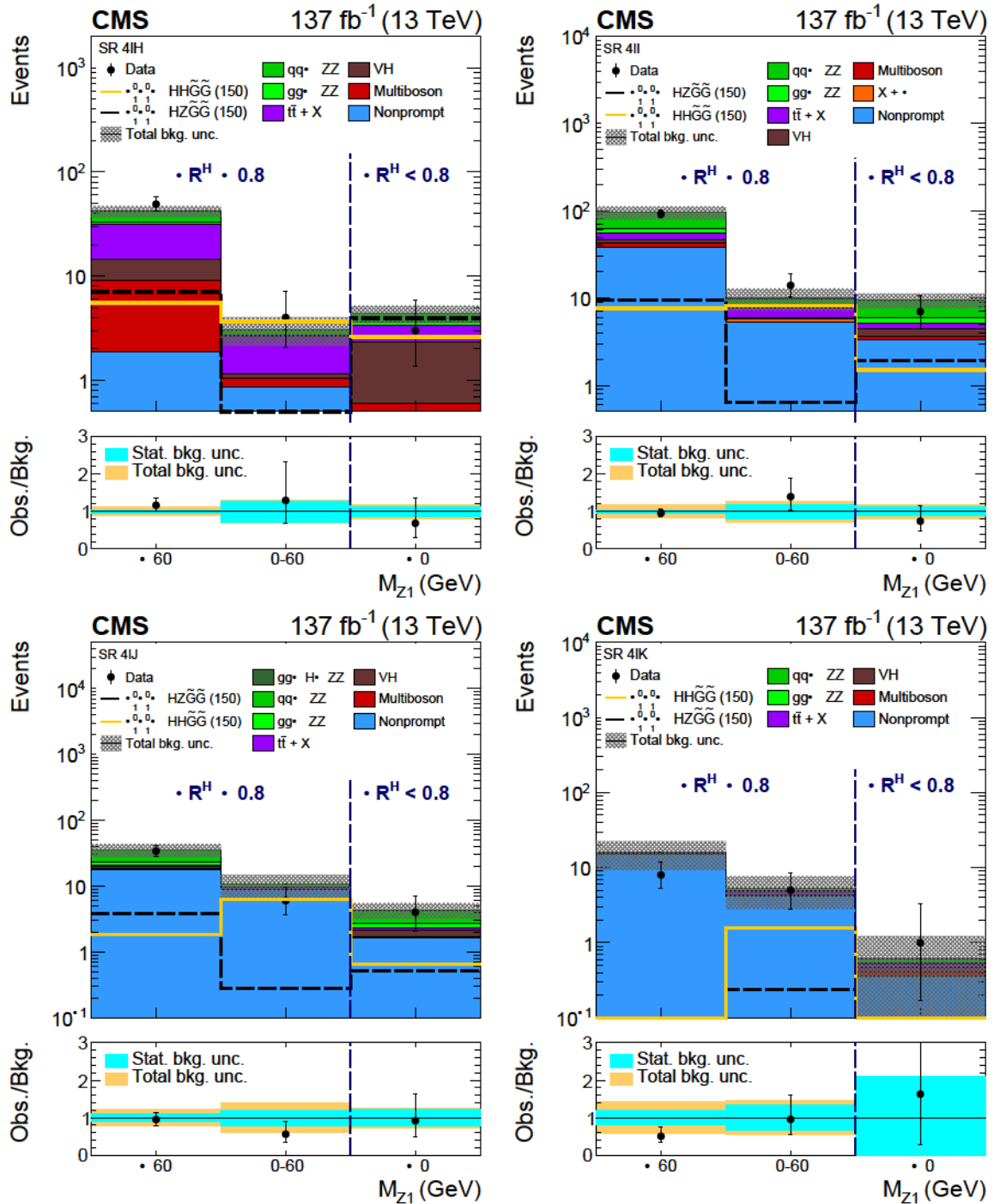
Figure 14: Observed and expected yields across the search regions in events with four light leptons not forming two OSSF pairs (4ℓH, upper left), events with three light leptons and a τ_h candidate (4ℓI, upper right), forming two OSSF pairs (4ℓJ, lower left), and forming one or less OSSF pairs (4ℓK, lower right). Several signal models are shown superimposed. They correspond to Higgsino pair production with decays to HZ (dashed black line, Higgsino mass of 150 GeV), and HH (dark yellow line, Higgsino mass of 150 GeV).
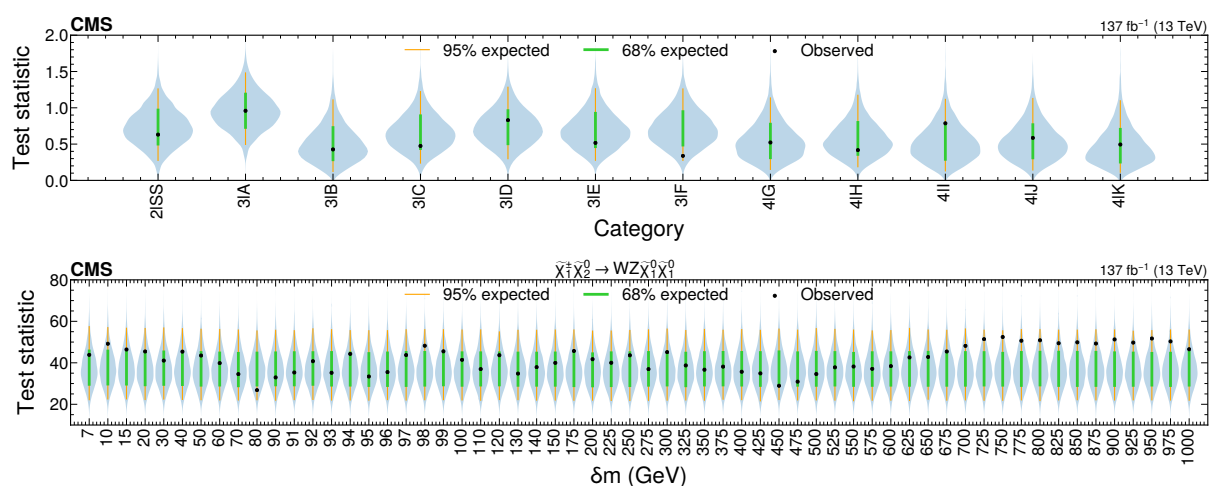
Figure 15: Expected test statistic distribution for a background-only fit compared to the observed test statistic value, drawn as black dots, for the search regions in each event category (upper plot) and the neural network targeting WZ-mediated superpartner decays for each m evaluation (lower plot). The gray shaded area represents the (symmetrized) probability density of the expected test statistic distribution, with 68 and 95% expected ranges respectively drawn in green and orange.

Table 13: Summary of the event categories used for the interpretation of the results in terms of different models, and references to the associated figure summarizing the expected and observed 95% CL upper limits.

Model	Categories used	Figure
$\tilde{\chi}_1^\pm\tilde{\chi}_2^0$ production, flavor-democratic	2 SS, 3 A (search regions and neural network fit separately)	16
$\tilde{\chi}_1^\pm\tilde{\chi}_2^0$ production, τ-enriched	3 A–3 F	17
$\tilde{\chi}_1^\pm\tilde{\chi}_2^0$ production, τ-dominated	3 B–3 F	18
$\tilde{\chi}_1^\pm\tilde{\chi}_2^0$ production, WZ-mediated decays	2 SS, 3 A (search regions and neural network fit separately)	19
$\tilde{\chi}_1^\pm\tilde{\chi}_2^0$ production, WH-mediated decays	2 SS, 3 A–3 F	20
$\tilde{\chi}_1^0\tilde{\chi}_1^0$ production	3 A–4 K	21

10 Interpretation

No significant excess of events over the SM-only hypothesis is observed, as shown in Section 9. The expected signal and background yields and the observed data are then used to determine 95% confidence level (CL) upper limits on $\tilde{\chi}_1^\pm\tilde{\chi}_2^0$ and effective $\tilde{\chi}_1^0\tilde{\chi}_1^0$ production cross sections for the different decay models introduced in Section 3, using the CL_s criterion [81, 82]. The asymptotic approximation of the distribution of the profile likelihood test statistic [83, 84] is used when computing these limits. The systematic uncertainties introduced in Section 8 are included as nuisance parameters with additional constrain terms into the likelihood function. Systematic uncertainties with an effect on overall process normalizations but not distributions are included through log-normal probability density functions while those that have an effect on both normalization and shape of any processes are included via the template morphing technique [85] and represented with Gaussian probability density functions. Uncertainties related to the limited size of the MC samples are introduced into the likelihood following the Barlow–Beeston approach [86].

For each model interpretation, a global fit of the analysis bins is performed, using the events from categories corresponding to the final state of the particular model. The event categories used to interpret each model are listed in Table 13. In the interpretations that include the neural network approach, the corresponding distributions used for the interpretation in the 3 A category in each signal point correspond to the evaluation of the neural network discriminant at the specific m value of the chosen point.

The sensitivity of $\tilde{\chi}_1^\pm\tilde{\chi}_2^0$ production models with slepton-mediated decays is mainly driven by 3 A events in case of flavor-democratic decays. In case of compressed models, in particular for $x \approx 0.05$ and 0.95, 2 SS events increase the sensitivity significantly, being the leading source of exclusion for mass splittings of $m_{\tilde{\chi}_2^0} - m_{\tilde{\chi}_1^0} \approx 30\,\text{GeV}$. For τ-enriched models, regions 3 B–3 F provide the bulk of the sensitivity, with 3 A and 2 SS events still adding sensitivity, the latter particularly for compressed models. For τ-dominated models, the sensitivity is driven by 3 B–3 F, and only these regions are included in the corresponding fits.

The observed and expected exclusion limits as a function of $m_{\tilde{\chi}_2^0}$ and $m_{\tilde{\chi}_1^0}$ are shown in Fig. 16 for flavor-democratic slepton-mediated decays. For each model the limits are separately computed by fitting 3 A events as a function of the output of the neural networks or the search regions. The 3 A search regions and neural networks contain the same events so are never simultaneously fit. In both cases, they are fit together with the 2 SS search regions as indicated in

Table 13. When the slepton mass is close to $m_{\tilde{\chi}_2^0}$ ($x = 0.95$), the neural network extends the observed limits by up to about 250 GeV in $m_{\tilde{\chi}_2^0}$ and 150 GeV in $m_{\tilde{\chi}_1^0}$ compared to the search regions. This corresponds to an excluded cross section that is almost of a factor 2 lower when only evaluating 3ℓA events, or a relative improvement slightly below 100%. In models where the mass difference between the sleptons and $\tilde{\chi}_2^0$ is bigger ($x = 0.5$ and 0.05), the leptons generally have harder p_T spectra and the gains from the neural networks over the search regions are smaller: up to around 100 GeV in both $m_{\tilde{\chi}_2^0}$ and $m_{\tilde{\chi}_1^0}$. This is equivalent to a relative improvement of about 50% in the excluded cross section. At very low δm values, the relative improvement varies more and can be greater than 100% for $x = 0.5$ while typically being smaller than 50% for the other x values. Chargino masses up to 1450 GeV and LSP masses up to 1000 GeV can be excluded by the neural networks depending on the model parameters. The reach of the previous iteration of the analysis has been improved up to 400 GeV in the chargino masses—a factor of 9 in terms of production cross-section—and up to 500 GeV in the LSP masses.
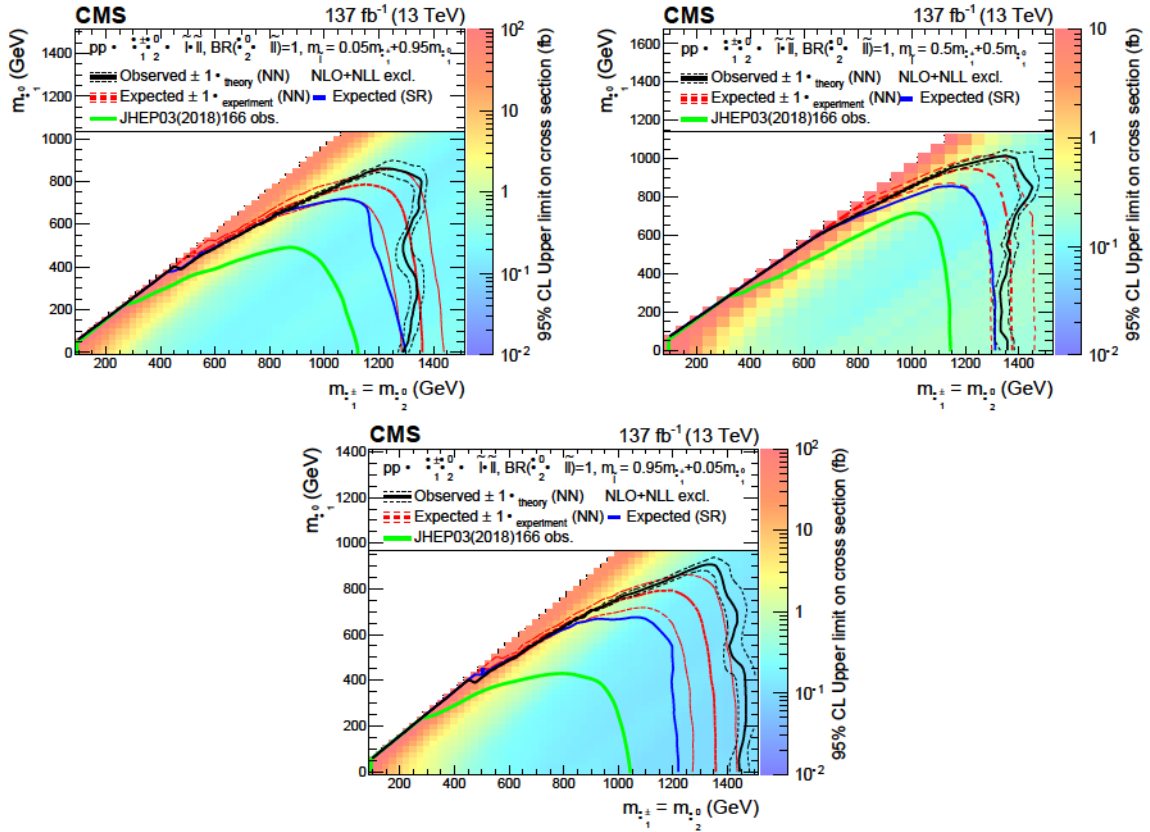
Figure 16: Interpretation of the results for $\tilde{\chi}_1^\pm \tilde{\chi}_2^0$ production with flavor-democratic slepton-mediated decays, and the parameter governing the mass splittings being $x = 0.05$ (upper left), $x = 0.5$ (upper right) and $x = 0.95$ (lower). The shading in the $m_{\tilde{\chi}_1^0}$ versus $m_{\tilde{\chi}_2^0}$ plane indicates the 95% CL upper limit on the $\tilde{\chi}_1^\pm \tilde{\chi}_2^0$ production cross sections. The contours delineate the mass regions excluded at 95% CL when assuming cross section computed at NLO plus NLL. All masses below the contours are excluded. The observed, observed $\pm 1\sigma_{\text{theory}}$ (± 1 standard deviation of the theoretical cross sections), median expected, and expected $\pm 1\sigma_{\text{experiment}}$ bounds obtained with the neural network strategy are shown in black and red. The median expected bound obtained with the search region strategy is shown in blue. The observed limits obtained in the CMS analysis using 2016 data [20] are shown in green.

For -enriched models, the exclusion limits are drawn in Fig. 17. The limits extend up to 1150 GeV in $m_{\tilde\chi_2^0}$ and 700 GeV in $m_{\tilde\chi_1^0}$ and provide improvements above the reach of previous iterations of the analysis of up to 150 GeV for chargino masses –around a factor 2 in cross section– and 100 GeV for LSP masses.

Limits for -dominated decay models are shown in Fig. 18, extending up to 970 GeV in $m_{\tilde\chi_2^0}$ and 450 GeV in $m_{\tilde\chi_1^0}$. For the -dominated models the limits for more compressed scenarios are significantly worse because of the relatively large p_T thresholds used in the $_h$ selection. Noticeable improvements, owing to the reoptimized search strategy and the updated lepton and identification criteria, lead to an improvement over the results obtained by previous iterations of the analysis of 350 GeV in chargino masses—around a factor 10 in cross section— and up to 200 GeV in the LSP mass.

Models of $_1$ $_2^0$ production with WZ-mediated decays are probed using category 3 A and 2 SS events, with the former dominating the sensitivity for most mass hypotheses. Similarly to the case of flavor-democratic slepton-mediated decays, the fits are performed twice: once using the neural network, and once using the 3 A search regions. Other regions provide minimal sensitivity to these models and are thus excluded from the interpretation. The interpretation is done separately, using the parametric neural network and the search region bins. The resulting exclusion limit curves are shown in Fig. 19. The neural network provides maximal sensitivity to the models we are probing, resulting in more stringent exclusion limits by about 130 GeV in $m_{\tilde\chi_2^0}$ and a bit less than 50 GeV in $m_{\tilde\chi_1^0}$. At most m values this corresponds to improvements between 30 and 40% in the excluded cross section, while at m values below 30 GeV the improvement is often larger than 200%. The current results improve the results of the 2016 analysis by 200 GeV in the excluded chargino masses –around a factor 6 in cross section– and 150 GeV in the LSP mass. Moreover, the current results provide coverage over the previously nonexcluded gap in the parameter space around mass splittings of $m_{\tilde\chi_2^0}$ $m_{\tilde\chi_1^0}$ m_Z.

Because of the diverse set of possible H decays, all event categories are used in the interpretation of models with H-mediated $_2^0$ decays. The most important event category in the interpretation of these models is 3 B, where the search regions are consequently designed to specifically target H decays. The resulting limits for this decay hypothesis are shown in Fig. 20, and range up to 300 GeV in $m_{\tilde\chi_2^0}$ and 70 GeV in $m_{\tilde\chi_1^0}$, excluding regions with cross sections up to four times smaller than those already reached by the previous iteration of the analysis.

The interpretation of $_1^0$ pair production models, with subsequent decays via H or Z bosons uses all event categories. In the case of decays via two Z bosons, 4 G events are the most important contributors to the final exclusion limits. In decays via an H and a Z boson, four lepton events provide the most sensitivity for low $_1^0$ mass hypotheses, while trilepton events become more important at higher $_1^0$ masses. When the $_1^0$ pair decays via two H, trilepton events drive the results. The exclusion limits as a function of $m_{\tilde\chi_1^0}$ for these models are shown in Fig. 21, and extend up to 600 GeV in case of ZZ-mediated decays, up to 400 GeV for decays via HZ, and up to 200 GeV for HH-mediated decays. These improved exclusion limits correspond to excluded cross-sections up to seven times better than those of the previous iteration of the analysis.
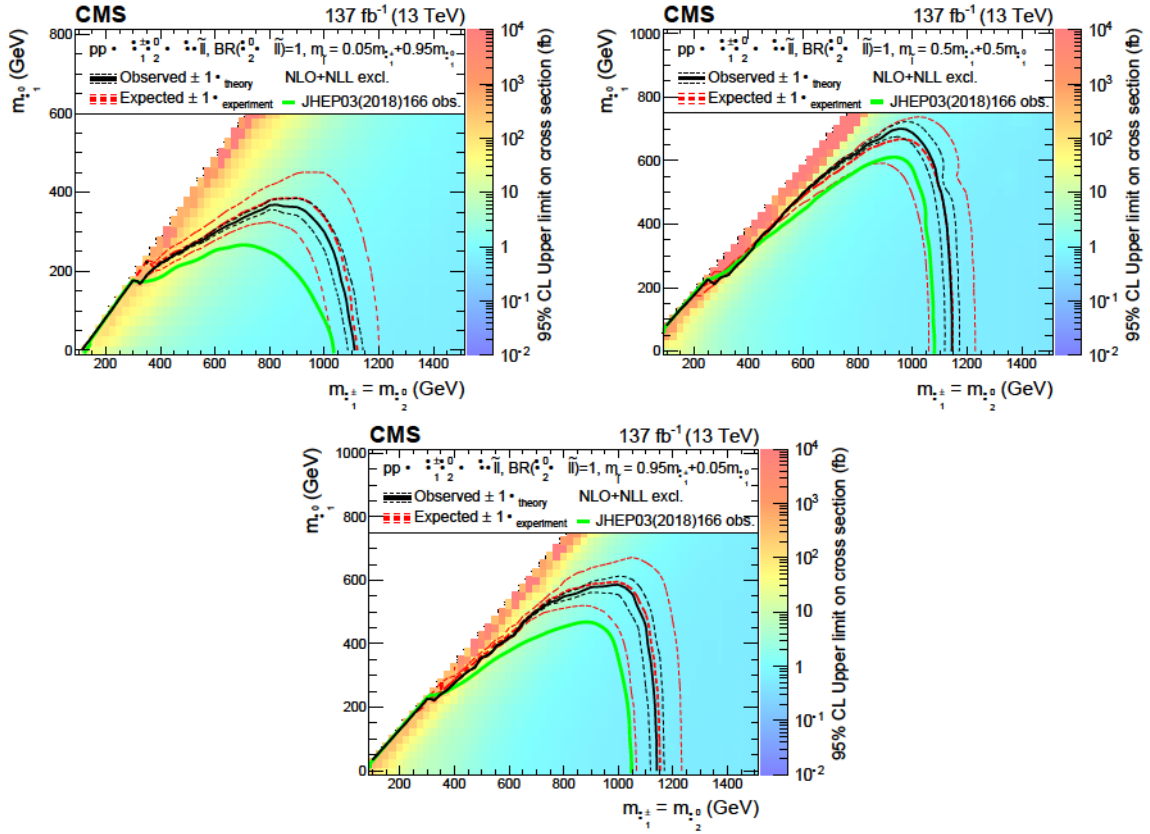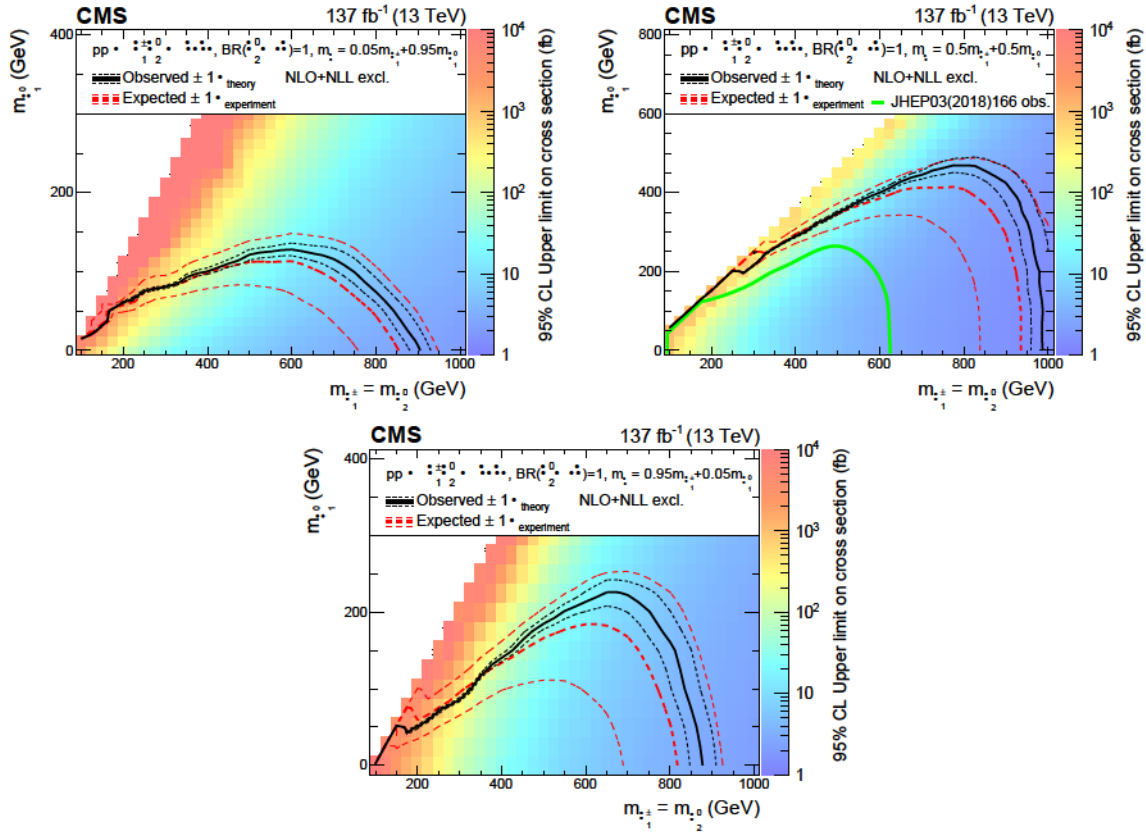
Figure 17: Interpretation of the results for $\widetilde{\chi}_1^{\pm}\widetilde{\chi}_2^0$ production with τ-enriched slepton-mediated decays, and the parameter governing the mass splittings being $x = 0.05$ (upper left), $x = 0.5$ (upper right) and $x = 0.95$ (lower). The shading in the $m_{\widetilde{\chi}_1^0}$ versus $m_{\widetilde{\chi}_2^0}$ plane indicates the 95% CL upper limits on the $\widetilde{\chi}_1^{\pm}\widetilde{\chi}_2^0$ production cross sections. The contours delineate the mass regions excluded at 95% CL when assuming cross sections computed at NLO plus NLL. The observed, observed $\pm 1\sigma_{\mathrm{theory}}$ (± 1 standard deviation of the theoretical cross sections), median expected, and expected $\pm 1\sigma_{\mathrm{experiment}}$ bounds are shown in black and red. The observed limits obtained in the CMS analysis using 2016 data [20] are shown in green.

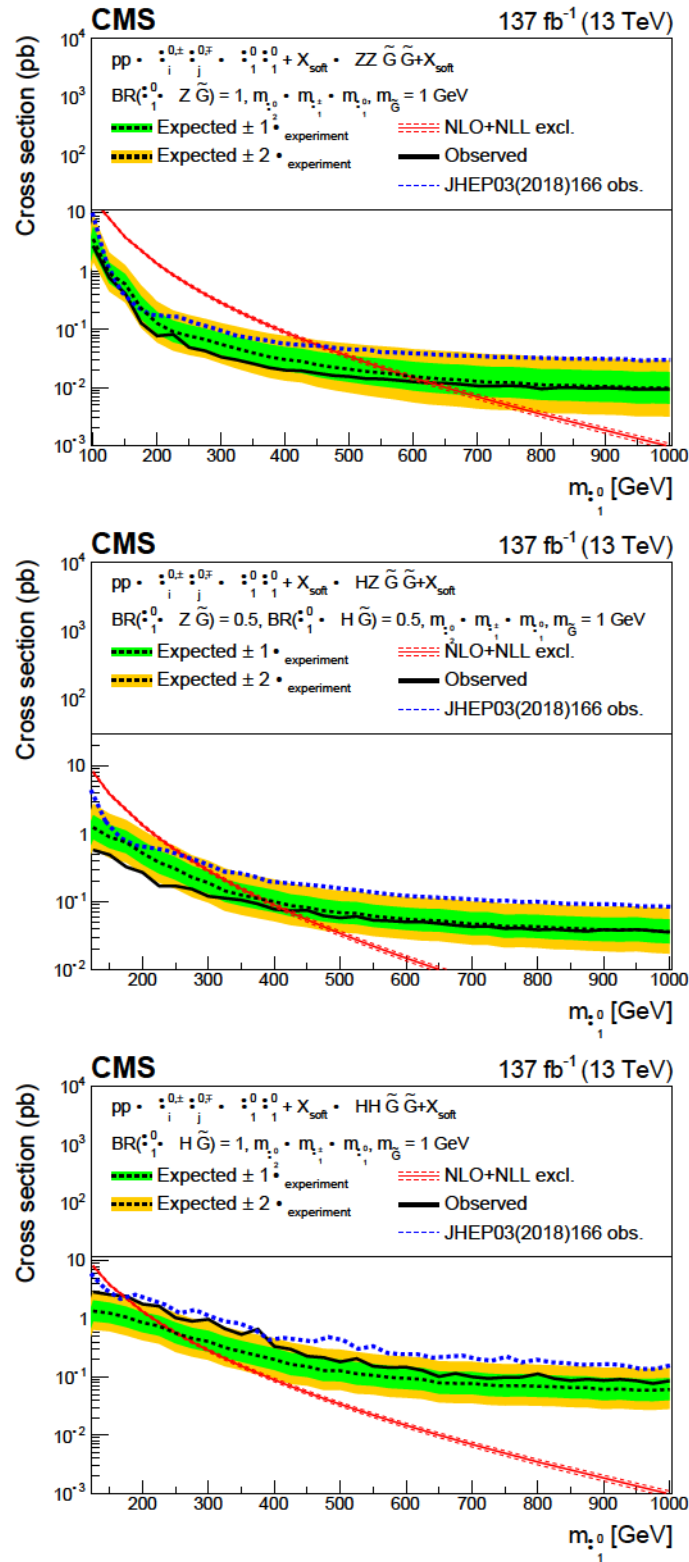Figure 18: Interpretation of the results for $\widetilde{\chi}_1^\pm \widetilde{\chi}_2^0$ production with τ-dominated slepton-mediated decays, and the parameter governing the mass splittings being $x = 0.05$ (upper left), $x = 0.5$ (upper right) and $x = 0.95$ (lower). The shading in the $m_{\widetilde{\chi}_1^0}$ versus $m_{\widetilde{\chi}_2^0}$ plane indicates the 95% CL upper limits on the $\widetilde{\chi}_1^\pm \widetilde{\chi}_2^0$ production cross sections. The contours delineate the mass regions excluded at 95% CL when assuming cross sections computed at NLO plus NLL. The observed, observed $\pm 1\sigma_{\text{theory}}$ (± 1 standard deviation of the theoretical cross sections), median expected, and expected $\pm 1\sigma_{\text{experiment}}$ bounds are shown in black and red. The median expected bound obtained with the search region strategy is shown in blue. The observed limits obtained in the CMS analysis using 2016 data [20] are shown in green, which only included interpretations in the $x = 0.5$ case.
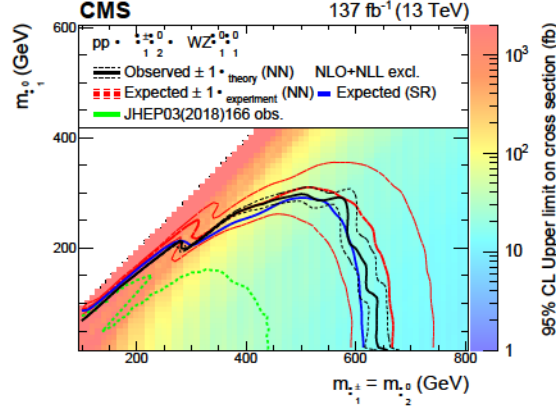
Figure 19: Interpretation of the results for $\widetilde{\chi}_1^\pm \widetilde{\chi}_2^0$ production with WZ-mediated decays. The shading in the $m_{\widetilde{\chi}_1^0}$ versus $m_{\widetilde{\chi}_2^0}$ plane indicates the 95% CL upper limits on the $\widetilde{\chi}_1^\pm \widetilde{\chi}_2^0$ production cross sections. The contours delineate the mass regions excluded at 95% CL when assuming cross sections computed at NLO plus NLL. The observed, observed $\pm 1\sigma_{\text{theory}}$ (± 1 standard deviation of the theoretical cross sections), median expected, and expected $\pm 1\sigma_{\text{experiment}}$ bounds obtained with the neural network strategy are shown in black and red. The median expected bound obtained with the search region strategy is shown in blue. The observed limits obtained in the CMS analysis using 2016 data [20] are shown in green.

Figure 20: Interpretation of the results for $\widetilde{\chi}_1^\pm \widetilde{\chi}_2^0$ production with WH-mediated decays. The shading in the $m_{\widetilde{\chi}_1^0}$ versus $m_{\widetilde{\chi}_2^0}$ plane indicates the 95% CL upper limits on the $\widetilde{\chi}_1^\pm \widetilde{\chi}_2^0$ production cross sections. The contours delineate the mass regions excluded at 95% CL when assuming cross sections computed at NLO plus NLL. The observed, observed $\pm 1\sigma_{\text{theory}}$ (± 1 standard deviation of the theoretical cross sections), median expected, and expected $\pm 1\sigma_{\text{experiment}}$ bounds are shown in black and red. The observed limits obtained in the CMS analysis using 2016 data [20] are shown in green.

Figure 21: Interpretation of the results for effective $\tilde{\chi}_1^0$ pair production, with ZZ-mediated decays (upper), HZ-mediated decays (middle), and HH-mediated decays (lower). The median expected upper limits (black line) are shown along with the $\pm 1\sigma$ (0.16 and 0.84 quantiles, green) and $\pm 2\sigma$ (0.05 and 0.95 quantiles, yellow) bands. The predicted production cross sections computed at NLO plus NLL are shown in red and the observed exclusion limits obtained in the CMS analysis using 2016 data [20] are shown in blue.

11 Summary

A search for new physics in events with two leptons of the same sign, or with three or more leptons with up to two hadronically decaying leptons, is presented. A data set of proton-proton collisions with $\bar{s}$ 13 TeV collected with the CMS detector at the LHC, corresponding to an integrated luminosity of 137 fb ^{1}, is analyzed. Events are categorized according to the number of leptons, their signs, and flavors. Events in each category are further binned using a plethora of kinematic quantities to maximize the sensitivity of the search to an extensive set of hypotheses of supersymmetric particle production via the electroweak interaction. In events with three light leptons, of which two have opposite sign and same flavor, parametric neural networks are used to significantly enhance the sensitivity of the search to several signal hypotheses.

No significant deviation from the standard model expectation is observed in any of the event categories. The results are interpreted in terms of a number of simplified models of superpartner production. Models of chargino-neutralino pair production with the neutralino forming the lightest supersymmetric particle (LSP), as well as models of effective neutralino pair production with a nearly massless gravitino as the LSP are considered. The signal topologies depend on the masses of the leptonic superpartners and the mixing of the gauge eigenstates.

If left-handed sleptons lighter than the chargino existed, the chargino-neutralino pair might undergo slepton-mediated decays resulting in final states with three leptons. The results of the analysis lead to a lower limit in the chargino mass up to 1450 GeV when using a parametric neural network. Searches in events with three light leptons including an opposite-sign, same-flavor pair provide sensitivity to these models. Events with two same-sign leptons further enhance the sensitivity in experimentally challenging scenarios with small mass differences between the chargino and the LSP.

If sleptons were right-handed, the chargino, or both the chargino and the neutralino, might decay almost exclusively to leptons. In the former scenario, a chargino mass up to 1150 GeV is excluded, while a mass up to 970 GeV is excluded in the latter.

If sleptons were sufficiently heavy, charginos and neutralinos would undergo direct decay to the LSP via the emission of W, Z, or Higgs bosons. For decays of the chargino-neutralino pair via a W and a Z boson, values of the chargino mass up to 650 GeV are excluded through the use of a parametric neural network. In case of a neutralino decay via the emission of a Higgs boson, charginos with a mass below 300 GeV are excluded for nearly massless LSPs.

In models of effective neutralino production we assume the neutralinos decay to almost massless gravitino LSPs via Z and Higgs bosons. This leads to excluded values of the neutralino mass up to 600 GeV.

The obtained results currently provide the most stringent limits for chargino-neutralino production with mass splittings close to the Z boson mass, nearly closing the gap in the exclusion plane found in this region of the parameter space. The exclusions obtained for the slepton-mediated decays are as well the most stringent results currently for all the considered branching fraction hypotheses. In the case of the flavor-democratic decay scenario, the obtained exclusion limits of up to 1450 GeV are the overall highest exclusion values obtained for the production of electroweak superpartners.

Acknowledgments

Havens Foundation (USA).

References

[1] P. Ramond, "Dual theory for free fermions", *Phys. Rev. D* **3** (1971) 2415, `doi:10.1103/PhysRevD.3.2415`.

[2] J. Wess and B. Zumino, "A Lagrangian model invariant under supergauge transformations", *Phys. Lett. B* **49** (1974) 52, `doi:10.1016/0370-2693(74)90578-4`.

[3] J. Wess and B. Zumino, "Supergauge transformations in four dimensions", *Nucl. Phys. B* **70** (1974) 39, `doi:10.1016/0550-3213(74)90355-1`.

[4] P. Fayet, "Supergauge invariant extension of the Higgs mechanism and a model for the electron and its neutrino", *Nucl. Phys. B* **90** (1975) 104, `doi:10.1016/0550-3213(75)90636-7`.

[5] H. P. Nilles, "Supersymmetry, supergravity and particle physics", *Phys. Rep.* **110** (1984) 1, `doi:10.1016/0370-1573(84)90008-5`.

[6] S. P. Martin, "A supersymmetry primer", volume 21, p. 1. 2010. `arXiv:hep-ph/9709356. doi:10.1142/9789812839657_0001`.

[7] CMS Collaboration, "Search for supersymmetry in proton-proton collisions at 13 TeV in final states with jets and missing transverse momentum", *JHEP* **10** (2019) 244, `doi:10.1007/JHEP10(2019)244, arXiv:1908.04722`.

[8] CMS Collaboration, "Searches for physics beyond the standard model with the M_{T2} variable in hadronic final states with and without disappearing tracks in proton-proton collisions at $\sqrt{s}$ 13 TeV", *Eur. Phys. J. C* **80** (2020) 3, `doi:10.1140/epjc/s10052-019-7493-x, arXiv:1909.03460`.

[9] CMS Collaboration, "Search for supersymmetry in pp collisions at $\sqrt{s}$ 13 TeV with 137 fb^{-1} in final states with a single lepton using the sum of masses of large-radius jets", *Phys. Rev. D* **101** (2020) 052010, `doi:10.1103/PhysRevD.101.052010, arXiv:1911.07558`.

[10] CMS Collaboration, "Search for physics beyond the standard model in events with jets and two same-sign or at least three charged leptons in proton-proton collisions at $\sqrt{s}$ 13 TeV", *Eur. Phys. J. C* **80** (2020) 752, `doi:10.1140/epjc/s10052-020-8168-3, arXiv:2001.10086`.

[11] CMS Collaboration, "Search for direct top squark pair production in events with one lepton, jets, and missing transverse momentum at 13 TeV with the CMS experiment", *JHEP* **05** (2020) 032, `doi:10.1007/JHEP05(2020)032, arXiv:1912.08887`.

[12] ATLAS Collaboration, "Search for top squarks in events with a Higgs or Z boson using 139 fb^{-1} of pp collision data at $\sqrt{s}$ 13 TeV with the ATLAS detector", *Eur. Phys. J. C* **80** (2020) 1080, `doi:10.1140/epjc/s10052-020-08469-8, arXiv:2006.05880`.

[13] ATLAS Collaboration, "Search for a scalar partner of the top quark in the all-hadronic $t\bar{t}$ plus missing transverse momentum final state at $\sqrt{s}$ 13 TeV with the ATLAS detector", *Eur. Phys. J. C* **80** (2020) 737, `doi:10.1140/epjc/s10052-020-8102-8, arXiv:2004.14060`.

[14] ATLAS Collaboration, "Search for long-lived, massive particles in events with a displaced vertex and a muon with large impact parameter in pp collisions at $\sqrt{s}$ 13 TeV with the ATLAS detector", *Phys. Rev. D* **102** (2020) 032006, `doi:10.1103/PhysRevD.102.032006`, `arXiv:2003.11956`.

[15] ATLAS Collaboration, "Search for squarks and gluinos in final states with same-sign leptons and jets using 139 fb^{-1} of data collected with the ATLAS detector", *JHEP* **06** (2020) 046, `doi:10.1007/JHEP06(2020)046`, `arXiv:1909.08457`.

[16] ATLAS Collaboration, "Search for bottom-squark pair production with the ATLAS detector in final states containing Higgs bosons, b-jets and missing transverse momentum", *JHEP* **12** (2019) 060, `doi:10.1007/JHEP12(2019)060`, `arXiv:1908.03122`.

[17] ATLAS Collaboration, "Search for chargino-neutralino production with mass splittings near the electroweak scale in three-lepton final states in $\sqrt{s}$ 13 TeV pp collisions with the ATLAS detector", *Phys. Rev. D* **101** (2020) 072001, `doi:10.1103/PhysRevD.101.072001`, `arXiv:1912.08479`.

[18] ATLAS Collaboration, "Search for electroweak production of supersymmetric particles in final states with two or three leptons at $\sqrt{s}$ 13 TeV with the ATLAS detector", *Eur. Phys. J. C* **78** (2018) 995, `doi:10.1140/epjc/s10052-018-6423-7`, `arXiv:1803.02762`.

[19] ATLAS Collaboration, "Search for supersymmetry in events with four or more leptons in $\sqrt{s}$ 13 TeV pp collisions with ATLAS", *Phys. Rev. D* **98** (2018) 032009, `doi:10.1103/PhysRevD.98.032009`, `arXiv:1804.03602`.

[20] CMS Collaboration, "Search for electroweak production of charginos and neutralinos in multilepton final states in proton-proton collisions at $\sqrt{s}$ 13 TeV", *JHEP* **03** (2018) 166, `doi:10.1007/JHEP03(2018)166`, `arXiv:1709.05406`.

[21] CMS Collaboration, "Combined search for electroweak production of charginos and neutralinos in proton-proton collisions at $\sqrt{s}$ 13 TeV", *JHEP* **03** (2018) 160, `doi:10.1007/JHEP03(2018)160`, `arXiv:1801.03957`.

[22] P. Baldi et al., "Parameterized neural networks for high-energy physics", *Eur. Phys. J. C* **76** (2016) 235, `doi:10.1140/epjc/s10052-016-4099-4`, `arXiv:1601.07913`.

[23] CMS Collaboration, "The CMS experiment at the CERN LHC", *JINST* **3** (2008) S08004, `doi:10.1088/1748-0221/3/08/S08004`.

[24] CMS Collaboration, "The CMS trigger system", *JINST* **12** (2017) P01020, `doi:10.1088/1748-0221/12/01/P01020`, `arXiv:1609.02366`.

[25] LHC New Physics Working Group Collaboration, "Simplified models for LHC new physics searches", *J. Phys. G* **39** (2012) 105005, `doi:10.1088/0954-3899/39/10/105005`, `arXiv:1105.2838`.

[26] CMS Collaboration, "Interpretation of searches for supersymmetry with simplified models", *Phys. Rev. D* **88** (2013) 052017, `doi:10.1103/PhysRevD.88.052017`, `arXiv:1301.2175`.

44

[27] LHC Higgs Cross Section Working Group, "Handbook of LHC Higgs cross sections: 4. deciphering the nature of the Higgs sector", *CERN* (2016) `doi:10.23731/CYRM-2017-002`, `arXiv:1610.07922`.

[28] K. T. Matchev and S. D. Thomas, "Higgs and Z boson signatures of supersymmetry", *Phys. Rev. D* **62** (2000) 077702, `doi:10.1103/PhysRevD.62.077702`, `arXiv:hep-ph/9908482`.

[29] J. T. Ruderman and D. Shih, "General neutralino NLSPs at the early LHC", *JHEP* **08** (2012) 159, `doi:10.1007/JHEP08(2012)159`, `arXiv:1103.6083`.

[30] P. Meade, M. Reece, and D. Shih, "Prompt decays of general neutralino NLSPs at the Tevatron", *JHEP* **05** (2010) 105, `doi:10.1007/JHEP05(2010)105`, `arXiv:0911.4130`.

[31] W. Beenakker et al., "The production of charginos/neutralinos and sleptons at hadron colliders", *Phys. Rev. Lett.* **83** (1999) 3780, `doi:10.1103/PhysRevLett.83.3780`, `arXiv:hep-ph/9906298`. [Erratum: `doi:10.1103/PhysRevLett.100.029901`].

[32] B. Fuks, M. Klasen, D. R. Lamprea, and M. Rothering, "Gaugino production in proton-proton collisions at a center-of-mass energy of 8 TeV", *JHEP* **10** (2012) 081, `doi:10.1007/JHEP10(2012)081`, `arXiv:1207.2159`.

[33] B. Fuks, M. Klasen, D. R. Lamprea, and M. Rothering, "Precision predictions for electroweak superpartner production at hadron colliders with Resummino", *Eur. Phys. J. C* **73** (2013) 2480, `doi:10.1140/epjc/s10052-013-2480-0`, `arXiv:1304.0790`.

[34] CMS Collaboration, "Particle-flow reconstruction and global event description with the CMS detector", *JINST* **12** (2017) P10003, `doi:10.1088/1748-0221/12/10/P10003`, `arXiv:1706.04965`.

[35] M. Cacciari, G. P. Salam, and G. Soyez, "The anti-k_T jet clustering algorithm", *JHEP* **04** (2008) 063, `doi:10.1088/1126-6708/2008/04/063`, `arXiv:0802.1189`.

[36] M. Cacciari and G. P. Salam, "Dispelling the N^3 myth for the k_t jet-finder", *Phys. Lett. B* **641** (2006) 57, `doi:10.1016/j.physletb.2006.08.037`, `arXiv:hep-ph/0512210`.

[37] M. Cacciari, G. P. Salam, and G. Soyez, "FastJet user manual", *Eur. Phys. J. C* **72** (2012) 1896, `doi:10.1140/epjc/s10052-012-1896-2`, `arXiv:1111.6097`.

[38] CMS Collaboration, "Jet performance in pp collisions at $\sqrt{s}$ 7 TeV", CMS Physics Analysis Summary CMS-PAS-JME-10-003, 2010.

[39] CMS Collaboration, "Determination of jet energy calibration and transverse momentum resolution in CMS", *JINST* **6** (2011) P11002, `doi:10.1088/1748-0221/6/11/P11002`, `arXiv:1107.4277`.

[40] CMS Collaboration, "Jet energy scale and resolution in the CMS experiment in pp collisions at 8 TeV", *JINST* **12** (2017) P02014, `doi:10.1088/1748-0221/12/02/P02014`, `arXiv:1607.03663`.

[41] CMS Collaboration, "Performance of electron reconstruction and selection with the CMS detector in proton-proton collisions at $\sqrt{s}$ = 8 TeV", *JINST* **10** (2015) P06005, `doi:10.1088/1748-0221/10/06/P06005`, `arXiv:1502.02701`.

[42] CMS Collaboration, "Performance of the CMS muon detector and muon reconstruction with proton-proton collisions at $\sqrt{s}$ 13 TeV", *JINST* **13** (2018) P06015, `doi:10.1088/1748-0221/13/06/P06015`, `arXiv:1804.04528`.

[43] CMS Collaboration, "Search for new physics in same-sign dilepton events in proton–proton collisions at $\sqrt{s}$ 13 TeV", *Eur. Phys. J. C* **76** (2016) 439, `doi:10.1140/epjc/s10052-016-4261-z`, `arXiv:1605.03171`.

[44] CMS Collaboration, "Evidence for associated production of a Higgs boson with a top quark pair in final states with electrons, muons, and hadronically decaying leptons at $\sqrt{s}$ 13 TeV", *JHEP* **08** (2018) 066, `doi:10.1007/JHEP08(2018)066`, `arXiv:1803.05485`.

[45] CMS Collaboration, "Observation of single top quark production in association with a Z boson in proton-proton collisions at $\sqrt{s}$ 13 TeV", *Phys. Rev. Lett.* **122** (2019) 132003, `doi:10.1103/PhysRevLett.122.132003`, `arXiv:1812.05900`.

[46] CMS Collaboration, "Performance of b tagging algorithms in proton-proton collisions at 13 TeV with Phase–1 CMS detector", CMS Detector Performance Summary CMS-DP-2018-33, 2018.

[47] CMS Collaboration, "Performance of reconstruction and identification of leptons decaying to hadrons and in pp collisions at $\sqrt{s}$ 13 TeV", *JINST* **13** (2018) P10005, `doi:10.1088/1748-0221/13/10/P10005`, `arXiv:1809.02816`.

[48] CMS Collaboration, "Identification of heavy-flavour jets with the CMS detector in pp collisions at 13 TeV", *JINST* **13** (2018) P05011, `doi:10.1088/1748-0221/13/05/P05011`, `arXiv:1712.07158`.

[49] S. Frixione and B. R. Webber, "Matching NLO QCD computations and parton shower simulations", *JHEP* **06** (2002) 029, `doi:10.1088/1126-6708/2002/06/029`, `arXiv:hep-ph/0204244`.

[50] J. Alwall et al., "The automated computation of tree-level and next-to-leading order differential cross sections, and their matching to parton shower simulations", *JHEP* **07** (2014) 079, `doi:10.1007/JHEP07(2014)079`, `arXiv:1405.0301`.

[51] P. Nason, "A new method for combining NLO QCD with shower Monte Carlo algorithms", *JHEP* **11** (2004) 040, `doi:10.1088/1126-6708/2004/11/040`, `arXiv:hep-ph/0409146`.

[52] S. Frixione, P. Nason, and C. Oleari, "Matching NLO QCD computations with parton shower simulations: the POWHEG method", *JHEP* **11** (2007) 070, `doi:10.1088/1126-6708/2007/11/070`, `arXiv:0709.2092`.

[53] T. Melia, P. Nason, R. Rontsch, and G. Zanderighi, "W W , WZ and ZZ production in the POWHEG BOX", *JHEP* **11** (2011) 078, `doi:10.1007/JHEP11(2011)078`, `arXiv:1107.5051`.

[54] P. Nason and G. Zanderighi, "W W , WZ and ZZ production in the POWHEG-BOX-V2", *Eur. Phys. J. C* **74** (2014) 2702, `doi:10.1140/epjc/s10052-013-2702-5`, `arXiv:1311.1365`.

[55] J. M. Campbell and R. K. Ellis, "MCFM for the Tevatron and the LHC", *Nucl. Phys. B Proc. Suppl.* **10** (2010) 205, `doi:10.1016/j.nuclphysbps.2010.08.011`, `arXiv:1007.3492`.

[56] NNPDF Collaboration, "Parton distributions for the LHC Run II", *JHEP* **04** (2015) 040, `doi:10.1007/JHEP04(2015)040`, `arXiv:1410.8849`.

[57] NNPDF Collaboration, "Parton distributions from high-precision collider data", *Eur. Phys. J. C* **77** (2017) 663, `doi:10.1140/epjc/s10052-017-5199-5`, `arXiv:1706.00428`.

[58] T. Sjöstrand et al., "An Introduction to PYTHIA 8.2", *Comput. Phys. Commun.* **191** (2015) 159, `doi:10.1016/j.cpc.2015.01.024`, `arXiv:1410.3012`.

[59] P. Skands, S. Carrazza, and J. Rojo, "Tuning PYTHIA 8.1: the Monash 2013 Tune", *Eur. Phys. J. C* **74** (2014) 3024, `doi:10.1140/epjc/s10052-014-3024-y`, `arXiv:1404.5630`.

[60] CMS Collaboration, "Event generator tunes obtained from underlying event and multiparton scattering measurements", *Eur. Phys. J. C* **76** (2016) 155, `doi:10.1140/epjc/s10052-016-3988-x`, `arXiv:1512.00815`.

[61] CMS Collaboration, "Extraction and validation of a new set of CMS PYTHIA8 tunes from underlying-event measurements", *Eur. Phys. J. C* **80** (2020) 4, `doi:10.1140/epjc/s10052-019-7499-4`, `arXiv:1903.12179`.

[62] R. Frederix and S. Frixione, "Merging meets matching in MC@NLO", *JHEP* **12** (2012) 061, `doi:10.1007/JHEP12(2012)061`, `arXiv:1209.6215`.

[63] J. Alwall et al., "Comparative study of various algorithms for the merging of parton showers and matrix elements in hadronic collisions", *Eur. Phys. J. C* **53** (2008) 473, `doi:10.1140/epjc/s10052-007-0490-5`, `arXiv:0706.2569`.

[64] B. Fuks, M. Klasen, D. R. Lamprea, and M. Rothering, "Revisiting slepton pair production at the Large Hadron Collider", *JHEP* **01** (2014) 168, `doi:10.1007/JHEP01(2014)168`, `arXiv:1310.2621`.

[65] GEANT4 Collaboration, "GEANT4—a simulation toolkit", *Nucl. Instrum. Meth. A* **506** (2003) 250, `doi:10.1016/S0168-9002(03)01368-8`.

[66] CMS Collaboration, "The fast simulation of the CMS detector at LHC", *J. Phys. Conf. Ser.* **331** (2011) 032049, `doi:10.1088/1742-6596/331/3/032049`.

[67] C. G. Lester and D. J. Summers, "Measuring masses of semiinvisibly decaying particles pair produced at hadron colliders", *Phys. Lett. B* **463** (1999) 99, `doi:10.1016/S0370-2693(99)00945-4`, `arXiv:hep-ph/9906349`.

[68] C. G. Lester, "The stransverse mass, MT2, in special cases", *JHEP* **05** (2011) 076, `doi:10.1007/JHEP05(2011)076`, `arXiv:1103.5682`.

[69] M. Abadi et al., "TensorFlow: Large-scale machine learning on heterogeneous systems", 2016. `arXiv:1603.04467`. Software available from `https://www.tensorflow.org/`.

[70] F. Chollet et al., "Keras", 2015. Software available from `https://keras.io`.

[71] D. P. Kingma and J. Ba, "Adam: A method for stochastic optimization", 2014.

[72] Y. Nesterov, "A method for unconstrained convex minimization problem with the rate of convergence O $1/k^2$ ", *Soviet Math. Dokl.* **269** (1983) 543.

[73] S. Ioffe and C. Szegedy, "Batch normalization: Accelerating deep network training by reducing internal covariate shift", 2015. `arXiv:1502.03167`.

[74] N. Srivastava et al., "Dropout: A simple way to prevent neural networks from overfitting", *JMLR* **15** (2014) 1929, `doi:10.5555/2627435.2670313`.

[75] CMS Collaboration, "Measurement of the inelastic proton-proton cross section at $\bar{s}$ 13 TeV", *JHEP* **07** (2018) 161, `doi:10.1007/JHEP07(2018)161`, `arXiv:1802.02613`.

[76] CMS Collaboration, "CMS luminosity measurement for the 2017 data-taking period at 13 TeV", CMS Physics Analysis Summary CMS-PAS-LUM-17-004, 2018.

[77] CMS Collaboration, "CMS luminosity measurements for the 2016 data-taking period", CMS Physics Analysis Summary CMS-PAS-LUM-17-001, 2017.

[78] CMS Collaboration, "CMS luminosity measurement for the 2018 data-taking period at $\bar{s}$ 13 TeV", CMS Physics Analysis Summary CMS-PAS-LUM-18-002, 2019.

[79] CMS Collaboration, "Search for top-squark pair production in the single-lepton final state in pp collisions at $\bar{s}$ = 8 TeV", *Eur. Phys. J. C* **73** (2013) 2677, `doi:10.1140/epjc/s10052-013-2677-2`, `arXiv:1308.1586`.

[80] R. D. Cousins, "Generalization of chisquare goodness-of-fit test for binned data using saturated models, with application to histograms", 2010. `www.physics.ucla.edu/˜cousins/stats/cousins_saturated.pdf`.

[81] T. Junk, "Confidence level computation for combining searches with small statistics", *Nucl. Instrum. Meth. A* **434** (1999) 435, `doi:10.1016/S0168-9002(99)00498-2`, `arXiv:hep-ex/9902006`.

[82] A. L. Read, "Presentation of search results: the CL$_s$ technique", *J. Phys. G* **28** (2002) 2693, `doi:10.1088/0954-3899/28/10/313`.

[83] G. Cowan, K. Cranmer, E. Gross, and O. Vitells, "Asymptotic formulae for likelihood-based tests of new physics", *Eur. Phys. J. C* **71** (2011) 1554, `doi:10.1140/epjc/s10052-011-1554-0`, `arXiv:1007.1727`. [Erratum: `doi:10.1140/epjc/s10052-013-2501-z`].

[84] ATLAS and CMS Collaborations, and the LHC Higgs Combination Group, "Procedure for the LHC Higgs boson search combination in Summer 2011", technical report, ATL-PHYS-PUB-2011-11, CMS-NOTE-2011-005, 2011.

[85] J. S. Conway, "Incorporating nuisance parameters in likelihoods for multisource spectra", in *Proceedings, workshop on statistical issues related to discovery claims in search experiments and unfolding (PHYSTAT 2011)*, p. 115. 2011. `arXiv:1103.0354`. `doi:10.5170/CERN-2011-006.115`.

[86] R. J. Barlow and C. Beeston, "Fitting using finite Monte Carlo samples", *Comput. Phys. Commun.* **77** (1993) 219, `doi:10.1016/0010-4655(93)90005-W`.

A   The CMS Collaboration

Yerevan Physics Institute, Yerevan, Armenia
A. Tumasyan

Institut für Hochenergiephysik, Wien, Austria
W. Adam, J.W. Andrejkovic, T. Bergauer, S. Chatterjee, M. Dragicevic, A. Escalante Del Valle,
R. Frühwirth[1], M. Jeitler[1], N. Krammer, L. Lechner, D. Liko, I. Mikulec, P. Paulitsch, F.M. Pitters,
J. Schieck[1], R. Schöfbeck, M. Spanring, S. Templ, W. Waltenberger, C.-E. Wulz[1]

Institute for Nuclear Problems, Minsk, Belarus
V. Chekhovsky, A. Litomin, V. Makarenko

Universiteit Antwerpen, Antwerpen, Belgium
M.R. Darwish[2], E.A. De Wolf, X. Janssen, T. Kello[3], A. Lelek, H. Rejeb Sfar, P. Van Mechelen,
S. Van Putte, N. Van Remortel

Vrije Universiteit Brussel, Brussel, Belgium
F. Blekman, E.S. Bols, J. D'Hondt, J. De Clercq, M. Delcourt, H. El Faham, S. Lowette,
S. Moortgat, A. Morton, D. Müller, A.R. Sahasransu, S. Tavernier, W. Van Doninck,
P. Van Mulders

Université Libre de Bruxelles, Bruxelles, Belgium
D. Beghin, B. Bilin, B. Clerbaux, G. De Lentdecker, L. Favart, A. Grebenyuk, A.K. Kalsi, K. Lee,
M. Mahdavikhorrami, I. Makarenko, L. Moureaux, L. Pétré, A. Popov, N. Postiau, E. Starling,
L. Thomas, M. Vanden Bemden, C. Vander Velde, P. Vanlaer, D. Vannerom, L. Wezenbeek

Ghent University, Ghent, Belgium
T. Cornelis, D. Dobur, J. Knolle, L. Lambrecht, G. Mestdach, M. Niedziela, C. Roskas,
A. Samalan, K. Skovpen, T.T. Tran, M. Tytgat, W. Verbeke, B. Vermassen, M. Vit

Université Catholique de Louvain, Louvain-la-Neuve, Belgium
A. Bethani, G. Bruno, F. Bury, C. Caputo, P. David, C. Delaere, I.S. Donertas, A. Giammanco,
K. Jaffel, V. Lemaitre, K. Mondal, J. Prisciandaro, A. Taliercio, M. Teklishyn, P. Vischia, S. Wertz,
S. Wuyckens

Centro Brasileiro de Pesquisas Fisicas, Rio de Janeiro, Brazil
G.A. Alves, C. Hensel, A. Moraes

Universidade do Estado do Rio de Janeiro, Rio de Janeiro, Brazil
W.L. Aldá Júnior, M. Alves Gallo Pereira, M. Barroso Ferreira Filho, H. BRANDAO MAL-
BOUISSON, W. Carvalho, J. Chinellato[4], E.M. Da Costa, G.G. Da Silveira[5], D. De Jesus Damiao,
S. Fonseca De Souza, D. Matos Figueiredo, C. Mora Herrera, K. Mota Amarilo, L. Mundim,
H. Nogima, P. Rebello Teles, A. Santoro, S.M. Silva Do Amaral, A. Sznajder, M. Thiel,
F. Torres Da Silva De Araujo, A. Vilela Pereira

Universidade Estadual Paulista [a], Universidade Federal do ABC [b], São Paulo, Brazil
C.A. Bernardes[a,a], L. Calligaris[a], T.R. Fernandez Perez Tomei[a], E.M. Gregores[a,b], D.S. Lemos[a],
P.G. Mercadante[a,b], S.F. Novaes[a], Sandra S. Padula[a]

**Institute for Nuclear Research and Nuclear Energy, Bulgarian Academy of Sciences, Sofia,
Bulgaria**
A. Aleksandrov, G. Antchev, R. Hadjiiska, P. Iaydjiev, M. Misheva, M. Rodozov, M. Shopova,
G. Sultanov

University of Sofia, Sofia, Bulgaria
A. Dimitrov, T. Ivanov, L. Litov, B. Pavlov, P. Petkov, A. Petrov

Beihang University, Beijing, China
T. Cheng, W. Fang[3], Q. Guo, T. Javaid[6], M. Mittal, H. Wang, L. Yuan

Department of Physics, Tsinghua University, Beijing, China
M. Ahmad, G. Bauer, C. Dozen[7], Z. Hu, J. Martins[8], Y. Wang, K. Yi[9,10]

Institute of High Energy Physics, Beijing, China
E. Chapon, G.M. Chen[6], H.S. Chen[6], M. Chen, F. Iemmi, A. Kapoor, D. Leggat, H. Liao, Z.-A. LIU[6], F. Monti, R. Sharma, J. Tao, J. Thomas-wilsker, J. Wang, H. Zhang, S. Zhang[6], J. Zhao

State Key Laboratory of Nuclear Physics and Technology, Peking University, Beijing, China
A. Agapitos, Y. Ban, C. Chen, Q. Huang, A. Levin, Q. Li, M. Lu, X. Lyu, Y. Mao, S.J. Qian, D. Wang, Q. Wang, J. Xiao

Sun Yat-Sen University, Guangzhou, China
Z. You

Institute of Modern Physics and Key Laboratory of Nuclear Physics and Ion-beam Application (MOE) - Fudan University, Shanghai, China
X. Gao[3], H. Okawa

Zhejiang University, Hangzhou, China
M. Xiao

Universidad de Los Andes, Bogota, Colombia
C. Avila, A. Cabrera, C. Florez, J. Fraga, A. Sarkar, M.A. Segura Delgado

Universidad de Antioquia, Medellin, Colombia
J. Mejia Guisao, F. Ramirez, J.D. Ruiz Alvarez, C.A. Salazar González

University of Split, Faculty of Electrical Engineering, Mechanical Engineering and Naval Architecture, Split, Croatia
D. Giljanovic, N. Godinovic, D. Lelas, I. Puljak

University of Split, Faculty of Science, Split, Croatia
Z. Antunovic, M. Kovac, T. Sculac

Institute Rudjer Boskovic, Zagreb, Croatia
V. Brigljevic, D. Ferencek, D. Majumder, M. Roguljic, A. Starodumov[11], T. Susa

University of Cyprus, Nicosia, Cyprus
A. Attikis, E. Erodotou, A. Ioannou, G. Kole, M. Kolosova, S. Konstantinou, J. Mousa, C. Nicolaou, F. Ptochos, P.A. Razis, H. Rykaczewski, H. Saka

Charles University, Prague, Czech Republic
M. Finger[12], M. Finger Jr.[12], A. Kveton

Escuela Politecnica Nacional, Quito, Ecuador
E. Ayala

Universidad San Francisco de Quito, Quito, Ecuador
E. Carrera Jarrin

Academy of Scientific Research and Technology of the Arab Republic of Egypt, Egyptian Network of High Energy Physics, Cairo, Egypt
A.A. Abdelalim[13,14], S. Khalil[14]

Center for High Energy Physics (CHEP-FU), Fayoum University, El-Fayoum, Egypt
A. Lotfy, M.A. Mahmoud

National Institute of Chemical Physics and Biophysics, Tallinn, Estonia
S. Bhowmik, A. Carvalho Antunes De Oliveira, R.K. Dewanjee, K. Ehataht, M. Kadastik, J. Pata, M. Raidal, C. Veelken

Department of Physics, University of Helsinki, Helsinki, Finland
P. Eerola, L. Forthomme, H. Kirschenmann, K. Osterberg, M. Voutilainen

Helsinki Institute of Physics, Helsinki, Finland
S. Bharthuar, E. Brücken, F. Garcia, J. Havukainen, M.S. Kim, R. Kinnunen, T. Lampén, K. Lassila-Perini, S. Lehti, T. Lindén, M. Lotti, L. Martikainen, J. Ott, H. Siikonen, E. Tuominen, J. Tuominiemi

Lappeenranta University of Technology, Lappeenranta, Finland
P. Luukka, H. Petrow, T. Tuuva

IRFU, CEA, Université Paris-Saclay, Gif-sur-Yvette, France
C. Amendola, M. Besancon, F. Couderc, M. Dejardin, D. Denegri, J.L. Faure, F. Ferri, S. Ganjour, A. Givernaud, P. Gras, G. Hamel de Monchenault, P. Jarry, B. Lenzi, E. Locci, J. Malcles, J. Rander, A. Rosowsky, M.Ö. Sahin, A. Savoy-Navarro[15], M. Titov, G.B. Yu

Laboratoire Leprince-Ringuet, CNRS/IN2P3, Ecole Polytechnique, Institut Polytechnique de Paris, Palaiseau, France
S. Ahuja, F. Beaudette, M. Bonanomi, A. Buchot Perraguin, P. Busson, A. Cappati, C. Charlot, O. Davignon, B. Diab, G. Falmagne, S. Ghosh, R. Granier de Cassagnac, A. Hakimi, I. Kucher, M. Nguyen, C. Ochando, P. Paganini, J. Rembser, R. Salerno, J.B. Sauvan, Y. Sirois, A. Zabi, A. Zghiche

Université de Strasbourg, CNRS, IPHC UMR 7178, Strasbourg, France
J.-L. Agram[16], J. Andrea, D. Apparu, D. Bloch, G. Bourgatte, J.-M. Brom, E.C. Chabert, C. Collard, D. Darej, J.-C. Fontaine[16], U. Goerlach, C. Grimault, A.-C. Le Bihan, E. Nibigira, P. Van Hove

Institut de Physique des 2 Infinis de Lyon (IP2I), Villeurbanne, France
E. Asilar, S. Beauceron, C. Bernet, G. Boudoul, C. Camen, A. Carle, N. Chanon, D. Contardo, P. Depasse, H. El Mamouni, J. Fay, S. Gascon, M. Gouzevitch, B. Ille, Sa. Jain, I.B. Laktineh, H. Lattaud, A. Lesauvage, M. Lethuillier, L. Mirabito, K. Shchablo, L. Torterotot, G. Touquet, M. Vander Donckt, S. Viret

Georgian Technical University, Tbilisi, Georgia
A. Khvedelidze[12], I. Lomidze, Z. Tsamalaidze[12]

RWTH Aachen University, I. Physikalisches Institut, Aachen, Germany
L. Feld, K. Klein, M. Lipinski, D. Meuser, A. Pauls, M.P. Rauch, N. Röwert, J. Schulz, M. Teroerde

RWTH Aachen University, III. Physikalisches Institut A, Aachen, Germany
D. Eliseev, M. Erdmann, P. Fackeldey, B. Fischer, S. Ghosh, T. Hebbeker, K. Hoepfner, F. Ivone, H. Keller, L. Mastrolorenzo, M. Merschmeyer, A. Meyer, G. Mocellin, S. Mondal, S. Mukherjee,

D. Noll, A. Novak, T. Pook, A. Pozdnyakov, Y. Rath, H. Reithler, J. Roemer, A. Schmidt, S.C. Schuler, A. Sharma, S. Wiedenbeck, S. Zaleski

RWTH Aachen University, III. Physikalisches Institut B, Aachen, Germany
C. Dziwok, G. Flügge, W. Haj Ahmad[17], O. Hlushchenko, T. Kress, A. Nowack, C. Pistone, O. Pooth, D. Roy, H. Sert, A. Stahl[18], T. Ziemons

Deutsches Elektronen-Synchrotron, Hamburg, Germany
H. Aarup Petersen, M. Aldaya Martin, P. Asmuss, I. Babounikau, S. Baxter, O. Behnke, A. Bermúdez Martínez, A.A. Bin Anuar, K. Borras[19], V. Botta, D. Brunner, A. Campbell, A. Cardini, C. Cheng, S. Consuegra Rodríguez, G. Correia Silva, V. Danilov, L. Didukh, G. Eckerlin, D. Eckstein, L.I. Estevez Banos, O. Filatov, E. Gallo[20], A. Geiser, A. Giraldi, A. Grohsjean, M. Guthoff, A. Jafari[21], N.Z. Jomhari, H. Jung, A. Kasem[19], M. Kasemann, H. Kaveh, C. Kleinwort, D. Krücker, W. Lange, J. Lidrych, K. Lipka, W. Lohmann[22], R. Mankel, I.-A. Melzer-Pellmann, J. Metwally, A.B. Meyer, M. Meyer, J. Mnich, A. Mussgiller, Y. Otarid, D. Pérez Adán, D. Pitzl, A. Raspereza, B. Ribeiro Lopes, J. Rübenach, A. Saggio, A. Saibel, M. Savitskyi, V. Scheurer, C. Schwanenberger[20], A. Singh, R.E. Sosa Ricardo, D. Stafford, N. Tonon, O. Turkot, M. Van De Klundert, R. Walsh, D. Walter, Y. Wen, K. Wichmann, C. Wissing, S. Wuchterl

University of Hamburg, Hamburg, Germany
R. Aggleton, S. Bein, L. Benato, A. Benecke, P. Connor, K. De Leo, M. Eich, F. Feindt, A. Fröhlich, C. Garbers, E. Garutti, P. Gunnellini, J. Haller, A. Hinzmann, G. Kasieczka, R. Klanner, R. Kogler, T. Kramer, V. Kutzner, J. Lange, T. Lange, A. Lobanov, A. Malara, A. Nigamova, K.J. Pena Rodriguez, O. Rieger, P. Schleper, M. Schröder, J. Schwandt, D. Schwarz, J. Sonneveld, H. Stadie, G. Steinbrück, A. Tews, B. Vormwald, I. Zoi

Karlsruher Institut fuer Technologie, Karlsruhe, Germany
J. Bechtel, T. Berger, E. Butz, R. Caspart, T. Chwalek, W. De Boer[†], A. Dierlamm, A. Droll, K. El Morabit, N. Faltermann, M. Giffels, J.o. Gosewisch, A. Gottmann, F. Hartmann[18], C. Heidecker, U. Husemann, I. Katkov[23], P. Keicher, R. Koppenhöfer, S. Maier, M. Metzler, S. Mitra, Th. Müller, M. Neukum, A. Nürnberg, G. Quast, K. Rabbertz, J. Rauser, D. Savoiu, M. Schnepf, D. Seith, I. Shvetsov, H.J. Simonis, R. Ulrich, J. Van Der Linden, R.F. Von Cube, M. Wassmer, M. Weber, S. Wieland, R. Wolf, S. Wozniewski, S. Wunsch

Institute of Nuclear and Particle Physics (INPP), NCSR Demokritos, Aghia Paraskevi, Greece
G. Anagnostou, P. Asenov, G. Daskalakis, T. Geralis, A. Kyriakis, D. Loukas, A. Stakia

National and Kapodistrian University of Athens, Athens, Greece
M. Diamantopoulou, D. Karasavvas, G. Karathanasis, P. Kontaxakis, C.K. Koraka, A. Manousakis-katsikakis, A. Panagiotou, I. Papavergou, N. Saoulidou, K. Theofilatos, E. Tziaferi, K. Vellidis, E. Vourliotis

National Technical University of Athens, Athens, Greece
G. Bakas, K. Kousouris, I. Papakrivopoulos, G. Tsipolitis, A. Zacharopoulou

University of Ioánnina, Ioánnina, Greece
I. Evangelou, C. Foudas, P. Gianneios, P. Katsoulis, P. Kokkas, N. Manthos, I. Papadopoulos, J. Strologas

MTA-ELTE Lendület CMS Particle and Nuclear Physics Group, Eötvös Loránd University,

Budapest, Hungary
M. Csanad, K. Farkas, M.M.A. Gadallah[24], S. Lökös[25], P. Major, K. Mandal, A. Mehta, G. Pasztor, A.J. Rádl, O. Surányi, G.I. Veres

Wigner Research Centre for Physics, Budapest, Hungary
M. Bartók[26], G. Bencze, C. Hajdu, D. Horvath[27], F. Sikler, V. Veszpremi, G. Vesztergombi[†]

Institute of Nuclear Research ATOMKI, Debrecen, Hungary
S. Czellar, J. Karancsi[26], J. Molnar, Z. Szillasi, D. Teyssier

Institute of Physics, University of Debrecen, Debrecen, Hungary
P. Raics, Z.L. Trocsanyi[28], B. Ujvari

Karoly Robert Campus, MATE Institute of Technology
T. Csorgo[29], F. Nemes[29], T. Novak

Indian Institute of Science (IISc), Bangalore, India
J.R. Komaragiri, D. Kumar, L. Panwar, P.C. Tiwari

National Institute of Science Education and Research, HBNI, Bhubaneswar, India
S. Bahinipati[30], D. Dash, C. Kar, P. Mal, T. Mishra, V.K. Muraleedharan Nair Bindhu[31], A. Nayak[31], P. Saha, N. Sur, S.K. Swain, D. Vats[31]

Panjab University, Chandigarh, India
S. Bansal, S.B. Beri, V. Bhatnagar, G. Chaudhary, S. Chauhan, N. Dhingra[32], R. Gupta, A. Kaur, M. Kaur, S. Kaur, P. Kumari, M. Meena, K. Sandeep, J.B. Singh, A.K. Virdi

University of Delhi, Delhi, India
A. Ahmed, A. Bhardwaj, B.C. Choudhary, R.B. Garg, M. Gola, S. Keshri, A. Kumar, M. Naimuddin, P. Priyanka, K. Ranjan, A. Shah

Saha Institute of Nuclear Physics, HBNI, Kolkata, India
M. Bharti[33], R. Bhattacharya, S. Bhattacharya, D. Bhowmik, S. Dutta, S. Dutta, B. Gomber[34], M. Maity[35], S. Nandan, P. Palit, P.K. Rout, G. Saha, B. Sahu, S. Sarkar, M. Sharan, B. Singh[33], S. Thakur[33]

Indian Institute of Technology Madras, Madras, India
P.K. Behera, S.C. Behera, P. Kalbhor, A. Muhammad, R. Pradhan, P.R. Pujahari, A. Sharma, A.K. Sikdar

Bhabha Atomic Research Centre, Mumbai, India
D. Dutta, V. Jha, V. Kumar, D.K. Mishra, K. Naskar[36], P.K. Netrakanti, L.M. Pant, P. Shukla

Tata Institute of Fundamental Research-A, Mumbai, India
T. Aziz, S. Dugad, M. Kumar, U. Sarkar

Tata Institute of Fundamental Research-B, Mumbai, India
S. Banerjee, S. Bhattacharya, R. Chudasama, M. Guchait, S. Karmakar, S. Kumar, G. Majumder, K. Mazumdar, S. Mukherjee

Indian Institute of Science Education and Research (IISER), Pune, India
K. Alpana, S. Dube, B. Kansal, S. Pandey, A. Rane, A. Rastogi, S. Sharma

Department of Physics, Isfahan University of Technology, Isfahan, Iran
H. Bakhshiansohi[37], M. Zeinali[38]

Institute for Research in Fundamental Sciences (IPM), Tehran, Iran
S. Chenarani[39], S.M. Etesami, M. Khakzad, M. Mohammadi Najafabadi

University College Dublin, Dublin, Ireland
M. Grunewald

INFN Sezione di Bari ^{a}, Università di Bari ^{b}, Politecnico di Bari ^{c}, Bari, Italy
M. Abbrescia^{a,b}, R. Aly^{a,b,40}, C. Aruta^{a,b}, A. Colaleo^a, D. Creanza^{a,c}, N. De Filippis^{a,c}, M. De Palma^{a,b}, A. Di Florio^{a,b}, A. Di Pilato^{a,b}, W. Elmetenawee^{a,b}, L. Fiore^a, A. Gelmi^{a,b}, M. Gul^a, G. Iaselli^{a,c}, M. Ince^{a,b}, S. Lezki^{a,b}, G. Maggi^{a,c}, M. Maggi^a, I. Margjeka^{a,b}, V. Mastrapasqua^{a,b}, J.A. Merlin^a, S. My^{a,b}, S. Nuzzo^{a,b}, A. Pellecchia^{a,b}, A. Pompili^{a,b}, G. Pugliese^{a,c}, A. Ranieri^a, G. Selvaggi^{a,b}, L. Silvestris^a, F.M. Simone^{a,b}, R. Venditti^a, P. Verwilligen^a

INFN Sezione di Bologna ^{a}, Università di Bologna ^{b}, Bologna, Italy
G. Abbiendi^a, C. Battilana^{a,b}, D. Bonacorsi^{a,b}, L. Borgonovi^a, L. Brigliadori^a, R. Campanini^{a,b}, P. Capiluppi^{a,b}, A. Castro^{a,b}, F.R. Cavallo^a, M. Cuffiani^{a,b}, G.M. Dallavalle^a, T. Diotalevi^{a,b}, F. Fabbri^a, A. Fanfani^{a,b}, P. Giacomelli^a, L. Giommi^{a,b}, C. Grandi^a, L. Guiducci^{a,b}, S. Lo Meo^{a,41}, L. Lunerti^{a,b}, S. Marcellini^a, G. Masetti^a, F.L. Navarria^{a,b}, A. Perrotta^a, F. Primavera^{a,b}, A.M. Rossi^{a,b}, T. Rovelli^{a,b}, G.P. Siroli^{a,b}

INFN Sezione di Catania ^{a}, Università di Catania ^{b}, Catania, Italy
S. Albergo^{a,b,42}, S. Costa^{a,b,42}, A. Di Mattia^a, R. Potenza^{a,b}, A. Tricomi^{a,b,42}, C. Tuve^{a,b}

INFN Sezione di Firenze ^{a}, Università di Firenze ^{b}, Firenze, Italy
G. Barbagli^a, A. Cassese^a, R. Ceccarelli^{a,b}, V. Ciulli^{a,b}, C. Civinini^a, R. D'Alessandro^{a,b}, E. Focardi^{a,b}, G. Latino^{a,b}, P. Lenzi^{a,b}, M. Lizzo^{a,b}, M. Meschini^a, S. Paoletti^a, R. Seidita^{a,b}, G. Sguazzoni^a, L. Viliani^a

INFN Laboratori Nazionali di Frascati, Frascati, Italy
L. Benussi, S. Bianco, D. Piccolo

INFN Sezione di Genova ^{a}, Università di Genova ^{b}, Genova, Italy
M. Bozzo^{a,b}, F. Ferro^a, R. Mulargia^{a,b}, E. Robutti^a, S. Tosi^{a,b}

INFN Sezione di Milano-Bicocca ^{a}, Università di Milano-Bicocca ^{b}, Milano, Italy
A. Benaglia^a, F. Brivio^{a,b}, F. Cetorelli^{a,b}, V. Ciriolo^{a,b,18}, F. De Guio^{a,b}, M.E. Dinardo^{a,b}, P. Dini^a, S. Gennai^a, A. Ghezzi^{a,b}, P. Govoni^{a,b}, L. Guzzi^{a,b}, M. Malberti^a, S. Malvezzi^a, A. Massironi^a, D. Menasce^a, L. Moroni^a, M. Paganoni^{a,b}, D. Pedrini^a, S. Ragazzi^{a,b}, N. Redaelli^a, T. Tabarelli de Fatis^{a,b}, D. Valsecchi^{a,b,18}, D. Zuolo^{a,b}

INFN Sezione di Napoli ^{a}, Università di Napoli 'Federico II' ^{b}, Napoli, Italy, Università della Basilicata ^{c}, Potenza, Italy, Università G. Marconi ^{d}, Roma, Italy
S. Buontempo^a, F. Carnevali^{a,b}, N. Cavallo^{a,c}, A. De Iorio^{a,b}, F. Fabozzi^{a,c}, A.O.M. Iorio^{a,b}, L. Lista^{a,b}, S. Meola^{a,d,18}, P. Paolucci^{a,18}, B. Rossi^a, C. Sciacca^{a,b}

INFN Sezione di Padova ^{a}, Università di Padova ^{b}, Padova, Italy, Università di Trento ^{c}, Trento, Italy
P. Azzi^a, N. Bacchetta^a, D. Bisello^{a,b}, P. Bortignon^a, A. Bragagnolo^{a,b}, R. Carlin^{a,b}, P. Checchia^a, P. De Castro Manzano^a, T. Dorigo^a, U. Dosselli^a, F. Gasparini^{a,b}, U. Gasparini^{a,b}, S.Y. Hoh^{a,b}, L. Layer^{a,43}, M. Margoni^{a,b}, A.T. Meneguzzo^{a,b}, J. Pazzini^{a,b}, M. Presilla^{a,b}, P. Ronchese^{a,b}, R. Rossin^{a,b}, F. Simonetto^{a,b}, G. Strong^a, M. Tosi^{a,b}, H. YARAR^{a,b}, M. Zanetti^{a,b}, P. Zotto^{a,b}, A. Zucchetta^{a,b}, G. Zumerle^{a,b}

INFN Sezione di Pavia ^{a}, Università di Pavia ^{b}, Pavia, Italy
C. Aime'^{a,b}, A. Braghieri^a, S. Calzaferri^{a,b}, D. Fiorina^{a,b}, P. Montagna^{a,b}, S.P. Ratti^{a,b}, V. Re^a, M. Ressegotti^{a,b}, C. Riccardi^{a,b}, P. Salvini^a, I. Vai^a, P. Vitulo^{a,b}

INFN Sezione di Perugia ^{a}, Università di Perugia ^{b}, Perugia, Italy
G.M. Bilei^a, D. Ciangottini^{a,b}, L. Fanò^{a,b}, P. Lariccia^{a,b}, M. Magherini^b, G. Mantovani^{a,b}, V. Mariani^{a,b}, M. Menichelli^a, F. Moscatelli^a, A. Piccinelli^{a,b}, A. Rossi^{a,b}, A. Santocchia^{a,b}, D. Spiga^a, T. Tedeschi^{a,b}

INFN Sezione di Pisa ^{a}, Università di Pisa ^{b}, Scuola Normale Superiore di Pisa ^{c}, Pisa Italy, Università di Siena ^{d}, Siena, Italy
P. Azzurri^a, G. Bagliesi^a, V. Bertacchi^{a,c}, L. Bianchini^a, T. Boccali^a, E. Bossini^{a,b}, R. Castaldi^a, M.A. Ciocci^{a,b}, R. Dell'Orso^a, M.R. Di Domenico^{a,d}, S. Donato^a, A. Giassi^a, M.T. Grippo^a, F. Ligabue^{a,c}, E. Manca^{a,c}, G. Mandorli^{a,c}, A. Messineo^{a,b}, F. Palla^a, S. Parolia^{a,b}, G. Ramirez-Sanchez^{a,c}, A. Rizzi^{a,b}, G. Rolandi^{a,c}, S. Roy Chowdhury^{a,c}, A. Scribano^a, N. Shafiei^{a,b}, P. Spagnolo^a, R. Tenchini^a, G. Tonelli^{a,b}, N. Turini^{a,d}, A. Venturi^a, P.G. Verdini^a

INFN Sezione di Roma ^{a}, Sapienza Università di Roma ^{b}, Rome, Italy
M. Campana^{a,b}, F. Cavallari^a, M. Cipriani^{a,b}, D. Del Re^{a,b}, E. Di Marco^a, M. Diemoz^a, E. Longo^{a,b}, P. Meridiani^a, G. Organtini^{a,b}, F. Pandolfi^a, R. Paramatti^{a,b}, C. Quaranta^{a,b}, S. Rahatlou^{a,b}, C. Rovelli^a, F. Santanastasio^{a,b}, L. Soffi^a, R. Tramontano^{a,b}

INFN Sezione di Torino ^{a}, Università di Torino ^{b}, Torino, Italy, Università del Piemonte Orientale ^{c}, Novara, Italy
N. Amapane^{a,b}, R. Arcidiacono^{a,c}, S. Argiro^{a,b}, M. Arneodo^{a,c}, N. Bartosik^a, R. Bellan^{a,b}, A. Bellora^{a,b}, J. Berenguer Antequera^{a,b}, C. Biino^a, N. Cartiglia^a, S. Cometti^a, M. Costa^{a,b}, R. Covarelli^{a,b}, N. Demaria^a, B. Kiani^{a,b}, F. Legger^a, C. Mariotti^a, S. Maselli^a, E. Migliore^{a,b}, E. Monteil^{a,b}, M. Monteno^a, M.M. Obertino^{a,b}, G. Ortona^a, L. Pacher^{a,b}, N. Pastrone^a, M. Pelliccioni^a, G.L. Pinna Angioni^{a,b}, M. Ruspa^{a,c}, R. Salvatico^{a,b}, K. Shchelina^{a,b}, F. Siviero^{a,b}, V. Sola^a, A. Solano^{a,b}, D. Soldi^{a,b}, A. Staiano^a, M. Tornago^{a,b}, D. Trocino^{a,b}, A. Vagnerini

INFN Sezione di Trieste ^{a}, Università di Trieste ^{b}, Trieste, Italy
S. Belforte^a, V. Candelise^{a,b}, M. Casarsa^a, F. Cossutti^a, A. Da Rold^{a,b}, G. Della Ricca^{a,b}, G. Sorrentino^{a,b}, F. Vazzoler^{a,b}

Kyungpook National University, Daegu, Korea
S. Dogra, C. Huh, B. Kim, D.H. Kim, G.N. Kim, J. Kim, J. Lee, S.W. Lee, C.S. Moon, Y.D. Oh, S.I. Pak, B.C. Radburn-Smith, S. Sekmen, Y.C. Yang

Chonnam National University, Institute for Universe and Elementary Particles, Kwangju, Korea
H. Kim, D.H. Moon

Hanyang University, Seoul, Korea
B. Francois, T.J. Kim, J. Park

Korea University, Seoul, Korea
S. Cho, S. Choi, Y. Go, B. Hong, K. Lee, K.S. Lee, J. Lim, J. Park, S.K. Park, J. Yoo

Kyung Hee University, Department of Physics, Seoul, Republic of Korea
J. Goh, A. Gurtu

Sejong University, Seoul, Korea
H.S. Kim, Y. Kim

Seoul National University, Seoul, Korea
J. Almond, J.H. Bhyun, J. Choi, S. Jeon, J. Kim, J.S. Kim, S. Ko, H. Kwon, H. Lee, S. Lee, B.H. Oh, M. Oh, S.B. Oh, H. Seo, U.K. Yang, I. Yoon

University of Seoul, Seoul, Korea
W. Jang, D. Jeon, D.Y. Kang, Y. Kang, J.H. Kim, S. Kim, B. Ko, J.S.H. Lee, Y. Lee, I.C. Park, Y. Roh, D. Song, I.J. Watson, S. Yang

Yonsei University, Department of Physics, Seoul, Korea
S. Ha, H.D. Yoo

Sungkyunkwan University, Suwon, Korea
Y. Jeong, H. Lee, Y. Lee, I. Yu

College of Engineering and Technology, American University of the Middle East (AUM), Egaila, Kuwait
T. Beyrouthy, Y. Maghrbi

Riga Technical University, Riga, Latvia
T. Torims, V. Veckalns[44]

Vilnius University, Vilnius, Lithuania
M. Ambrozas, A. Juodagalvis, A. Rinkevicius, G. Tamulaitis, A. Vaitkevicius

National Centre for Particle Physics, Universiti Malaya, Kuala Lumpur, Malaysia
N. Bin Norjoharuddeen, W.A.T. Wan Abdullah, M.N. Yusli, Z. Zolkapli

Universidad de Sonora (UNISON), Hermosillo, Mexico
J.F. Benitez, A. Castaneda Hernandez, M. León Coello, J.A. Murillo Quijada, A. Sehrawat, L. Valencia Palomo

Centro de Investigacion y de Estudios Avanzados del IPN, Mexico City, Mexico
G. Ayala, H. Castilla-Valdez, I. Heredia-De La Cruz[45], R. Lopez-Fernandez, C.A. Mondragon Herrera, D.A. Perez Navarro, A. Sanchez-Hernandez

Universidad Iberoamericana, Mexico City, Mexico
S. Carrillo Moreno, C. Oropeza Barrera, M. Ramirez-Garcia, F. Vazquez Valencia

Benemerita Universidad Autonoma de Puebla, Puebla, Mexico
I. Pedraza, H.A. Salazar Ibarguen, C. Uribe Estrada

University of Montenegro, Podgorica, Montenegro
J. Mijuskovic[46], N. Raicevic

University of Auckland, Auckland, New Zealand
D. Krofcheck

University of Canterbury, Christchurch, New Zealand
S. Bheesette, P.H. Butler

National Centre for Physics, Quaid-I-Azam University, Islamabad, Pakistan
A. Ahmad, M.I. Asghar, A. Awais, M.I.M. Awan, H.R. Hoorani, W.A. Khan, M.A. Shah, M. Shoaib, M. Waqas

AGH University of Science and Technology Faculty of Computer Science, Electronics and Telecommunications, Krakow, Poland
V. Avati, L. Grzanka, M. Malawski

National Centre for Nuclear Research, Swierk, Poland
H. Bialkowska, M. Bluj, B. Boimska, M. Górski, M. Kazana, M. Szleper, P. Zalewski

Institute of Experimental Physics, Faculty of Physics, University of Warsaw, Warsaw, Poland
K. Bunkowski, K. Doroba, A. Kalinowski, M. Konecki, J. Krolikowski, M. Walczak

Laboratório de Instrumentação e Física Experimental de Partículas, Lisboa, Portugal
M. Araujo, P. Bargassa, D. Bastos, A. Boletti, P. Faccioli, M. Gallinaro, J. Hollar, N. Leonardo, T. Niknejad, M. Pisano, J. Seixas, O. Toldaiev, J. Varela

Joint Institute for Nuclear Research, Dubna, Russia
S. Afanasiev, D. Budkouski, I. Golutvin, I. Gorbunov, V. Karjavine, V. Korenkov, A. Lanev, A. Malakhov, V. Matveev[47,48], V. Palichik, V. Perelygin, M. Savina, D. Seitova, V. Shalaev, S. Shmatov, S. Shulha, V. Smirnov, O. Teryaev, N. Voytishin, B.S. Yuldashev[49], A. Zarubin, I. Zhizhin

Petersburg Nuclear Physics Institute, Gatchina (St. Petersburg), Russia
G. Gavrilov, V. Golovtcov, Y. Ivanov, V. Kim[50], E. Kuznetsova[51], V. Murzin, V. Oreshkin, I. Smirnov, D. Sosnov, V. Sulimov, L. Uvarov, S. Volkov, A. Vorobyev

Institute for Nuclear Research, Moscow, Russia
Yu. Andreev, A. Dermenev, S. Gninenko, N. Golubev, A. Karneyeu, D. Kirpichnikov, M. Kirsanov, N. Krasnikov, A. Pashenkov, G. Pivovarov, D. Tlisov[†], A. Toropin

Institute for Theoretical and Experimental Physics named by A.I. Alikhanov of NRC 'Kurchatov Institute', Moscow, Russia
V. Epshteyn, V. Gavrilov, N. Lychkovskaya, A. Nikitenko[52], V. Popov, A. Spiridonov, A. Stepennov, M. Toms, E. Vlasov, A. Zhokin

Moscow Institute of Physics and Technology, Moscow, Russia
T. Aushev

National Research Nuclear University 'Moscow Engineering Physics Institute' (MEPhI), Moscow, Russia
M. Chadeeva[53], A. Oskin, P. Parygin, E. Popova, E. Zhemchugov[54]

P.N. Lebedev Physical Institute, Moscow, Russia
V. Andreev, M. Azarkin, I. Dremin, M. Kirakosyan, A. Terkulov

Skobeltsyn Institute of Nuclear Physics, Lomonosov Moscow State University, Moscow, Russia
A. Belyaev, E. Boos, V. Bunichev, M. Dubinin[55], L. Dudko, A. Gribushin, V. Klyukhin, O. Kodolova, I. Lokhtin, S. Obraztsov, M. Perfilov, S. Petrushanko, V. Savrin

Novosibirsk State University (NSU), Novosibirsk, Russia
V. Blinov[56], T. Dimova[56], L. Kardapoltsev[56], A. Kozyrev[56], I. Ovtin[56], Y. Skovpen[56]

Institute for High Energy Physics of National Research Centre 'Kurchatov Institute', Protvino, Russia
I. Azhgirey, I. Bayshev, D. Elumakhov, V. Kachanov, D. Konstantinov, P. Mandrik, V. Petrov, R. Ryutin, S. Slabospitskii, A. Sobol, S. Troshin, N. Tyurin, A. Uzunian, A. Volkov

National Research Tomsk Polytechnic University, Tomsk, Russia
A. Babaev, V. Okhotnikov

Tomsk State University, Tomsk, Russia
V. Borchsh, V. Ivanchenko, E. Tcherniaev

University of Belgrade: Faculty of Physics and VINCA Institute of Nuclear Sciences, Belgrade, Serbia
P. Adzic[57], M. Dordevic, P. Milenovic, J. Milosevic, V. Milosevic

Centro de Investigaciones Energéticas Medioambientales y Tecnológicas (CIEMAT), Madrid, Spain
M. Aguilar-Benitez, J. Alcaraz Maestre, A. Álvarez Fernández, I. Bachiller, M. Barrio Luna, Cristina F. Bedoya, C.A. Carrillo Montoya, M. Cepeda, M. Cerrada, N. Colino, B. De La Cruz, A. Delgado Peris, J.P. Fernández Ramos, J. Flix, M.C. Fouz, O. Gonzalez Lopez, S. Goy Lopez, J.M. Hernandez, M.I. Josa, J. León Holgado, D. Moran, Á. Navarro Tobar, A. Pérez-Calero Yzquierdo, J. Puerta Pelayo, I. Redondo, L. Romero, S. Sánchez Navas, L. Urda Gómez, C. Willmott

Universidad Autónoma de Madrid, Madrid, Spain
J.F. de Trocóniz, R. Reyes-Almanza

Universidad de Oviedo, Instituto Universitario de Ciencias y Tecnologías Espaciales de Asturias (ICTEA), Oviedo, Spain
B. Alvarez Gonzalez, J. Cuevas, C. Erice, J. Fernandez Menendez, S. Folgueras, I. Gonzalez Caballero, E. Palencia Cortezon, C. Ramón Álvarez, J. Ripoll Sau, V. Rodríguez Bouza, A. Trapote, N. Trevisani

Instituto de Física de Cantabria (IFCA), CSIC-Universidad de Cantabria, Santander, Spain
J.A. Brochero Cifuentes, I.J. Cabrillo, A. Calderon, B. Chazin Quero, J. Duarte Campderros, M. Fernandez, C. Fernandez Madrazo, P.J. Fernández Manteca, A. García Alonso, G. Gomez, C. Martinez Rivero, P. Martinez Ruiz del Arbol, F. Matorras, P. Matorras Cuevas, J. Piedra Gomez, C. Prieels, T. Rodrigo, A. Ruiz-Jimeno, L. Scodellaro, I. Vila, J.M. Vizan Garcia

University of Colombo, Colombo, Sri Lanka
MK Jayananda, B. Kailasapathy[58], D.U.J. Sonnadara, DDC Wickramarathna

University of Ruhuna, Department of Physics, Matara, Sri Lanka
W.G.D. Dharmaratna, K. Liyanage, N. Perera, N. Wickramage

CERN, European Organization for Nuclear Research, Geneva, Switzerland
T.K. Aarrestad, D. Abbaneo, J. Alimena, E. Auffray, G. Auzinger, J. Baechler, P. Baillon[†], D. Barney, J. Bendavid, M. Bianco, A. Bocci, T. Camporesi, M. Capeans Garrido, G. Cerminara, S.S. Chhibra, L. Cristella, D. d'Enterria, A. Dabrowski, N. Daci, A. David, A. De Roeck, M.M. Defranchis, M. Deile, M. Dobson, M. Dünser, N. Dupont, A. Elliott-Peisert, N. Emriskova, F. Fallavollita[59], D. Fasanella, S. Fiorendi, A. Florent, G. Franzoni, W. Funk, S. Giani, D. Gigi, K. Gill, F. Glege, L. Gouskos, M. Haranko, J. Hegeman, Y. Iiyama, V. Innocente, T. James, P. Janot, J. Kaspar, J. Kieseler, M. Komm, N. Kratochwil, C. Lange, S. Laurila, P. Lecoq, K. Long, C. Lourenço, L. Malgeri, S. Mallios, M. Mannelli, A.C. Marini, F. Meijers, S. Mersi, E. Meschi, F. Moortgat, M. Mulders, S. Orfanelli, L. Orsini, F. Pantaleo, L. Pape, E. Perez, M. Peruzzi, A. Petrilli, G. Petrucciani, A. Pfeiffer, M. Pierini, D. Piparo, M. Pitt, H. Qu, T. Quast, D. Rabady, A. Racz, M. Rieger, M. Rovere, H. Sakulin, J. Salfeld-Nebgen, S. Scarfi, C. Schäfer, C. Schwick, M. Selvaggi, A. Sharma, P. Silva, W. Snoeys, P. Sphicas[60], S. Summers, V.R. Tavolaro, D. Treille, A. Tsirou, G.P. Van Onsem, M. Verzetti, J. Wanczyk[61], K.A. Wozniak, W.D. Zeuner

Paul Scherrer Institut, Villigen, Switzerland

L. Caminada[62], A. Ebrahimi, W. Erdmann, R. Horisberger, Q. Ingram, H.C. Kaestli, D. Kotlinski, U. Langenegger, M. Missiroli, T. Rohe

ETH Zurich - Institute for Particle Physics and Astrophysics (IPA), Zurich, Switzerland
K. Androsov[61], M. Backhaus, P. Berger, A. Calandri, N. Chernyavskaya, A. De Cosa, G. Dissertori, M. Dittmar, M. Donegà, C. Dorfer, F. Eble, T.A. Gómez Espinosa, C. Grab, D. Hits, W. Lustermann, A.-M. Lyon, R.A. Manzoni, C. Martin Perez, M.T. Meinhard, F. Micheli, F. Nessi-Tedaldi, J. Niedziela, F. Pauss, V. Perovic, G. Perrin, S. Pigazzini, M.G. Ratti, M. Reichmann, C. Reissel, T. Reitenspiess, B. Ristic, D. Ruini, D.A. Sanz Becerra, M. Schönenberger, V. Stampf, J. Steggemann[61], R. Wallny, D.H. Zhu

Universität Zürich, Zurich, Switzerland
C. Amsler[63], P. Bärtschi, C. Botta, D. Brzhechko, M.F. Canelli, K. Cormier, A. De Wit, R. Del Burgo, J.K. Heikkilä, M. Huwiler, A. Jofrehei, B. Kilminster, S. Leontsinis, A. Macchiolo, P. Meiring, V.M. Mikuni, U. Molinatti, I. Neutelings, G. Rauco, A. Reimers, P. Robmann, S. Sanchez Cruz, K. Schweiger, Y. Takahashi

National Central University, Chung-Li, Taiwan
C. Adloff[64], C.M. Kuo, W. Lin, A. Roy, T. Sarkar[35], S.S. Yu

National Taiwan University (NTU), Taipei, Taiwan
L. Ceard, Y. Chao, K.F. Chen, P.H. Chen, W.-S. Hou, Y.y. Li, R.-S. Lu, E. Paganis, A. Psallidas, A. Steen, E. Yazgan, P.r. Yu

Chulalongkorn University, Faculty of Science, Department of Physics, Bangkok, Thailand
B. Asavapibhop, C. Asawatangtrakuldee, N. Srimanobhas

Çukurova University, Physics Department, Science and Art Faculty, Adana, Turkey
F. Boran, S. Damarseckin[65], Z.S. Demiroglu, F. Dolek, I. Dumanoglu[66], E. Eskut, Y. Guler, E. Gurpinar Guler[67], I. Hos[68], C. Isik, O. Kara, A. Kayis Topaksu, U. Kiminsu, G. Onengut, K. Ozdemir[69], A. Polatoz, A.E. Simsek, B. Tali[70], U.G. Tok, S. Turkcapar, I.S. Zorbakir, C. Zorbilmez

Middle East Technical University, Physics Department, Ankara, Turkey
B. Isildak[71], G. Karapinar[72], K. Ocalan[73], M. Yalvac[74]

Bogazici University, Istanbul, Turkey
B. Akgun, I.O. Atakisi, E. Gülmez, M. Kaya[75], O. Kaya[76], Ö. Özçelik, S. Tekten[77], E.A. Yetkin[78]

Istanbul Technical University, Istanbul, Turkey
A. Cakir, K. Cankocak[66], Y. Komurcu, S. Sen[79]

Istanbul University, Istanbul, Turkey
S. Cerci[70], B. Kaynak, S. Ozkorucuklu, D. Sunar Cerci[70]

Institute for Scintillation Materials of National Academy of Science of Ukraine, Kharkov, Ukraine
B. Grynyov

National Scientific Center, Kharkov Institute of Physics and Technology, Kharkov, Ukraine
L. Levchuk

University of Bristol, Bristol, United Kingdom
D. Anthony, E. Bhal, S. Bologna, J.J. Brooke, A. Bundock, E. Clement, D. Cussans, H. Flacher, J. Goldstein, G.P. Heath, H.F. Heath, L. Kreczko, B. Krikler, S. Paramesvaran, S. Seif El Nasr-Storey, V.J. Smith, N. Stylianou[80], R. White

Rutherford Appleton Laboratory, Didcot, United Kingdom
K.W. Bell, A. Belyaev[81], C. Brew, R.M. Brown, D.J.A. Cockerill, K.V. Ellis, K. Harder, S. Harper, J. Linacre, K. Manolopoulos, D.M. Newbold, E. Olaiya, D. Petyt, T. Reis, T. Schuh, C.H. Shepherd-Themistocleous, I.R. Tomalin, T. Williams

Imperial College, London, United Kingdom
R. Bainbridge, P. Bloch, S. Bonomally, J. Borg, S. Breeze, O. Buchmuller, V. Cepaitis, G.S. Chahal[82], D. Colling, P. Dauncey, G. Davies, M. Della Negra, S. Fayer, G. Fedi, G. Hall, M.H. Hassanshahi, G. Iles, J. Langford, L. Lyons, A.-M. Magnan, S. Malik, A. Martelli, J. Nash[83], M. Pesaresi, D.M. Raymond, A. Richards, A. Rose, E. Scott, C. Seez, A. Shtipliyski, A. Tapper, K. Uchida, T. Virdee[18], N. Wardle, S.N. Webb, D. Winterbottom, A.G. Zecchinelli

Brunel University, Uxbridge, United Kingdom
K. Coldham, J.E. Cole, A. Khan, P. Kyberd, I.D. Reid, L. Teodorescu, S. Zahid

Baylor University, Waco, USA
S. Abdullin, A. Brinkerhoff, B. Caraway, J. Dittmann, K. Hatakeyama, A.R. Kanuganti, B. McMaster, N. Pastika, S. Sawant, C. Smith, C. Sutantawibul, J. Wilson

Catholic University of America, Washington, DC, USA
R. Bartek, A. Dominguez, R. Uniyal, A.M. Vargas Hernandez

The University of Alabama, Tuscaloosa, USA
A. Buccilli, S.I. Cooper, D. Di Croce, S.V. Gleyzer, C. Henderson, C.U. Perez, P. Rumerio[84], C. West

Boston University, Boston, USA
A. Akpinar, A. Albert, D. Arcaro, C. Cosby, Z. Demiragli, E. Fontanesi, D. Gastler, J. Rohlf, K. Salyer, D. Sperka, D. Spitzbart, I. Suarez, A. Tsatsos, S. Yuan, D. Zou

Brown University, Providence, USA
G. Benelli, B. Burkle, X. Coubez[19], D. Cutts, Y.t. Duh, M. Hadley, U. Heintz, J.M. Hogan[85], G. Landsberg, K.T. Lau, J. Lee, M. Lukasik, J. Luo, M. Narain, S. Sagir[86], E. Usai, W.Y. Wong, X. Yan, D. Yu, W. Zhang

University of California, Davis, Davis, USA
J. Bonilla, C. Brainerd, R. Breedon, M. Calderon De La Barca Sanchez, M. Chertok, J. Conway, P.T. Cox, R. Erbacher, G. Haza, F. Jensen, O. Kukral, R. Lander, M. Mulhearn, D. Pellett, B. Regnery, D. Taylor, Y. Yao, F. Zhang

University of California, Los Angeles, USA
M. Bachtis, R. Cousins, A. Datta, D. Hamilton, J. Hauser, M. Ignatenko, M.A. Iqbal, T. Lam, N. Mccoll, W.A. Nash, S. Regnard, D. Saltzberg, B. Stone, V. Valuev

University of California, Riverside, Riverside, USA
K. Burt, Y. Chen, R. Clare, J.W. Gary, M. Gordon, G. Hanson, G. Karapostoli, O.R. Long, N. Manganelli, M. Olmedo Negrete, W. Si, S. Wimpenny, Y. Zhang

University of California, San Diego, La Jolla, USA
J.G. Branson, P. Chang, S. Cittolin, S. Cooperstein, N. Deelen, J. Duarte, R. Gerosa, L. Giannini, D. Gilbert, J. Guiang, R. Kansal, V. Krutelyov, R. Lee, J. Letts, M. Masciovecchio, S. May, M. Pieri, B.V. Sathia Narayanan, V. Sharma, M. Tadel, A. Vartak, F. Würthwein, Y. Xiang, A. Yagil

University of California, Santa Barbara - Department of Physics, Santa Barbara, USA
N. Amin, C. Campagnari, M. Citron, A. Dorsett, V. Dutta, J. Incandela, M. Kilpatrick, J. Kim, B. Marsh, H. Mei, M. Oshiro, M. Quinnan, J. Richman, U. Sarica, D. Stuart, S. Wang

California Institute of Technology, Pasadena, USA
A. Bornheim, O. Cerri, I. Dutta, J.M. Lawhorn, N. Lu, J. Mao, H.B. Newman, J. Ngadiuba, T.Q. Nguyen, M. Spiropulu, J.R. Vlimant, C. Wang, S. Xie, Z. Zhang, R.Y. Zhu

Carnegie Mellon University, Pittsburgh, USA
J. Alison, S. An, M.B. Andrews, P. Bryant, T. Ferguson, A. Harilal, T. Mudholkar, M. Paulini, A. Sanchez

University of Colorado Boulder, Boulder, USA
J.P. Cumalat, W.T. Ford, E. MacDonald, R. Patel, A. Perloff, K. Stenson, K.A. Ulmer, S.R. Wagner

Cornell University, Ithaca, USA
J. Alexander, Y. Cheng, J. Chu, D.J. Cranshaw, K. Mcdermott, J. Monroy, J.R. Patterson, D. Quach, J. Reichert, A. Ryd, W. Sun, S.M. Tan, Z. Tao, J. Thom, P. Wittich, M. Zientek

Fermi National Accelerator Laboratory, Batavia, USA
M. Albrow, M. Alyari, G. Apollinari, A. Apresyan, A. Apyan, S. Banerjee, L.A.T. Bauerdick, D. Berry, J. Berryhill, P.C. Bhat, K. Burkett, J.N. Butler, A. Canepa, G.B. Cerati, H.W.K. Cheung, F. Chlebana, M. Cremonesi, K.F. Di Petrillo, V.D. Elvira, Y. Feng, J. Freeman, Z. Gecse, L. Gray, D. Green, S. Grünendahl, O. Gutsche, R.M. Harris, R. Heller, T.C. Herwig, J. Hirschauer, B. Jayatilaka, S. Jindariani, M. Johnson, U. Joshi, T. Klijnsma, B. Klima, K.H.M. Kwok, S. Lammel, D. Lincoln, R. Lipton, T. Liu, C. Madrid, K. Maeshima, C. Mantilla, D. Mason, P. McBride, P. Merkel, S. Mrenna, S. Nahn, V. O'Dell, V. Papadimitriou, K. Pedro, C. Pena[55], O. Prokofyev, F. Ravera, A. Reinsvold Hall, L. Ristori, B. Schneider, E. Sexton-Kennedy, N. Smith, A. Soha, W.J. Spalding, L. Spiegel, S. Stoynev, J. Strait, L. Taylor, S. Tkaczyk, N.V. Tran, L. Uplegger, E.W. Vaandering, H.A. Weber

University of Florida, Gainesville, USA
D. Acosta, P. Avery, D. Bourilkov, L. Cadamuro, V. Cherepanov, F. Errico, R.D. Field, D. Guerrero, B.M. Joshi, M. Kim, E. Koenig, J. Konigsberg, A. Korytov, K.H. Lo, K. Matchev, N. Menendez, G. Mitselmakher, A. Muthirakalayil Madhu, N. Rawal, D. Rosenzweig, S. Rosenzweig, K. Shi, J. Sturdy, J. Wang, E. Yigitbasi, X. Zuo

Florida State University, Tallahassee, USA
T. Adams, A. Askew, D. Diaz, R. Habibullah, V. Hagopian, K.F. Johnson, R. Khurana, T. Kolberg, G. Martinez, H. Prosper, C. Schiber, R. Yohay, J. Zhang

Florida Institute of Technology, Melbourne, USA
M.M. Baarmand, S. Butalla, T. Elkafrawy[87], M. Hohlmann, R. Kumar Verma, D. Noonan, M. Rahmani, M. Saunders, F. Yumiceva

University of Illinois at Chicago (UIC), Chicago, USA
M.R. Adams, H. Becerril Gonzalez, R. Cavanaugh, X. Chen, S. Dittmer, O. Evdokimov, C.E. Gerber, D.A. Hangal, D.J. Hofman, C. Mills, G. Oh, T. Roy, M.B. Tonjes, N. Varelas, J. Viinikainen, X. Wang, Z. Wu, Z. Ye

The University of Iowa, Iowa City, USA
M. Alhusseini, K. Dilsiz[88], R.P. Gandrajula, O.K. Köseyan, J.-P. Merlo, A. Mestvirishvili[89], J. Nachtman, H. Ogul[90], Y. Onel, A. Penzo, C. Snyder, E. Tiras[91]

Johns Hopkins University, Baltimore, USA
O. Amram, B. Blumenfeld, L. Corcodilos, J. Davis, M. Eminizer, A.V. Gritsan, S. Kyriacou, P. Maksimovic, J. Roskes, M. Swartz, T.Á. Vámi

The University of Kansas, Lawrence, USA
J. Anguiano, C. Baldenegro Barrera, P. Baringer, A. Bean, A. Bylinkin, T. Isidori, S. Khalil, J. King, G. Krintiras, A. Kropivnitskaya, C. Lindsey, N. Minafra, M. Murray, C. Rogan, C. Royon, S. Sanders, E. Schmitz, J.D. Tapia Takaki, Q. Wang, J. Williams, G. Wilson

Kansas State University, Manhattan, USA
S. Duric, A. Ivanov, K. Kaadze, D. Kim, Y. Maravin, T. Mitchell, A. Modak, K. Nam

Lawrence Livermore National Laboratory, Livermore, USA
F. Rebassoo, D. Wright

University of Maryland, College Park, USA
E. Adams, A. Baden, O. Baron, A. Belloni, S.C. Eno, N.J. Hadley, S. Jabeen, R.G. Kellogg, T. Koeth, A.C. Mignerey, S. Nabili, M. Seidel, A. Skuja, L. Wang, K. Wong

Massachusetts Institute of Technology, Cambridge, USA
D. Abercrombie, G. Andreassi, R. Bi, S. Brandt, W. Busza, I.A. Cali, Y. Chen, M. D'Alfonso, J. Eysermans, G. Gomez Ceballos, M. Goncharov, P. Harris, M. Hu, M. Klute, D. Kovalskyi, J. Krupa, Y.-J. Lee, B. Maier, C. Mironov, C. Paus, D. Rankin, C. Roland, G. Roland, Z. Shi, G.S.F. Stephans, K. Tatar, J. Wang, Z. Wang, B. Wyslouch

University of Minnesota, Minneapolis, USA
R.M. Chatterjee, A. Evans, P. Hansen, J. Hiltbrand, Sh. Jain, M. Krohn, Y. Kubota, J. Mans, M. Revering, R. Rusack, R. Saradhy, N. Schroeder, N. Strobbe, M.A. Wadud

University of Nebraska-Lincoln, Lincoln, USA
K. Bloom, M. Bryson, S. Chauhan, D.R. Claes, C. Fangmeier, L. Finco, F. Golf, J.R. González Fernández, C. Joo, I. Kravchenko, M. Musich, I. Reed, J.E. Siado, G.R. Snow[†], W. Tabb, F. Yan

State University of New York at Buffalo, Buffalo, USA
G. Agarwal, H. Bandyopadhyay, L. Hay, I. Iashvili, A. Kharchilava, C. McLean, D. Nguyen, J. Pekkanen, S. Rappoccio, A. Williams

Northeastern University, Boston, USA
G. Alverson, E. Barberis, C. Freer, Y. Haddad, A. Hortiangtham, J. Li, G. Madigan, B. Marzocchi, D.M. Morse, V. Nguyen, T. Orimoto, A. Parker, L. Skinnari, A. Tishelman-Charny, T. Wamorkar, B. Wang, A. Wisecarver, D. Wood

Northwestern University, Evanston, USA
S. Bhattacharya, J. Bueghly, Z. Chen, A. Gilbert, T. Gunter, K.A. Hahn, N. Odell, M.H. Schmitt, M. Velasco

University of Notre Dame, Notre Dame, USA
R. Band, R. Bucci, N. Dev, R. Goldouzian, M. Hildreth, K. Hurtado Anampa, C. Jessop, K. Lannon, N. Loukas, N. Marinelli, I. Mcalister, T. McCauley, F. Meng, K. Mohrman, Y. Musienko[47], R. Ruchti, P. Siddireddy, M. Wayne, A. Wightman, M. Wolf, M. Zarucki, L. Zygala

The Ohio State University, Columbus, USA
B. Bylsma, B. Cardwell, L.S. Durkin, B. Francis, C. Hill, M. Nunez Ornelas, K. Wei, B.L. Winer, B.R. Yates

Princeton University, Princeton, USA
F.M. Addesa, B. Bonham, P. Das, G. Dezoort, P. Elmer, A. Frankenthal, B. Greenberg, N. Haubrich, S. Higginbotham, A. Kalogeropoulos, G. Kopp, S. Kwan, D. Lange, M.T. Lucchini, D. Marlow, K. Mei, I. Ojalvo, J. Olsen, C. Palmer, D. Stickland, C. Tully

University of Puerto Rico, Mayaguez, USA
S. Malik, S. Norberg

Purdue University, West Lafayette, USA
A.S. Bakshi, V.E. Barnes, R. Chawla, S. Das, L. Gutay, M. Jones, A.W. Jung, S. Karmarkar, M. Liu, G. Negro, N. Neumeister, G. Paspalaki, C.C. Peng, S. Piperov, A. Purohit, J.F. Schulte, M. Stojanovic[15], J. Thieman, F. Wang, R. Xiao, W. Xie

Purdue University Northwest, Hammond, USA
J. Dolen, N. Parashar

Rice University, Houston, USA
A. Baty, M. Decaro, S. Dildick, K.M. Ecklund, S. Freed, P. Gardner, F.J.M. Geurts, A. Kumar, W. Li, B.P. Padley, R. Redjimi, W. Shi, A.G. Stahl Leiton, S. Yang, L. Zhang, Y. Zhang

University of Rochester, Rochester, USA
A. Bodek, P. de Barbaro, R. Demina, J.L. Dulemba, C. Fallon, T. Ferbel, M. Galanti, A. Garcia-Bellido, O. Hindrichs, A. Khukhunaishvili, E. Ranken, R. Taus

Rutgers, The State University of New Jersey, Piscataway, USA
B. Chiarito, J.P. Chou, A. Gandrakota, Y. Gershtein, E. Halkiadakis, A. Hart, M. Heindl, E. Hughes, S. Kaplan, O. Karacheban[22], I. Laflotte, A. Lath, R. Montalvo, K. Nash, M. Osherson, S. Salur, S. Schnetzer, S. Somalwar, R. Stone, S.A. Thayil, S. Thomas, H. Wang

University of Tennessee, Knoxville, USA
H. Acharya, A.G. Delannoy, S. Spanier

Texas A&M University, College Station, USA
O. Bouhali[92], M. Dalchenko, A. Delgado, R. Eusebi, J. Gilmore, T. Huang, T. Kamon[93], H. Kim, S. Luo, S. Malhotra, R. Mueller, D. Overton, D. Rathjens, A. Safonov

Texas Tech University, Lubbock, USA
N. Akchurin, J. Damgov, V. Hegde, S. Kunori, K. Lamichhane, S.W. Lee, T. Mengke, S. Muthumuni, T. Peltola, I. Volobouev, Z. Wang, A. Whitbeck

Vanderbilt University, Nashville, USA
E. Appelt, S. Greene, A. Gurrola, W. Johns, A. Melo, H. Ni, K. Padeken, F. Romeo, P. Sheldon, S. Tuo, J. Velkovska

University of Virginia, Charlottesville, USA
M.W. Arenton, B. Cox, G. Cummings, J. Hakala, R. Hirosky, M. Joyce, A. Ledovskoy, A. Li, C. Neu, B. Tannenwald, S. White, E. Wolfe

Wayne State University, Detroit, USA
N. Poudyal, P. Thapa

University of Wisconsin - Madison, Madison, WI, USA
K. Black, T. Bose, J. Buchanan, C. Caillol, S. Dasu, I. De Bruyn, P. Everaerts, F. Fienga,
C. Galloni, H. He, M. Herndon, A. Hervé, U. Hussain, A. Lanaro, A. Loeliger, R. Loveless,
J. Madhusudanan Sreekala, A. Mallampalli, A. Mohammadi, D. Pinna, A. Savin, V. Shang,
V. Sharma, W.H. Smith, D. Teague, S. Trembath-reichert, W. Vetens

†: Deceased
1: Also at TU Wien, Wien, Austria
2: Also at Institute of Basic and Applied Sciences, Faculty of Engineering, Arab Academy for
Science, Technology and Maritime Transport, Alexandria, Egypt, Alexandria, Egypt
3: Also at Université Libre de Bruxelles, Bruxelles, Belgium
4: Also at Universidade Estadual de Campinas, Campinas, Brazil
5: Also at Federal University of Rio Grande do Sul, Porto Alegre, Brazil
6: Also at University of Chinese Academy of Sciences, Beijing, China
7: Also at Department of Physics, Tsinghua University, Beijing, China, Beijing, China
8: Also at UFMS, Nova Andradina, Brazil
9: Also at Nanjing Normal University Department of Physics, Nanjing, China
10: Now at The University of Iowa, Iowa City, USA
11: Also at Institute for Theoretical and Experimental Physics named by A.I. Alikhanov of
NRC 'Kurchatov Institute', Moscow, Russia
12: Also at Joint Institute for Nuclear Research, Dubna, Russia
13: Also at Helwan University, Cairo, Egypt
14: Now at Zewail City of Science and Technology, Zewail, Egypt
15: Also at Purdue University, West Lafayette, USA
16: Also at Université de Haute Alsace, Mulhouse, France
17: Also at Erzincan Binali Yildirim University, Erzincan, Turkey
18: Also at CERN, European Organization for Nuclear Research, Geneva, Switzerland
19: Also at RWTH Aachen University, III. Physikalisches Institut A, Aachen, Germany
20: Also at University of Hamburg, Hamburg, Germany
21: Also at Department of Physics, Isfahan University of Technology, Isfahan, Iran, Isfahan,
Iran
22: Also at Brandenburg University of Technology, Cottbus, Germany
23: Also at Skobeltsyn Institute of Nuclear Physics, Lomonosov Moscow State University,
Moscow, Russia
24: Also at Physics Department, Faculty of Science, Assiut University, Assiut, Egypt
25: Also at Karoly Robert Campus, MATE Institute of Technology, Gyongyos, Hungary
26: Also at Institute of Physics, University of Debrecen, Debrecen, Hungary, Debrecen,
Hungary
27: Also at Institute of Nuclear Research ATOMKI, Debrecen, Hungary
28: Also at MTA-ELTE Lendület CMS Particle and Nuclear Physics Group, Eötvös Loránd
University, Budapest, Hungary, Budapest, Hungary
29: Also at Wigner Research Centre for Physics, Budapest, Hungary
30: Also at IIT Bhubaneswar, Bhubaneswar, India, Bhubaneswar, India
31: Also at Institute of Physics, Bhubaneswar, India
32: Also at G.H.G. Khalsa College, Punjab, India
33: Also at Shoolini University, Solan, India
34: Also at University of Hyderabad, Hyderabad, India
35: Also at University of Visva-Bharati, Santiniketan, India
36: Also at Indian Institute of Technology (IIT), Mumbai, India
37: Also at Deutsches Elektronen-Synchrotron, Hamburg, Germany

38: Also at Sharif University of Technology, Tehran, Iran
39: Also at Department of Physics, University of Science and Technology of Mazandaran, Behshahr, Iran
40: Now at INFN Sezione di Bari ^{a}, Università di Bari ^{b}, Politecnico di Bari ^{c}, Bari, Italy
41: Also at Italian National Agency for New Technologies, Energy and Sustainable Economic Development, Bologna, Italy
42: Also at Centro Siciliano di Fisica Nucleare e di Struttura Della Materia, Catania, Italy
43: Also at Università di Napoli 'Federico II', NAPOLI, Italy
44: Also at Riga Technical University, Riga, Latvia, Riga, Latvia
45: Also at Consejo Nacional de Ciencia y Tecnología, Mexico City, Mexico
46: Also at IRFU, CEA, Université Paris-Saclay, Gif-sur-Yvette, France
47: Also at Institute for Nuclear Research, Moscow, Russia
48: Now at National Research Nuclear University 'Moscow Engineering Physics Institute' (MEPhI), Moscow, Russia
49: Also at Institute of Nuclear Physics of the Uzbekistan Academy of Sciences, Tashkent, Uzbekistan
50: Also at St. Petersburg State Polytechnical University, St. Petersburg, Russia
51: Also at University of Florida, Gainesville, USA
52: Also at Imperial College, London, United Kingdom
53: Also at Moscow Institute of Physics and Technology, Moscow, Russia, Moscow, Russia
54: Also at P.N. Lebedev Physical Institute, Moscow, Russia
55: Also at California Institute of Technology, Pasadena, USA
56: Also at Budker Institute of Nuclear Physics, Novosibirsk, Russia
57: Also at Faculty of Physics, University of Belgrade, Belgrade, Serbia
58: Also at Trincomalee Campus, Eastern University, Sri Lanka, Nilaveli, Sri Lanka
59: Also at INFN Sezione di Pavia ^{a}, Università di Pavia ^{b}, Pavia, Italy, Pavia, Italy
60: Also at National and Kapodistrian University of Athens, Athens, Greece
61: Also at Ecole Polytechnique Fédérale Lausanne, Lausanne, Switzerland
62: Also at Universität Zürich, Zurich, Switzerland
63: Also at Stefan Meyer Institute for Subatomic Physics, Vienna, Austria, Vienna, Austria
64: Also at Laboratoire d'Annecy-le-Vieux de Physique des Particules, IN2P3-CNRS, Annecy-le-Vieux, France
65: Also at Şırnak University, Sirnak, Turkey
66: Also at Near East University, Research Center of Experimental Health Science, Nicosia, Turkey
67: Also at Konya Technical University, Konya, Turkey
68: Also at Istanbul University - Cerrahpasa, Faculty of Engineering, Istanbul, Turkey
69: Also at Piri Reis University, Istanbul, Turkey
70: Also at Adiyaman University, Adiyaman, Turkey
71: Also at Ozyegin University, Istanbul, Turkey
72: Also at Izmir Institute of Technology, Izmir, Turkey
73: Also at Necmettin Erbakan University, Konya, Turkey
74: Also at Bozok Universitetesi Rektörlügü, Yozgat, Turkey, Yozgat, Turkey
75: Also at Marmara University, Istanbul, Turkey
76: Also at Milli Savunma University, Istanbul, Turkey
77: Also at Kafkas University, Kars, Turkey
78: Also at Istanbul Bilgi University, Istanbul, Turkey
79: Also at Hacettepe University, Ankara, Turkey
80: Also at Vrije Universiteit Brussel, Brussel, Belgium

81: Also at School of Physics and Astronomy, University of Southampton, Southampton, United Kingdom

82: Also at IPPP Durham University, Durham, United Kingdom

83: Also at Monash University, Faculty of Science, Clayton, Australia

84: Also at Università di Torino, TORINO, Italy

85: Also at Bethel University, St. Paul, Minneapolis, USA, St. Paul, USA

86: Also at Karamanoğlu Mehmetbey University, Karaman, Turkey

87: Also at Ain Shams University, Cairo, Egypt

88: Also at Bingol University, Bingol, Turkey

89: Also at Georgian Technical University, Tbilisi, Georgia

90: Also at Sinop University, Sinop, Turkey

91: Also at Erciyes University, KAYSERI, Turkey

92: Also at Texas A&M University at Qatar, Doha, Qatar

93: Also at Kyungpook National University, Daegu, Korea, Daegu, Korea